INVESTIGATION OF OPTICAL AND ELECTRONIC PROPERTIES OF Au DECORATED MoS_2

by

UDAI BHANU
M.S. University of Central Florida, 2012

A dissertation submitted in partial fulfillment of requirements
for the degree of Doctor of Philosophy
in the Department of Physics
in the College of Sciences
at the University of Central Florida
Orlando, Florida

Spring Term
2015

Major Professor: Saiful I. Khondaker

© 2015 Udai Bhanu

ABSTRACT

Achieving tunability of two dimensional (2D) transition metal dichalcogenides (TMDs) functions calls for the introduction of hybrid 2D materials by means of localized interactions with zero dimensional (0D) materials. A metal-semiconductor interface, as in gold (Au) - molybdenum disulfide (MoS_2), is of great interest from the standpoint of fundamental science as it constitutes an outstanding platform to investigate optical and electronic properties due to charge transfer. The applied aspects of such systems introduce new options for electronics, photovoltaics, detectors, catalysis, and biosensing. Here in this dissertation, we study the charge transfer interaction between Au nanoparticals and MoS_2 flakes and its effect on Photoluminescence and electronic transport properties. The MoS_2 was mechanically exfoliated from bulk single crystal. Number of layers in the flake was identified with the help of AFM and Raman Spectra. Au was deposited by physical vapor deposition method (PVD) in multiple steps to decorate MoS_2 flakes.

We first study the photoluminescence of pristine and Au decorated MoS_2 and shows that in the presence of Au, the photoluminescence of MoS_2 quenches significantly. We infer that the PL quenching can be attributed to a change in the electronic structure of the MoS_2-Au system. The difference in Fermi level of a of MoS_2 and Au results in a 0.4 eV energy level offset, which causes a band bending in the MoS_2-Au hybrid. Upon illumination, the electrons in the excited state of MoS_2 transfer to Au, leaving a hole behind, thus cause p-doping in MoS_2. As electrons from MoS_2 are transferred to Au, they do not decay back to their initial ground state, leading to PL quenching in the hybrid system.

To study the effect of Au deposition on electronic properties of ultra-thin and multilayers MoS_2 flakes, we have fabricated MoS_2 FETs from (1) ultra-thin sample (2-4 MoS_2 layers) and (2) multilayers samples (more than 20 layers). After each deposition of Au, we measured the electrical characteristics of FET at room temperature. We show that the threshold voltage shifts towards the positive gate voltage as we increase the thickness of Au. This shift in threshold voltage is indicative of p doping of the MoS_2. We further show that the field effect mobility of MoS_2 FET decrease with Au thickness. We have quantitatively estimated the charge transferring from MoS_2 to Au.

To my loving family

ACKNOWLEDGMENT

With much gratitude and fondness, I would like to recognize my family, friends, mentors and committee members who contributed to completion of my PhD degree.

First of all I would like thank my supervisor Dr. Saiful Khondaker, for giving me an opportunity to pursue a topic of my interest and helping me in many possible ways. His critical comments and commitment helped me throughout my graduate life.

I am equally grateful to my dissertation committee members Dr. Sergei Stolbov, Dr. Lee Chow and Dr. Lei Zhai for their encouragement, guidance, time and their attention.

I am also thankful to Dr. Laurene Tetrad who helped me in recording and analyzing Raman and Photoluminescence data.

I am truly indebted to my parents whose love, patience and faith inspired me to begin this journey. Their prayers, teachings, continuous motivation and support have been immeasurably valuable. To all other family members, my brothers, sister-in-law and Unnabh who gave me their unconditional love and affection, thank you.

I would like to thank my fellow coworker, Rakib for his valuable scientific discussion and continuous moral support and Narae for making environment cheerful inside the lab. Among the colleagues who left the group I acknowledge Dr. Daeha Joung for teaching me the device fabrication and Dr. Biddut Sarker, Dr. Feras Alzubi, Dr. Shashank Shekhar, Kristy Kormondy, and Edvards Jimenez for sharing their enthusiasm and comments on my work.

I have many friends who have encouraged and supported me during the five years of graduate school. I would like to thanks Aniruddha Dutta, Deep Panjawani, Aditya Reddy Koli and Anupama Yadav for sharing my stress and joy.

I would also like to acknowledge Department of Physics, University of Central Florida (UCF) for financially supporting me for almost 4 years and Nanoscience and Technology Center (NSTC) & Materials Characterization Facility (MCF) at UCF for allowing me to use their characterization facility and other scientific instruments.

At the end of my formal education with this PhD, I remember all my teachers for providing me good education.

TABLE OF CONTENTS

LIST OF FIGURES

LIST OF ABBREVIATIONS

AFM	Atomic Force Microscopy
CNT	Carbon Nanotube
CVD	Chemical Vapor Deposition
DEP	Dielectophoreis
DI	Deionized
EBL	Electron Beam Lithography
FET	Field Effect Transistor
IPA	Isopropyl-alcohol Methyl-isobutyl-ketone
MIBK	Methyl-isobutyl-ketone
MOS	Metals Oxide Semiconductor
MoS_2	molybdenum disulphide
NPGS	Nano-Patterned- Generation-System
NPs	Nanoparticles
SB	Schottky Barrier
SEM	Scanning Electron Microscopy
SiO_2	Silicon Dioxide
TMDs	Transition Metal Dichalcogenides
VdW	Van der Waals

CHAPTER 1: INTRODUCTION

1.1 Motivation

Two-dimensional (2D) materials are substances with a thickness of a few nanometres or less. Electrons in these 2D materials are free to move in a 2D plane however the electron motion in third dimension is governed by quantum mechanics. Most of layered materials, because of their property of strong in-plane chemical bond and very weak coupling between layers it has been possible to synthesize/isolate single and few layers from bulk layered materials to obtain a 2D material. These layered materials often called as Van der Waals (VdW) material because of the presence of weak VdW forces between its layers that binds them together.

Technological point of view, 2D materials are very important in designing the future nanoelectronic devices. On one hand, starting from 2D materials it is possible to stack different other 2D materials on top of each other and create non-naturally existent 3D materials with completely different properties and on the other hand we can chemically synthesize and/or etch out the 2D materials to further scale down its dimensionality to create 1D nano structures. Stacking 2D materials on top of each other has resulted in the emergence of a new class of materials: heterostructures based on 2D atomic crystals. It has significance in both fundamental physics point of view and application point of view. In particular, by stacking graphene, hexagonal Boron Nitride (hBN) and Molybdenum disulphide (MoS_2), a tunnel transistor could be realized and uncommon phenomenon like quantum Hall Effect could be observed. On the other hand, scaling down the dimensions of 2D materials also generates equally exciting results.

For instance, the chemically derived 1D graphene (Nanoribbon) shows completely different electronic properties than 2D graphene. Reducing dimension of graphene to 1D opens up band gap in it therefore 1D graphene shows semiconducting properties in contrary to 2D graphene which is well known as semimetal.

A step further towards technological development is the realization of atomically thin pn junctions which could be possible only because of 2d semiconductors. An n-type 2D semiconducting material can either brought directly in contact with another p-type 2D semiconducting materials (vertical stack geometry), or a part of 2D semiconductor can be doped with molecules/atom to realize (planer geometry) atomically thin pn junction. Such a pn junction made form VdW materials would reach to ultimate quantum limit. In particular, these atomically thin pn junctions are predicted to exhibits a completely different charge transport mechanism than their bulk counterpart. In bulk pn junctions, the carrier transport is governed by diffusion and drift process across the depletion region. Unlike bulk, atomically thin pn junctions do not have depletion region, hence are predicted to have completely different charge transport mechanism.

Another interesting aspect of 2D materials is that they only consist of two surfaces with no materials in underneath these surfaces. In other words, in 2D material the whole material is exposed to surface modifications (doping, functionalization, plasma treatment, adsorption). Therefore the surface chemistry can play a very active role in tuning the properties of these materials. Band gap tuning of graphene by organic molecules have already been demonstrated. Hence 2D materials give room to tune their properties by external control.

In addition, the most 2D semiconductors are flexible and transparent which give them advantage over conventional bulk semiconductor for being capable to be used in flexible and transparent device.

The most extensively studied 2D material is graphene. Besides having rich physics and high career mobility its use in electronic applications is limited by the absence of band gap in it. A number of methods have been devised to introduce band gap in graphene for example substrate induced band gap, strain induced band gap, chemical functionalization, nanomesh method and nano ribbon method. Despite so many efforts, creation of sufficient band gap in graphene to make it compete with other semiconductor remains a challenge to till date.

On the other hand hexagonal boron nitride, another commonly studied layered Van der Waals material has a band gap of 5.2eV which makes it insulator. Therefor such a 2D material can be used as insulator or atomically flat substrate but not as an active material in nano electronic devices. However another kind of 2D materials called transition metal dichalcogenides (TMDs) exists in semiconductor, semi-metal and metallic, magnetic and super conducting (at low temperature) forms. For example MoS_2 and WS_2 is semiconducting, $NbSe_2$ and TaS_2 are super conductors at low temperature and $TcSe_2$ is small gap semiconductor[1]. The general stoichiometric formula for TMDs is MX_2 where "M" represents a transition metal atom and "X" represents a chalcogen atom. The transition metal atoms are coordinated with six nearby chalcogen atoms to form either octahedral or trigonal prismatic polyhedron structures. Ataca et al. studied the stability of about 44 TDMs and the results are presented in figure 1.1. The grey color indicates that the compound is not stable. Brown and green indicates their H and T phase respectively.

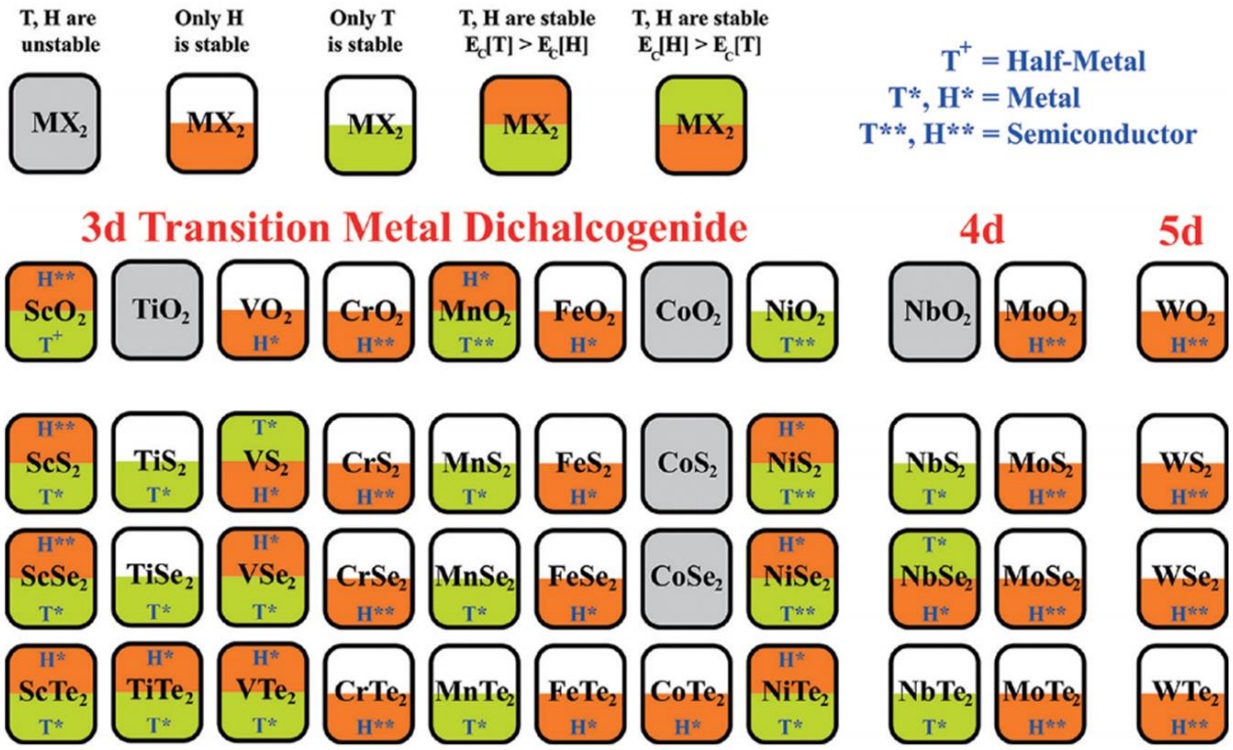

Figure 1.1 Summary of the calculated stability analysis of 44 different Metal Dichalcogenides compounds of type MX_2 that can form stable 2D single-layer H and/or T structures. M indicates Transition-metal atoms which are further characterized into 3d, 4d and 5d groups and X indicated the chalcogen atom. Grey color indicates that MX_2 compounds do not form stable H nor T structure. The half-metallic compounds are represented by (+), metallic by (*) and semiconducting by (**) in the figure[2].

Recently, one of the TMD materials, molybdenum disulfide (MoS_2), has attracted tremendous interest. In particular, single layer and few layers MoS_2 exhibit promising behavior for applications in transistor with high current switching[3,4], light emitting devices[5] , photo-transistors[6-8], catalysis[9] and solar cells[10,11]. Another interesting property of MoS_2 is its transition from bulk indirect semiconductor to a direct bandgap in pristine MoS_2 monolayers[12-16]. Since the

monolayer of MoS_2 is a direct semiconductor material, it exhibits a strong photoluminescence (PL). Spelndiani et al. have shown ultrathin MoS_2 exhibits enhanced PL peaks assigned as A1 and B1 at 1.85 and 1.98eV respectively. Radisavljevic et. al. have shown that a single layer MoS_2 transistor can have room temperature on/off ratio $1x10^8$ and mobility 200 cm^2/Vs and such transistor shows ultralow power dissipation. The enhanced PL observed in monolayers have also triggered interesting work on electroluminescence[5], valley-Spin polarization[17-19], and tunable p-n diodes[20]. Other 2D layered materials and heterostructures resulting from stacking of different 2D layers are also believed to hold exciting promises[21-23]. However, in most cases the production of such heterostructures is hindered by significant challenges due to the complications in obtaining other 2D materials and their control placements on top of each other. Hence, 0D-2D hybrid structures may offer a more immediate benefit for tunability of 2D transition metal dichalcogenides (TMDs) functions: because layers of VdW (2D) materials are so thin, physical or chemical modifications of their surface can significantly impact their functionalities. Thus, exploring the interactions of 0D and 2D materials is crucial to the quest for highly efficient and functional hybrid nanodevices. Here, by creating hybrid 0D-2D systems, we propose to modify the properties of MoS_2. Once such immediate modification could be doping of 2D material by nano particles.

Hence, here in this dissertation, I investigate the effect of Au nanostructures on the electronic properties of MoS_2 and discuss the consequences of MoS_2-Au interactions in electronics and optoelectronics.

1.2 Chapter Outline

Chapter 2 provides the historical and technical background and basic theoretical concepts necessary for my dissertation. I shall introduced MoS_2 to the readers in the beginning of the chapter followed by a discussion about the structural, electronic and optical properties of it. Thereafter I shall discuss the characterization strategies followed to accurately identify the number of layers in mechanically exfoliated flakes. In the end of the chapter 2, I shall briefly explain my device structure (FET structure) and its characteristics for the readers. In the last section of the chapter, I shall be discussing some of the previous reported work on Au decorated MoS_2.

Chapter 3 will focus on micro and nano fabrication strategies followed during MoS_2 FET fabrication process. I shall enlist and explain all the fabrication steps by order. Starting from the shape, size and spacing consideration for the marker on the Si chip used for mechanical exfoliation, I shall explain the nitty-gritty of mechanical exfoliation followed by discussion on parameters for Au NP formation and electrode deposition during my experiments. Towards the end of the chapter, I shall present my measurement set put including room temperature and low temperature setup for electronics properties and PL/Raman setup for measurement of optical properties to the readers.

Chapter 4 will focus on Optical properties Au decorated MoS_2. In particular, I shall discuss the effect of Au deposition on photoluminescence properties of MoS_2. A detailed study and minor details were taken care of by creating 2D PL maps of the decorated flakes.

Chapter 5 will focus on room temperature electronic properties Au decorated MoS_2. I shall discuss the effect of controlled Au deposition on mobility and threshold voltage of few and

multi layers MoS_2 FET. In the end, I shall quantitatively estimate the charge transfer from MoS_2 to Au as a function of Au thickness. Adequate discussion about the alignment of energy band and Fermi level has been added.

Chapter 6 will focus answering the very fundamental question of charge transport at low temperature in Au decorated MoS_2. I shall discuss the results of electron transport experiment conducted at 77K (liquid N_2 temperature). Adequate discussion has been added in the end of the chapter to convince readers.

Chapter 7 will focus on further possible extension of this work. I shall be purposing some of future directions and experiments for continuation of my work. I shall also present some of preliminary data I have obtained on those lines.

1.3 References

1 Chhowalla, M. *et al.* The chemistry of two-dimensional layered transition metal dichalcogenide nanosheets. *Nat Chem* **5**, 263-275 (2013).

2 Ataca, C., Şahin, H. & Ciraci, S. Stable, Single-Layer MX_2 Transition-Metal Oxides and Dichalcogenides in a Honeycomb-Like Structure. *The Journal of Physical Chemistry C* **116**, 8983-8999, (2012).

3 RadisavljevicB, RadenovicA, BrivioJ, GiacomettiV & KisA. Single-layer MoS_2 transistors. *Nat Nano* **6**, 147-150, (2011).

4 Pu, J. *et al.* Highly Flexible MoS_2 Thin-Film Transistors with Ion Gel Dielectrics. *Nano Letters* **12**, 4013-4017, (2012).

5 Sundaram, R. S. *et al.* Electroluminescence in Single Layer MoS_2. *Nano Letters* **13**, 1416-1421, (2013).

6 Lee, H. S. *et al.* MoS_2 Nanosheet Phototransistors with Thickness-Modulated Optical Energy Gap. *Nano Letters* **12**, 3695-3700, (2012).

7 Liu, M. *et al.* A graphene-based broadband optical modulator. *Nature* **474**, 64-67 (2011).

8 Choi, W. *et al.* High-Detectivity Multilayer MoS_2 Phototransistors with Spectral Response from Ultraviolet to Infrared. *Advanced Materials* **24**, 5832-5836, (2012).

9 Voiry, D. *et al.* Conducting MoS_2 Nanosheets as Catalysts for Hydrogen Evolution Reaction. *Nano Letters* **13**, 6222-6227, (2013).

10 Feng, J., Qian, X., Huang, C.-W. & Li, J. Strain-engineered artificial atom as a broad-spectrum solar energy funnel. *Nat Photon* **6**, 866-872, (2012).

11 Wang, Q. H., Kalantar-Zadeh, K., Kis, A., Coleman, J. N. & Strano, M. S. Electronics and optoelectronics of two-dimensional transition metal dichalcogenides. *Nat Nano* **7**, 699-712 (2012).

12 Splendiani, A. *et al.* Emerging Photoluminescence in Monolayer MoS_2. *Nano Letters* **10**, 1271-1275, (2010).

13 Mak, K. F., Lee, C., Hone, J., Shan, J. & Heinz, T. F. Atomically Thin MoS_2: A New Direct-Gap Semiconductor. *Physical Review Letters* **105**, 136805 (2010).

14 Molina-Sánchez, A. & Wirtz, L. Phonons in single-layer and few-layer MoS_2 and WS_2. *Physical Review B* **84**, 155413 (2011).

15 Korn, T., Heydrich, S., Hirmer, M., Schmutzler, J. & Schüller, C. Low-temperature photocarrier dynamics in monolayer MoS_2. *Applied Physics Letters* **99**, 102109, (2011).

16 Ghatak, S., Pal, A. N. & Ghosh, A. Nature of Electronic States in Atomically Thin MoS_2 Field-Effect Transistors. *ACS Nano* **5**, 7707-7712, (2011).

17 Mak, K. F., He, K., Shan, J. & Heinz, T. F. Control of valley polarization in monolayer MoS_2 by optical helicity. *Nat Nano* **7**, 494-498, (2012).

18 Zeng, H., Dai, J., Yao, W., Xiao, D. & Cui, X. Valley polarization in MoS_2 monolayers by optical pumping. *Nat Nano* **7**, 490-493, (2012).

19 Xiao, D., Liu, G.-B., Feng, W., Xu, X. & Yao, W. Coupled Spin and Valley Physics in Monolayers of MoS_2 and Other Group-VI Dichalcogenides. *Physical Review Letters* **108**, 196802 (2012).

20 Jariwala, D. *et al.* Gate-tunable carbon nanotube–MoS_2 heterojunction p-n diode. *Proceedings of the National Academy of Sciences* **110**, 18076-18080, (2013).

21 Geim, A. K. & Grigorieva, I. V. Van der Waals heterostructures. *Nature* **499**, 419-425, (2013).

22 Zhang, W. *et al.* Ultrahigh-Gain Photodetectors Based on Atomically Thin Graphene-MoS_2 Heterostructures. *Sci. Rep.* **4**, (2014).

23 Eda, G. *et al.* Coherent Atomic and Electronic Heterostructures of Single-Layer MoS_2. *ACS Nano* **6**, 7311-7317, (2012).

CHAPTER 2: BACKGROUND

2.1 Two Dimension Materials: A New Class of Materials

In recent years two dimensional (2D) materials have gained a lot of attention primarily because of their exceptional properties which lead to their applications in nano electronics, optoelectronics, spintronics, catalysts, chemical and biological sensors, supercapacitors, solar cells and lithium ion batteries[1-18]. Since the discovery of graphene in 2004 which lead to Nobel Prize in the field of 2D materials, the other 2D materials for example Transition Metal Dichalcogenides (TDM), hBN, Silicene and Germanene have also being explored in great details[19-24]. Out of these other 2D materials, TDM are widely studied because of the fact of their wide range of band gap makes them promising candidate for future electronics, optoelectronics and logics applications[25-35].

2.2 Emergence of MoS_2

MoS_2 is the most extensively studied material among TDM family. It has been studied for more than five decades[36-48]. R. V. Kasowski was one of early researchers who studied the band structure of MoS2 back in 1973. Fivaz et al. studies the charge career mobility in layers semiconducting materials in 1967[38]. The early researchers had just scratched the surface in exploring the properties of MoS_2. The electronic and optoelectronics properties have never been investigated extensively until recently. In last few years, the number of publications in this field have increased manifold. Only in 2014, the total numbers of articles published on MoS_2 alone

were 1506. The MoS_2 articles have been cited by 132059 times in last 20 years. Figure 2.1 illustrates the number of publications in last 20 years according to web of science database on the date of 02/15/2015.

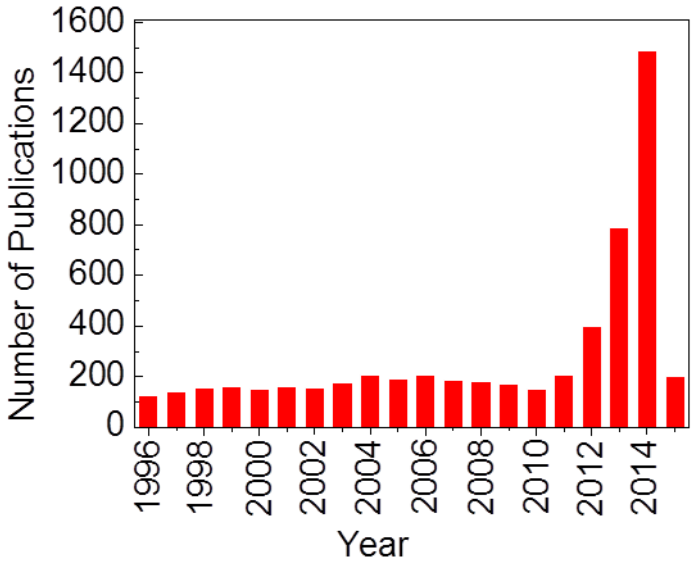

Figure 2.1 Number of publications in last 20 years containing the term "MoS_2". (determined by searching for "MoS_2" in Web of Knowledge database).

2.2.1 Structural Properties of MoS_2

MoS_2 belongs to family of transition metal dichalcogenides materials consists of layer of Mo atoms covalently bonded to 3 S atoms on top and 3 S atoms at the bottom as shown in figure 2.2. It can be seen that the Mo atoms sits at the center and the S atoms sit at the edges. This repeating arrangement constitutes a single layer of MoS_2. In bulk MoS_2, hundreds and thousands of layers of MoS_2 are held together by Van der Waals forces. Due to weak Van der Waals force, it is possible to exfoliate MoS_2 bulk crystal into 2D mono layers. The exfoliation method will be explained in details in chapter 3.

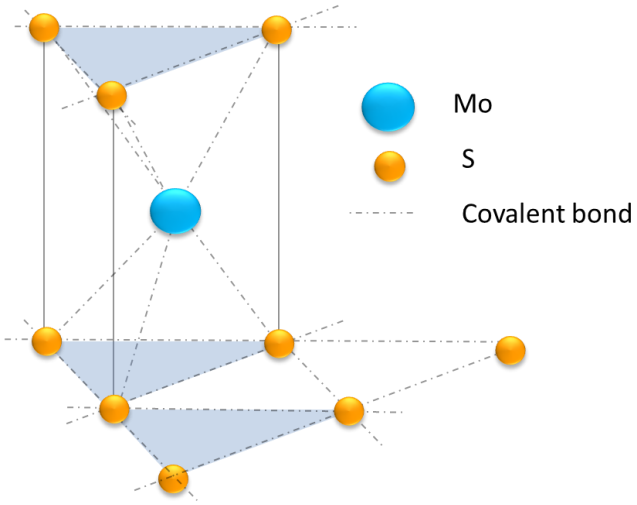

Figure 2.2 A simplified schematic of MoS_2 structure. Blue spheres indicate the Mo atom and the yellow spheres indicate S atoms.

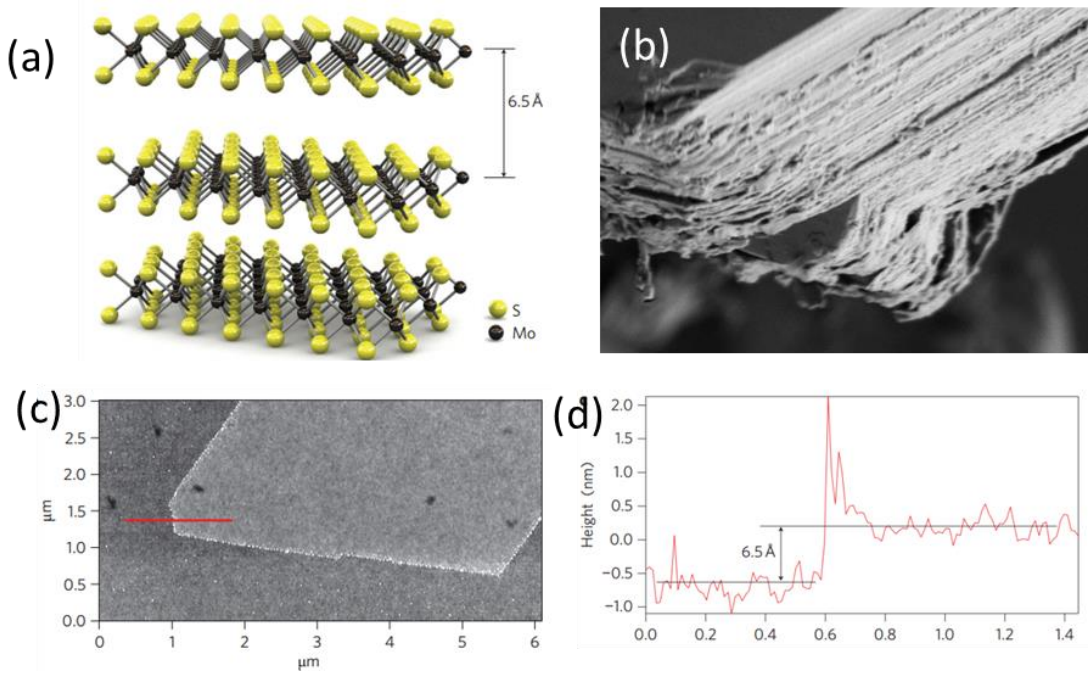

Figure 2.3 Structural representations of layers in MoS_2 bulk crystal[12]. (b) SEM image of actual MoS_2 bulk crystal (c) AFM image of single layer MoS_2 produced by mechanical exfoliation[12] (d) the height profile extracted from the AFM image[12].

Figure 2.3a illustrates the layered structure in MoS_2 bulk crystal. Figure 2.3b illustrates the SEM image of actual bulk MoS_2 crystal where hundreds of stacked monolayers can be seen. Each monolayer of MoS_2 is 6.5nm thick. Figure 2.3c and 2.3d illustrates the AFM image of a mechanically exfoliated monolayer and its height profile respectively.

2.2.2 Optical Properties

MoS_2 is a semiconducting material and has numerous applications in optics and optoelectronics as discussed earlier. In this section I shall briefly discuss about some important optical properties of MoS_2.

2.2.2.1 Photoluminescence and Band Gap dependence

Photoluminescence (PL) is a process where a photon is emitted due to recombination of optically created electron with a hole. A prerequisite condition for PL to occur in a semiconducting material is that an electron must be promoted from valence band to conduction band by the incident laser light. Hence the incident photon energy must have to be equal to or larger than the band gap of the semiconducting material. If the incident photon energy is larger than the band gap of the material, often times a non-radiative relaxation occur within the vibrations levels. This is also called vibrational relaxation. Figure 2.4 illustrates the possible electronic transition that can lead to photoluminescence in the material.

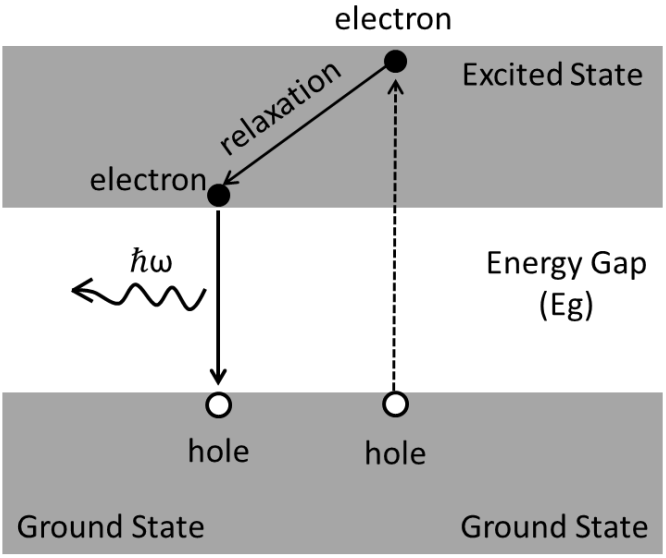

Figure 2.4 Electronic energy level diagram showing the transitions between ground state and excited state responsible for photoluminescence.

When a photo-excited electron comes back to ground sate it recombines with the electron. Such optical recombinations occur at energies close to the edge of bandgap[51]. When band edges have same wave vector (ie when band edges have same position of Brillouin Zone in momentum space) the energy and momentum remain conserve in the process of photon emission. In other words, such an emission occurs without generation of any phonon. However if the band edges do not have the same position of Brillouin Zone in momentum space (ie. different wave vectors) then the emission of photon happens by second order process which require generation of a phonon in order to conserve momentum[51]. The first order process is related to direct band gap semiconductors (for example monolayer MoS_2) and the later second order process is related to the indirect semiconductors. Figure 2.5 illustrates the electronic band diagram for direct and indirect band gap materials in momentum space.

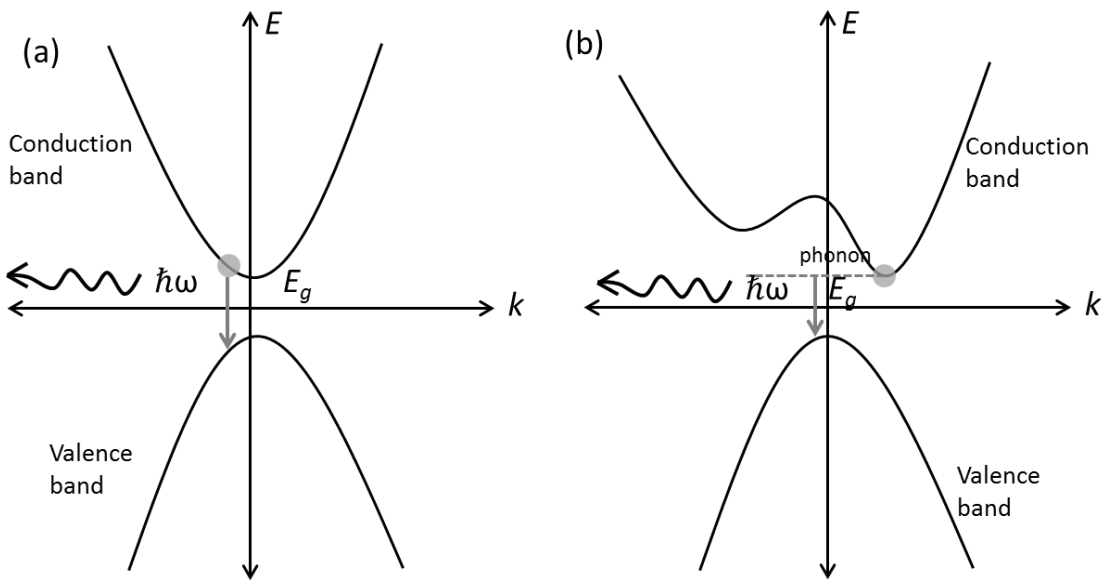

Figure 2.5 Position of valence and conduction band minimum in momentum space for direct (a) and indirect (b) band gaps and it illustrates the direct and indirect transition in semiconductors.

In most of semiconductors, we see broadened PL spectral peaks. The broadening of PL peak in semiconductors occurs due to thermal distribution K_BT of electron before recombination, where K_B is Boltzmann Constant and T is temperature, along with the homogeneity in the crystal. Figure 2.6 illustrates that because of disorder in the semiconductor, the different Eg values because of different transition can lead to broadening of the spectrum.

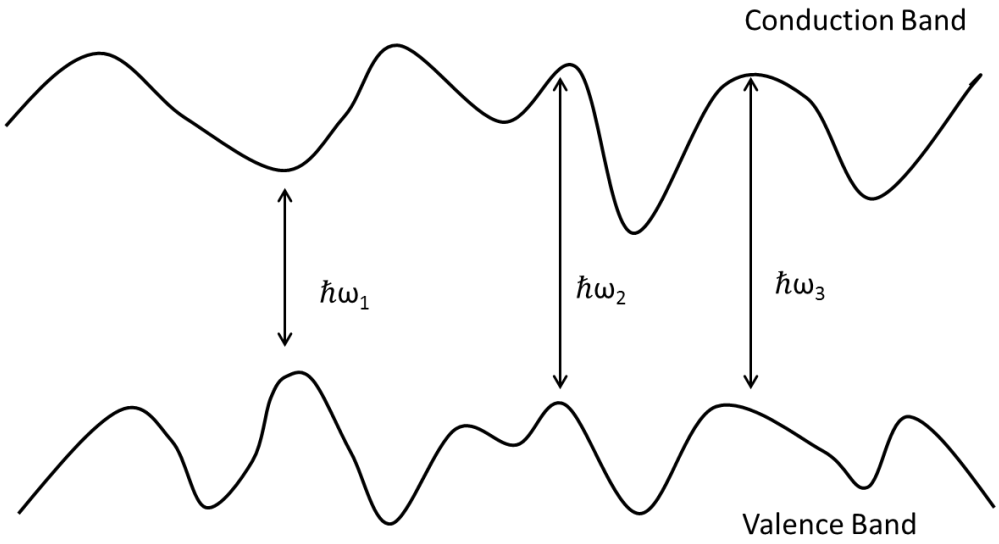

Figure 2.6 Broadening of PL line due to inhomogeneities in the semiconductor.

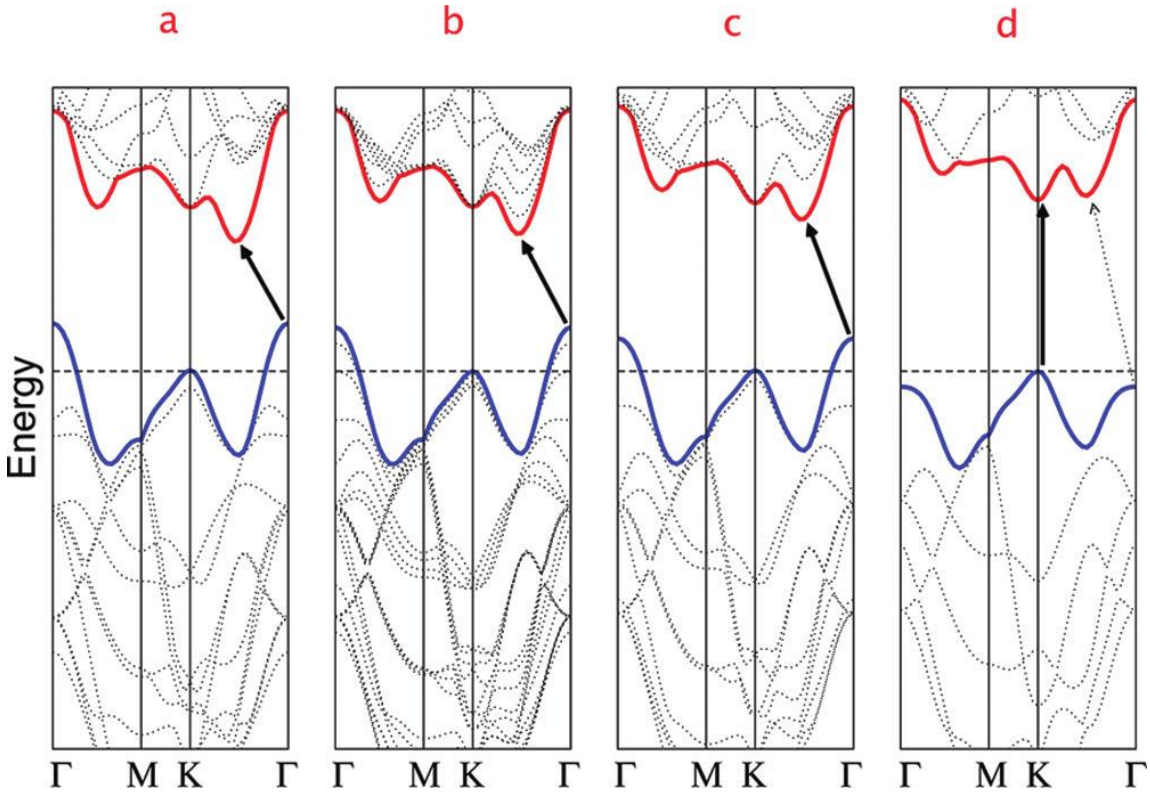

Figure 2.7 Calculated band structure of (a) bulk (b) 4 layer (c) bilayer (d) monolayer MoS_2 by Splendiani at al[49].

A very interesting aspect of MoS_2 is that its band gap is thickness dependent. The band gap of bulk MoS_2 crystal is 1.2eV whereas the band gap of monolayer MoS_2 is reported to be 1.9eV[50]. Figure 2.7 illustrates the change in band gap as the thickness of MoS_2 flake changes. The blue solid line represents the valence band, red solid line represents the conduction band and the black solid arrows shows the lowest energy transition. As the number of layers in MoS_2 decreases, the indirect band gap becomes larger and larger. In monolayer case, the lowest energy transition becomes the direct transition at K point between highest of valence band and lowest of conduction band. Hence the monolayer MoS_2 becomes a direct band gap semiconductor.

Splendiani et al, studied the photoluminescence of ultrathin MoS_2 prepared by microfabrication techniques on both quartz and Si/SiO_2 substrate[49]. It has been suggested that the optical transitions in ultrathin MoS_2 are dominated by excitons[50]. Hence the optical absorption of ultrathin MoS_2 spectrum shows two distinct peaks assigned to A and B excitations at Brillouin zone K point. The difference in their energy of these two peaks is due to spin orbital splitting of valence band. The luminescence quantum efficiency was found to be much higher in single layer than bulk and the reason of such enhanced luminescence has been attributed to slower electronic relaxation. Eda et al studied the photoluminescence properties of chemically exfoliated MoS_2 and found very similar PL results as in case of mechanically exfoliated MoS_2 layers[51].

Mak et al.[50] studied the PL spectrum of monolayer MoS_2 of suspended sample. They found that PL spectrum is dominant by a single exciton peak (A peak) as shown in figure 2.8b. The reason for absence of B exciton peak in suspended sample is still not clear. This may be because of the Si substrate effect. A similar PL spectrum was also found on grown monolayer

samples on intert and nearly lattice matching mica by low pressure chemical vapor deposition method[52].

In another report by Mak et al.[53] where they studied the PL spectrum of monolayer MoS_2 on hexagonal boron nitride (h-BN) substrate at low temperature (10K), they found that the A exciton peak evolves into two resonances. A new low energy resonance named A^- feature was found. The origin on this new feature is assigned to quasi particles called trion which is made up of two electrons and one hole. The PL spectrum taken by Mak et al. is presented in figure 2.8c

Mouri et al, reported the tunability of photoluminescence of mechanically exfoliated monolayer MoS_2 on Si/SiO_2 substrate by chemical doping. It is suggested that chemical doping of MoS_2 by p-dopant like 7,7,8,8-tetracyanoquinodimethane (TCQN) drastically enhance the photoluminescence properties. Where the doping MoS_2 by n-dopant like nicotinamide adenine dinucleotide (NADH) can suppress the PL properties due to injection of excess of electrons from n-dopant to MoS_2 monolayer[54].

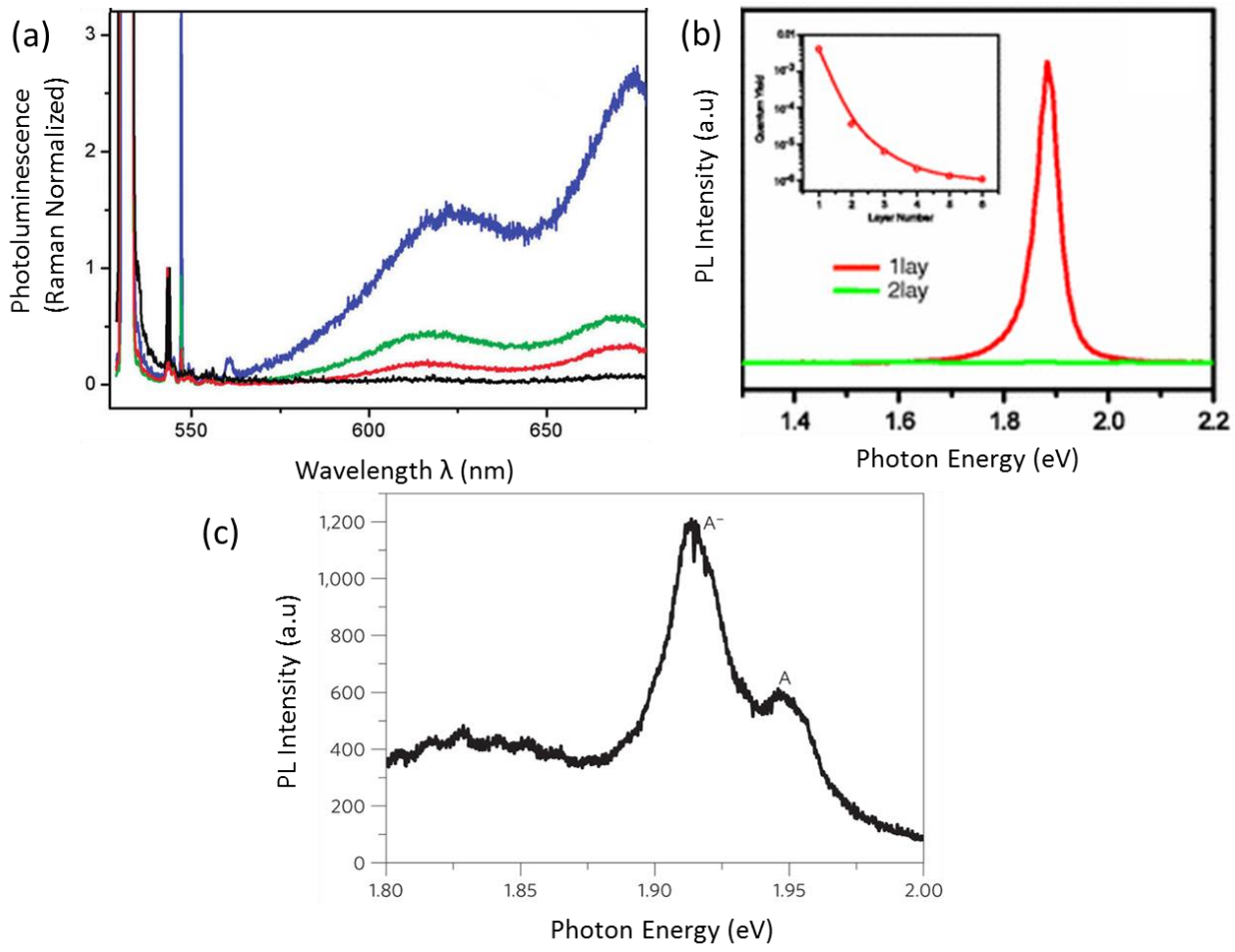

Figure 2.8 (a) Photoluminescence of monolayer (blue), bilayer (green), hexa-layer (red) and bulk (black)MoS_2 by splendiani et al[49] (b) photoluminescence of MoS_2 on suspended sample[50] (c) photoluminescence of MoS_2 at low temperature showing the trion peak[53].

2.2.3 Characterization of MoS_2

Before conducting any kind of optical and/or charge transport measurements on MoS_2, it is very important to accurately find out the number of layers in the flake in hand. Numerous techniques have been developed for characterizing of MoS_2 flake. Following are the few techniques that I have used in characterize MoS_2 flakes throughout my research.

2.2.3.1 Optical Contrast and Visibility of Flakes

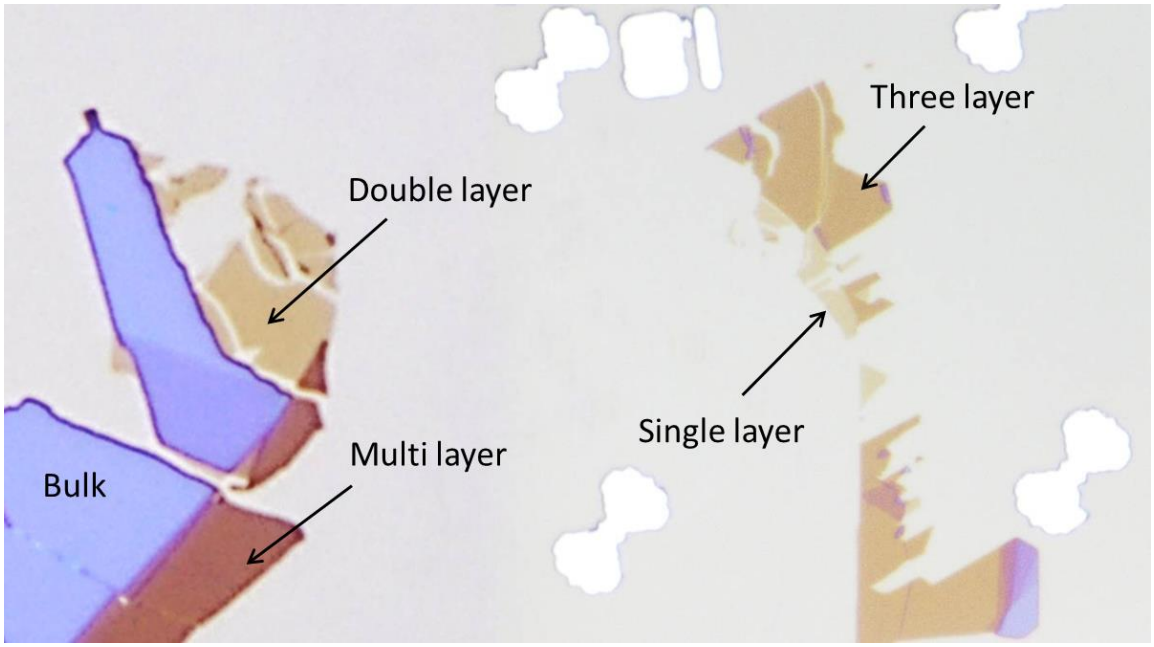

Figure 2.9 Optical image of mechanically exfoliated MoS_2 flakes on 250nm thick SiO_2 substrate. Different color contrast is indicative of the different thickness within the flake[55].

Thin sheets of MoS_2 are mostly transparent. However the optical contrast of MoS_2 flake on Si/SiO_2 substrate can be enhanced by choice of suitable thickness of the SiO_2 layer on the Si wafer. By choosing suitably thick substrate, the visibility of flake gets enhance due to constructive interference of light which is being reflected back from SiO_2 underneath[55-57]. According to Benameur et al. ~90nm and ~270nm thick SiO_2 substrate are best suited for identification of number of layers in MoS_2 flake by optical contrast method[58].

Figure 2.9 illustrate the optical image of mechanically exfoliated MoS_2 flake. The optical contrast has been used to estimate the thickness of flake to monolayer accuracy. In my

dissertation research, I have used the optical contrast as an initial indicator to estimate the number of layers in the flake.

2.2.3.2 Atomic Force Microscopy

AFM was developed by Binning et al. back in the year 1986. It is very powerful tool to measure nanometer heights and surface topography. Before AFM measurement, it is necessary to hot plate bake the flake at 100C for 2 hours. By doing so, we make sure that there are no adsorbed water molecules left on the surface of flake. The height of mono layer (ML) of MoS_2 is expected to be 0.65nm, however often time the ML height comes out to be slightly larger than 6.5nm. This slight increase in height can be because of different interaction of MoS_2 with substrate. The height should not increase more than 1.3nm in any case (for ML). In addition to height measurement, AFM is also very powerful tool for determining the surface topology, cleanliness and the surface roughness of the flakes.

2.2.3.3 Raman Spectra: Determination of Layer Thickness

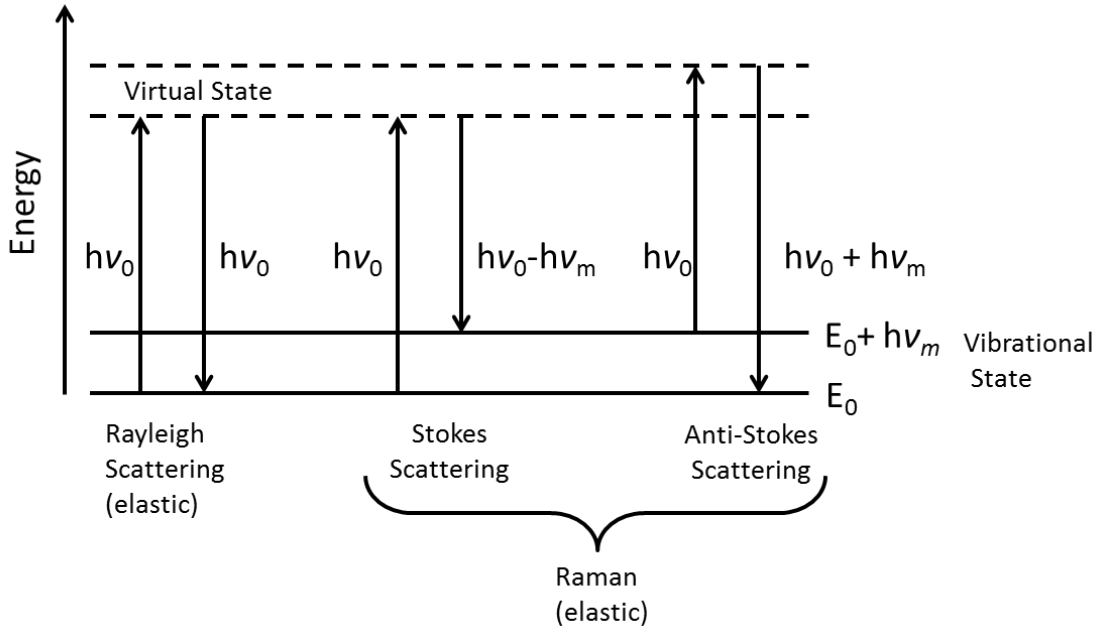

Figure 2.10 Energy level diagram for Rayleigh (elastic) and Raman (inelastic) scattering.

Characterization of MoS_2 by raman spectroscope is based upon Raman effect. When the sample is irritated by lase of a particular wave length, some of the light gets absorbed by the sample and results in heating of sample or reemitted and some of the light gets scattered. A small portion of scattered light is scattered at a wavelength either higher or lower than the incident light as shown in figure 2.10. This inelastically scattered light (called raman scattering) carries information with it about the material from which it is being inelastically scattered. If the inelastically scatterd light have wavelength smaller than the incident light, it is called Stokes scattering whereas if the inelastically scattered light have wavelength larger than incident light, it is called Anti-Stokes scattering. The difference between the wavelengths of irradiated light and inelastically scattered light provides information about the vibrations modes of the material.

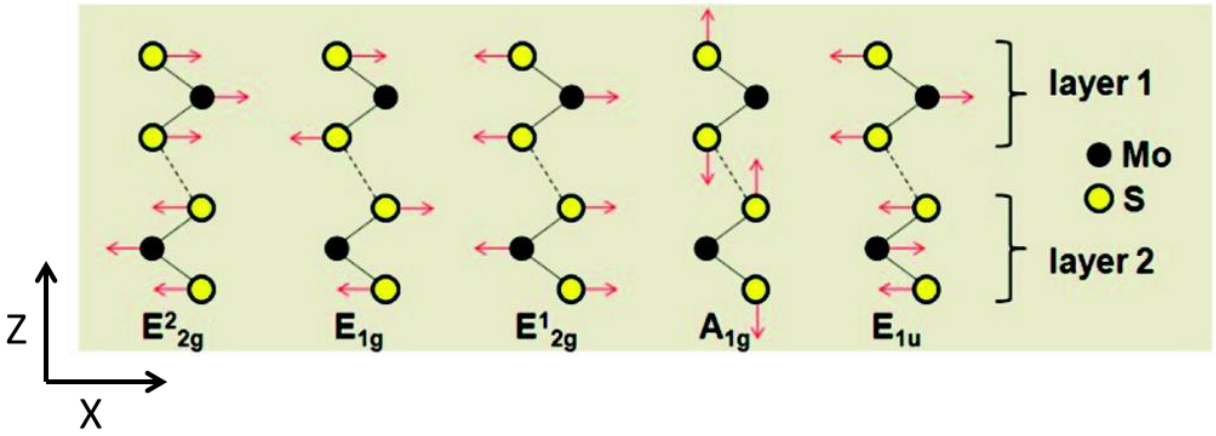

Figure 2.11 Atomic displacements of the four Raman-active modes and one IR-active mode (E_{1u}) in the unit cell of the bulk MoS_2 crystal as viewed along the [1000] direction[59].

Figure 2.12 illustrates the vibrational modes of MoS_2. Among all these modes, E^1_{2g} and A_{1g} modes are the strongest one. Detection of E_{1g} and E^2_{2g} mode cannot be done due to selection rule. The last E_{1u} mode is not a Raman active mode[59], hence cannot be detected.

These vibrational modes are often called as fingerprints of a material. In case of MoS_2, Thickness of atomically thin flakes of 2D sheet can be accurately determined by studying all the raman active modes by Raman spectroscopy[59,60]. Figure 2.12a illustrates the Raman spectra of thin (nL) and bulk MoS_2 flake taken by Lee et al. There are two prominent peaks (originating from raman active modes) present in the spectrum. It has been found that as the number of layers in the flake increase, the position of these two peaks also changes correspondingly. The change in position of these is two prominent signature modes of vibrations called E^1_{2g} and A_{1g} can be accurately correlated to the thickness of the flake. In ML MoS_2 the strong in plane vibration mode (E^1_{2g}) is found to be at 384 cm^{-1} and a strong out of plane mode (A_{1g}) is found at 303cm^{-1}. The difference in position ($\Delta\omega$) of these two modes of is related to the distinctive behavior which

can be related to the thickness of the flake. Therefore $\Delta\omega = 19cm^{-1}$ corresponds to single layer flake. In igure 2.12a the change in peak position can be clearly seen. Figure 2.12b quantitatively relates the change in peak position to the number of layers in the flake.

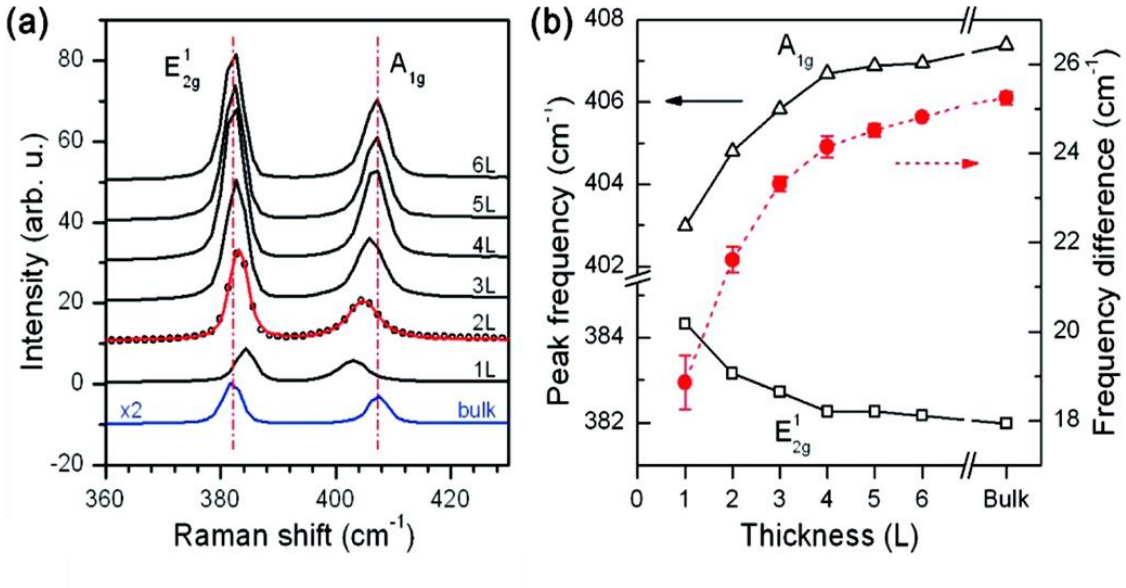

Figure 2.12 (a) Raman spectra of thin (nL) and bulk MoS_2 films. (b) Frequencies of E_{2g} and A_{1g} Raman modes (left vertical axis) and their difference (right vertical axis) as a function of layer thickness[59].

2.3 FET Device Structure and Characteristics

Field effect transistors are the fundamental building block of modern electronics. MOSFETs are currently most prevalent used design. A MOSFET is a three terminal device named Source (S), Drain (D) and Gate (G). Figure 2.13 illustrates the schematic diagram of n-type MOSFET. A bias voltage is applied at two terminals of MOSFET and a third terminal is used to control the flow of current through it. Gate terminal is responsible in establishing a channel of majority careers connecting the S and D by field effect mechanism. In conventional MOSFETs, the channel material is same as substrate (ie. Si). However in case of 2D FETs, the

active material which act as channel is the 2D materials itself and not the semiconducting substrate. Rest of the design and working principle remains same.

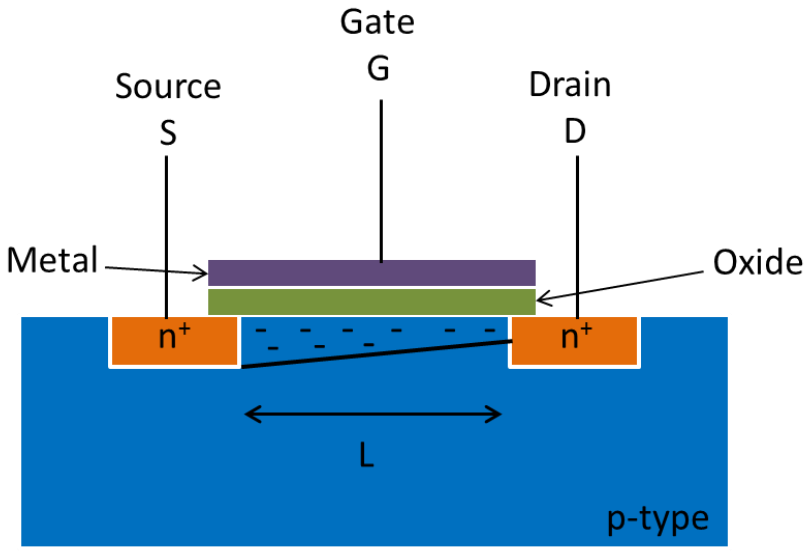

Figure 2.13 Schematic of metal oxide semiconductor field effect transistor (MOSFET).

2.3.1 MoS_2 Field Effect Transistor

In this section I will review the basics of MoS_2 field effect transistors, which will lay the background for the results mainly discussed in chapter 5 & 6. The first MoS_2 field effect transistors were reported by Radisavljevic et. al in 2011 using top gate geometry as shown in figure 2.14a. A monolayer of MoS_2 was contacted between two Au metal electrodes called source and drain. The monolayer was capacitively coupled by a third top electrode called gate which control the flow of current between source and drain similar to standard metal oxide field effect transistor. A 30 nm thick HfO_2 was used as dielectric layer.

Figure 2.14b illustrates a representative plot of the conductance as a function of gate voltage for an n-type MoS_2 device. The MoS_2 conducts well at high positive gate voltages and shuts off at high negative gate voltages. The gate voltage where the MoS_2 shuts off is known as the threshold voltage (V_{th}).

From the current versus gate voltage curve (i.e. transfer characteristics) one can characterize the performance of a device by extraction of several parameters. One such parameter is transconductance,

$$g = \frac{dI_{DS}}{dV_G} \tag{2.1}$$

which is proportional to the capacitance between the MoS_2 and the gate. From the transconductance we can calculate the field effect mobility using the following formula:

$$\mu = \frac{dI_{DS}}{dV_G} \frac{L}{WC_iV_{DS}} \tag{2.2}$$

Where C_i is the capacitance per unit area, L, W are channel length and channel width respectively, V_{DS} is drain to source voltage. Gate capacitance is given by

$$C = \frac{kA\varepsilon_0}{d} \tag{2.3}$$

A very important parameter for MoS_2 Field effect transistor is the subthreshold slope, which is measured by

$$S = \frac{dV}{d(\log(I))}. \tag{2.4}$$

can also be measured from the current vs gate voltage plot. The subthreshold slope (in units of mV/decade) basically determines the amount of voltage needed to change the current by an order of. For low power and fast FET operation, a small values of the subthreshold swing and low threshold voltage is desired[61].

2.3.2 Electronic Properties of MoS_2

Figure 2.14b illustrates the current voltage characteristics of a typical MoS_2 transistor. It is clear from the figure that at negative applied gate voltage, the drain current is zero. Such a state in FET is depletion mode. As we increases the gate voltage, a positive current starts for flow between source to drain and it increases with the gate voltage until it reaches saturation. This is a signature of typical n-type semiconductor material. The carrier mobility of MoS_2 was found to be ~ 200 cm^2/Vs[12,55]. Whereas the mobility for duel gate multilayer MoS_2 transistor was found to be 517 cm^2/Vs[56]. An on/off ratio of MoS_2 transistor up to 10^8 has been reported by Radisavljevic et al[12].

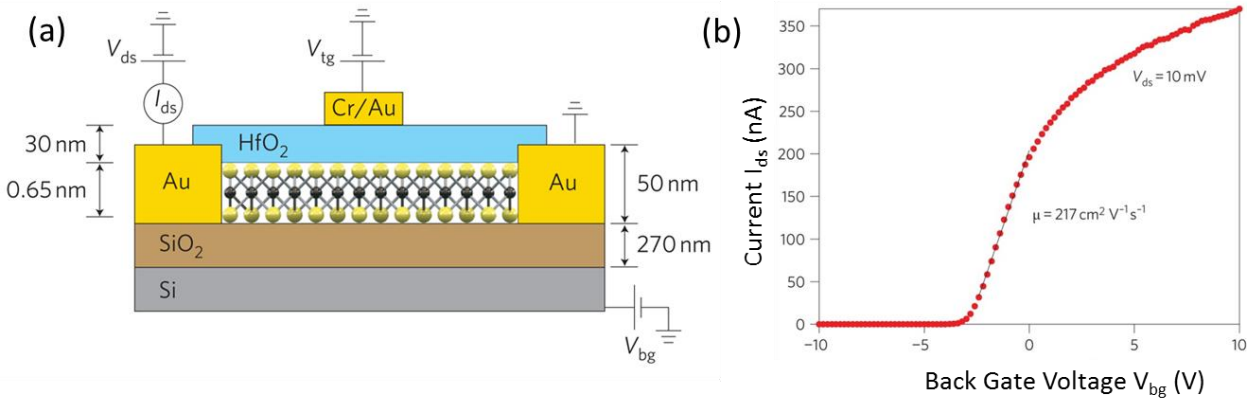

Figure 2.14 Side view of a MoS_2 field effect transistor. The MoS_2 flake is contacted by source and drain electrodes on each side to apply a source drain bias to and a conducting gate electrode is separated by a thin layer of dielectric (HfO_2) (b) Typical conductance versus gate voltage curve showing an increase in current at positive gate bias indicating n-type transport by Radisavljevic et al.[12].

2.4 References

1 Ganatra, R. & Zhang, Q. Few-Layer MoS_2: A Promising Layered Semiconductor. *ACS Nano* **8**, 4074-4099, (2014).

2 Geim, A. K. Graphene: Status and Prospects. *Science* **324**, 1530-1534, (2009).

3 Geim, A. K. & Novoselov, K. S. The rise of graphene. *Nat Mater* **6**, 183-191 (2007).

4 Larentis, S., Fallahazad, B. & Tutuc, E. Field-effect transistors and intrinsic mobility in ultra-thin $MoSe_2$ layers. *Applied Physics Letters* **101**, 223104, (2012).

5 Late, D. J. *et al.* Sensing Behavior of Atomically Thin-Layered MoS_2 Transistors. *ACS Nano* **7**, 4879-4891, (2013).

6 Lee, C., Wei, X., Kysar, J. W. & Hone, J. Measurement of the Elastic Properties and Intrinsic Strength of Monolayer Graphene. *Science* **321**, 385-388, (2008).

7 Liu, M. *et al.* A graphene-based broadband optical modulator. *Nature* **474**, 64-67 (2011).

8 Mueller, T., Xia, F. & Avouris, P. Graphene photodetectors for high-speed optical communications. *Nat Photon* **4**, 297-301, (2010).

9 Novoselov, K. S. *et al.* A roadmap for graphene. *Nature* **490**, 192-200 (2012).

10 Ovchinnikov, D., Allain, A., Huang, Y.-S., Dumcenco, D. & Kis, A. Electrical Transport Properties of Single-Layer WS_2. *ACS Nano* **8**, 8174-8181, (2014).

11 Perkins, F. K. *et al.* Chemical Vapor Sensing with Monolayer MoS_2. *Nano Letters* **13**, 668-673, (2013).

12 RadisavljevicB, RadenovicA, BrivioJ, GiacomettiV & KisA. Single-layer MoS_2 transistors. *Nat Nano* **6**, 147-150, (2011).

13 Sanchez, V. C., Jachak, A., Hurt, R. H. & Kane, A. B. Biological Interactions of Graphene-Family Nanomaterials: An Interdisciplinary Review. *Chemical Research in Toxicology* **25**, 15-34, (2011).

14 Schwierz, F. Graphene transistors. *Nat Nano* **5**, 487-496 (2010).

15 Stampfer, C. *et al.* Tunable Graphene Single Electron Transistor. *Nano Letters* **8**, 2378-2383, (2008).

16 Xia, F., Mueller, T., Lin, Y.-m., Valdes-Garcia, A. & Avouris, P. Ultrafast graphene photodetector. *Nat Nano* **4**, 839-843, (2009).

17 Xu, M., Liang, T., Shi, M. & Chen, H. Graphene-Like Two-Dimensional Materials. *Chemical Reviews* **113**, 3766-3798, (2013).

18 Yoo, E. *et al.* Enhanced Electrocatalytic Activity of Pt Subnanoclusters on Graphene Nanosheet Surface. *Nano Letters* **9**, 2255-2259, (2009).

19 Morishita, T. *et al.* First-principles study of structural and electronic properties of ultrathin silicon nanosheets. *Physical Review B* **82**, 045419 (2010).

20 Spencer, M. J. S., Morishita, T. & Snook, I. K. Reconstruction and electronic properties of silicon nanosheets as a function of thickness. *Nanoscale* **4**, 2906-2913, (2012).

21 Garcia, J. C., de Lima, D. B., Assali, L. V. C. & Justo, J. F. Group IV Graphene- and Graphane-Like Nanosheets. *The Journal of Physical Chemistry C* **115**, 13242-13246, (2011).

22 De Padova, P. *et al.* Evidence of graphene-like electronic signature in silicene nanoribbons. *Applied Physics Letters* **96**, 261905, (2010).

23 Cahangirov, S., Topsakal, M., Aktürk, E., Şahin, H. & Ciraci, S. Two- and One-Dimensional Honeycomb Structures of Silicon and Germanium. *Physical Review Letters* **102**, 236804 (2009).

24 Ding, Y. & Ni, J. Electronic structures of silicon nanoribbons. *Applied Physics Letters* **95**, 083115, (2009).

25 Wang, Q. H., Kalantar-Zadeh, K., Kis, A., Coleman, J. N. & Strano, M. S. Electronics and optoelectronics of two-dimensional transition metal dichalcogenides. *Nat Nano* **7**, 699-712 (2012).

26 Yin, Z. *et al.* Single-Layer MoS_2 Phototransistors. *ACS Nano* **6**, 74-80, (2011).

27 Wang, H. *et al.* Integrated Circuits Based on Bilayer MoS_2 Transistors. *Nano Letters* **12**, 4674-4680, (2012).

28 Radisavljevic, B., Whitwick, M. B. & Kis, A. Integrated Circuits and Logic Operations Based on Single-Layer MoS_2. *ACS Nano* **5**, 9934-9938, (2011).

29 Lopez-Sanchez, O., Lembke, D., Kayci, M., Radenovic, A. & Kis, A. Ultrasensitive photodetectors based on monolayer MoS_2. *Nat Nano* **8**, 497-501, (2013).

30 Lee, H. S. *et al.* MoS_2 Nanosheet Phototransistors with Thickness-Modulated Optical Energy Gap. *Nano Letters* **12**, 3695-3700, (2012).

31 Bernardi, M., Palummo, M. & Grossman, J. C. Extraordinary Sunlight Absorption and One Nanometer Thick Photovoltaics Using Two-Dimensional Monolayer Materials. *Nano Letters* **13**, 3664-3670, (2013).

32 Baugher, B. W. H., Churchill, H. O. H., Yang, Y. & Jarillo-Herrero, P. Optoelectronic devices based on electrically tunable p-n diodes in a monolayer dichalcogenide. *Nat Nano* **9**, 262-267, (2014).

33 Yu, W. J. *et al.* Highly efficient gate-tunable photocurrent generation in vertical heterostructures of layered materials. *Nat Nano* **8**, 952-958, (2013).

34 Tongay, S. *et al.* Broad-Range Modulation of Light Emission in Two-Dimensional Semiconductors by Molecular Physisorption Gating. *Nano Letters* **13**, 2831-2836, (2013).

35 Chen, Y. *et al.* Tunable Band Gap Photoluminescence from Atomically Thin Transition-Metal Dichalcogenide Alloys. *ACS Nano* **7**, 4610-4616, (2013).

36 Novoselov, K. S. *et al.* Two-dimensional atomic crystals. *Proceedings of the National Academy of Sciences of the United States of America* **102**, 10451-10453, (2005).

37 Frindt, R. F. Single Crystals of MoS_2 Several Molecular Layers Thick. *Journal of Applied Physics* **37**, 1928-1929, (1966).

38 Fivaz, R. & Mooser, E. Mobility of Charge Carriers in Semiconducting Layer Structures. *Physical Review* **163**, 743-755 (1967).

39 Mattheiss, L. F. Band Structures of Transition-Metal-Dichalcogenide Layer Compounds. *Physical Review B* **8**, 3719-3740 (1973).

40 Mattheiss, L. F. Energy Bands for 2H-$NbSe_2$ and 2H-MoS_2. *Physical Review Letters* **30**, 784-787 (1973).

41 Kasowski, R. V. Band Structure of MoS_2 and NbS_2. *Physical Review Letters* **30**, 1175-1178 (1973).

42 Joensen, P., Frindt, R. F. & Morrison, S. R. Single-layer MoS_2. *Materials Research Bulletin* **21**, 457-461, (1986).

43 Miremadi, B. K., Cowan, T. & Morrison, S. R. New structures from exfoliated MoS_2. *Journal of Applied Physics* **69**, 6373-6379, (1991).

44 Wypych, F. & Schollhorn, R. 1T-MoS_2, a new metallic modification of molybdenum disulfide. *Journal of the Chemical Society, Chemical Communications*, 1386-1388, (1992).

45 Byskov, L. S., Hammer, B., Nørskov, J. K., Clausen, B. S. & Topsøe, H. Sulfur bonding in MoS_2 and Co-Mo-S structures. *Catalysis Letters* **47**, 177-182, (1997).

46 Wypych, F., Weber, T. & Prins, R. Scanning Tunneling Microscopic Investigation of 1T-MoS_2. *Chemistry of Materials* **10**, 723-727, (1998).

47 Böker, T. *et al.* Band structure of MoS_2, $MoSe_2$, and $MoTe_2$: Angle-resolved photoelectron spectroscopy and ab initio calculations. *Physical Review B* **64**, 235305 (2001).

48 Lauritsen, J. V. *et al.* Size-dependent structure of MoS_2 nanocrystals. *Nat Nano* **2**, 53-58 (2007).

49 Splendiani, A. *et al.* Emerging Photoluminescence in Monolayer MoS_2. *Nano Letters* **10**, 1271-1275, (2010).

50 Mak, K. F., Lee, C., Hone, J., Shan, J. & Heinz, T. F. Atomically Thin MoS_2: A New Direct-Gap Semiconductor. *Physical Review Letters* **105**, 136805 (2010).

51 Eda, G. *et al.* Photoluminescence from Chemically Exfoliated MoS_2. *Nano Letters* **11**, 5111-5116, (2011).

52 Ji, Q. *et al.* Epitaxial Monolayer MoS_2 on Mica with Novel Photoluminescence. *Nano Letters* **13**, 3870-3877, (2013).

53 Mak, K. F. *et al.* Tightly bound trions in monolayer MoS_2. *Nat Mater* **12**, 207-211, (2013).

54 Mouri, S., Miyauchi, Y. & Matsuda, K. Tunable Photoluminescence of Monolayer MoS_2 via Chemical Doping. *Nano Letters* **13**, 5944-5948, (2013).

55 Optical identification of atomically thin dichalcogenide crystals. *Applied Physics Letters* **96**, 213116 (2010).

56 Wang, Y. Y. *et al.* Thickness identification of two-dimensional materials by optical imaging. *Nanotechnology* **23**, (2012).

57 Shaharin Fadzli Abd, R., Abdul Manaf, H. & Seiya, K. Identification of Graphene Layer Numbers from Color Combination Contrast Image for Wide-Area Characterization. *Japanese Journal of Applied Physics* **51**, (2012).

58 Benameur, M. M. *et al.* Visibility of dichalcogenide nanolayers. *Nanotechnology* **22**, (2011).

59 Lee, C. *et al.* Anomalous Lattice Vibrations of Single- and Few-Layer MoS_2. *ACS Nano* **4**, 2695-2700, (2010).

60 Castellanos-Gomez, A. *et al.* Fast and reliable identification of atomically thin layers of $TaSe_2$ crystals. *Nano Res.* **6**, 191-199, (2013).

61 Krasnozhon, D., Lembke, D., Nyffeler, C., Leblebici, Y. & Kis, A. MoS_2 Transistors Operating at Gigahertz Frequencies. *Nano Letters* **14**, 5905-5911, (2014).

62 Kaasbjerg, K., Thygesen, K. S. & Jacobsen, K. W. Phonon-limited mobility in n-type single-layer MoS_2 from first principles. *Physical Review B* **85**, 115317 (2012).

63 Liu, H. & Ye, P. D. MoS_2 Dual-Gate MOSFET With Atomic-Layer-Deposited Al_2O_3 as Top-Gate Dielectric. *Electron Device Letters, IEEE* **33**, 546-548, (2012).

64 Yoon, Y., Ganapathi, K. & Salahuddin, S. How Good Can Monolayer MoS_2 Transistors Be? *Nano Letters* **11**, 3768-3773, (2011).

CHAPTER 3: METHODS, DEVICE FABRICATION AND EXPERIMENTAL SETUP

3.1 Introduction

To get nice, clean flakes and reproducible data, the optimization of exfoliation process, and fabrication steps play very significant role. Here in this chapter first I shall explain in details my method of mechanical exfoliation for obtaining single and few layers MoS_2.

The second most crucial part in my research is the device fabrication. A lot of efforts have been given to fabricate cleaner devices. It involves many steps as shown in flow chart in figure 3.1. Later in this chapter I shall discuss all the device fabrication steps and the parameter to be considered during fabrication process in chronological order. Fabrication includes starting from cleaning the substrate, cleaning the exfoliated flake and defining electrodes by both photolithography and electron beam lithography and deposition of Au electrodes.

After exfoliation and identification of flake thickness, the photoluminescence of pristine and Au decorated MoS_2 was studied. Photoluminescence data is presented in Chapter 4 in this dissertation. In the end, after the device fabrication the last part is measurement of electrical transport properties. In the end of this chapter, I have discuss the experimental setup for all of my electrical measurements, low temperature measurements, optical measurement and topological and height measurement of the flakes. The electrical measurement data is presented in chapter 5 and chapter 6 of this dissertation.

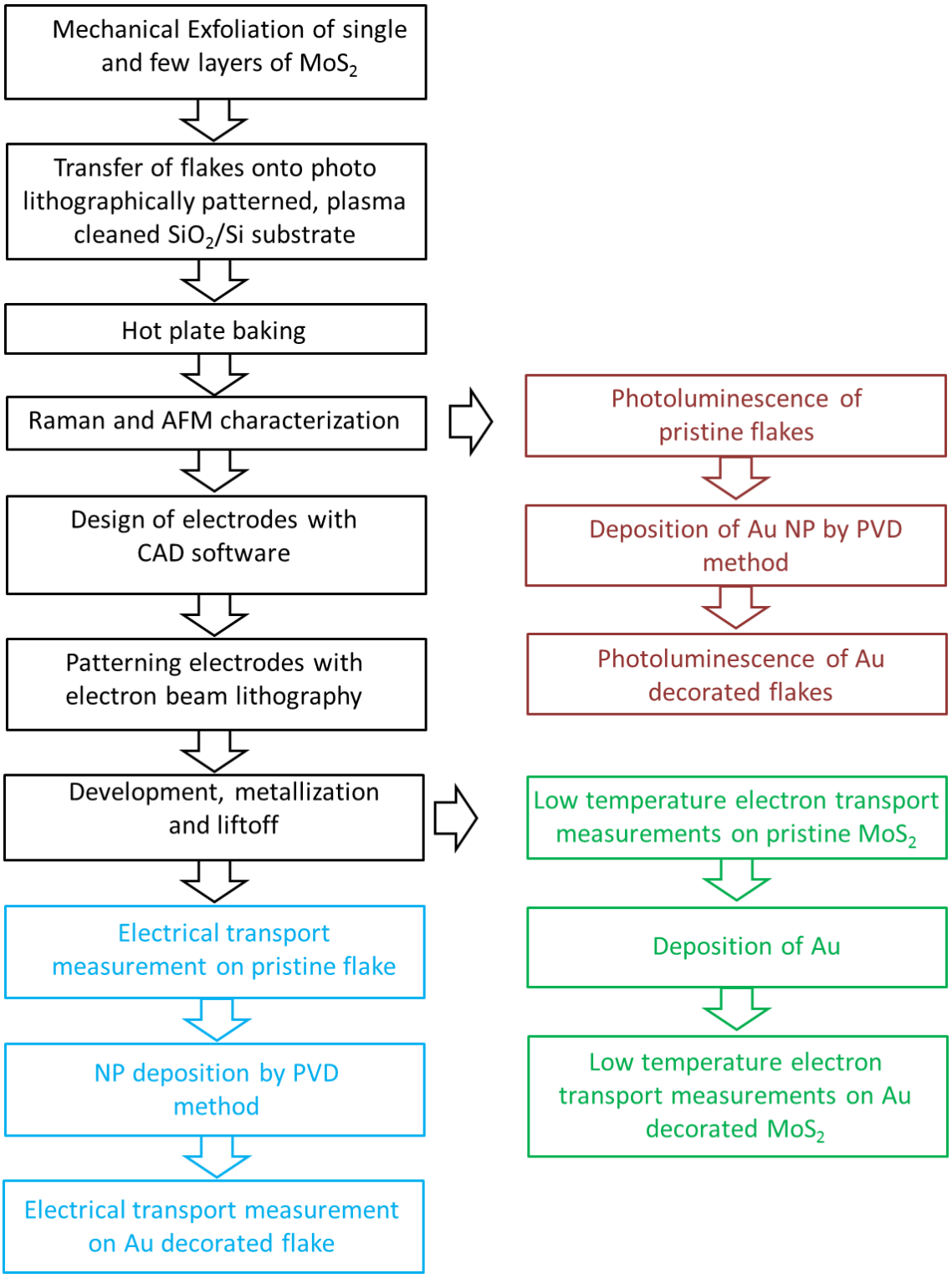

Figure 3.1 Flow-chart for experimental procedures.

3.2 Design of Markers

A prerequisite for any kind of study on exfoliated MoS_2 flake is that we should be able to locate the position of exfoliated flake on the substrate. The need for accurately locating the position of MoS_2 becomes more urgent when we want to fabricate FET device, because with any few hundred nanometers offset in electron beam writing pattern we might end up with a bad device or no device at all (in case we completely miss the flake during lithography process due to offset). The shape of the markers can help in minimizing the offset during lithography. Hence the design of markers becomes very important. Figure 3.2 illustrate the design of my markers which were patterened over the entire 3 inch wafer used for mechanical exfoliation and device fabrication.

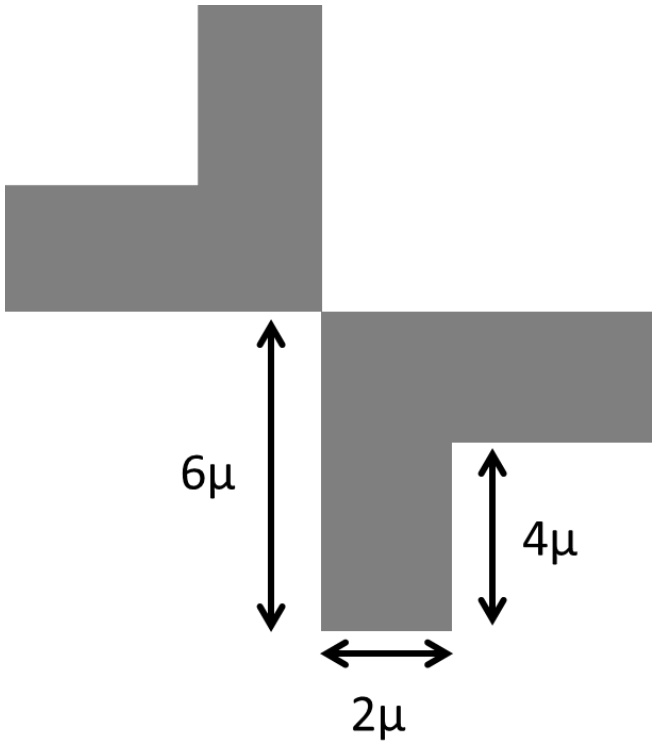

Figure 3.2 Schematic design of markers made by photolithography on 3 inch wafer used for mechanical exfoliation and device making.

The markers were separated by 50µm distance from each other. The distance between two markers was kept 50µm so that the optical microscope which has field of view (100X lens) of about 75µm can take an image of at least 4 markers in one picture. These four markers then later help us to accurately locate the position of the flake on the wafer. Figure 3.3 illustrates the design of 3 inch optical mask. The actual image of the markers at different magnifications is shown in figure 3.4.

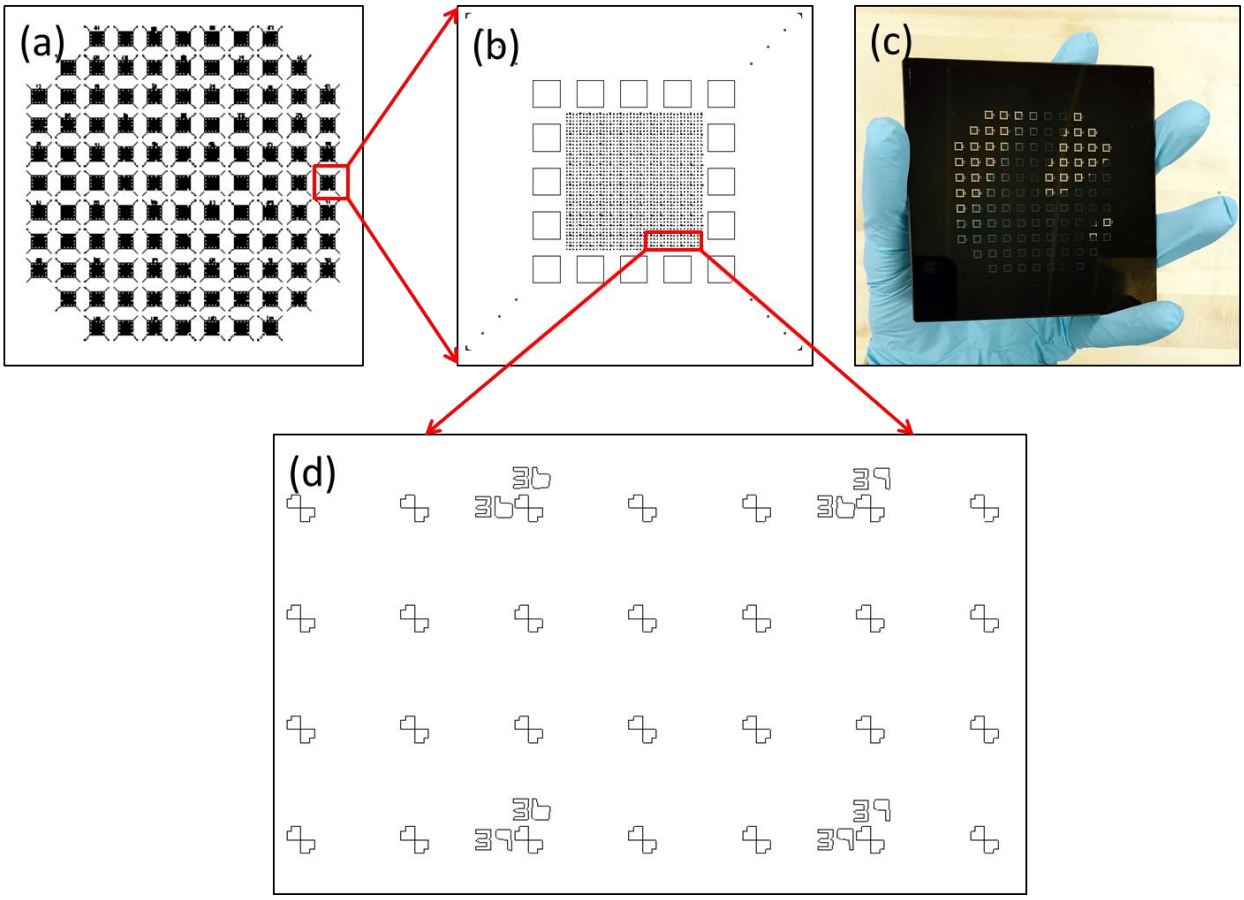

Figure 3.3 (a) 3 inch mask design (b) zoomed in image of portion of mask (c) actual image of our own photo mask.

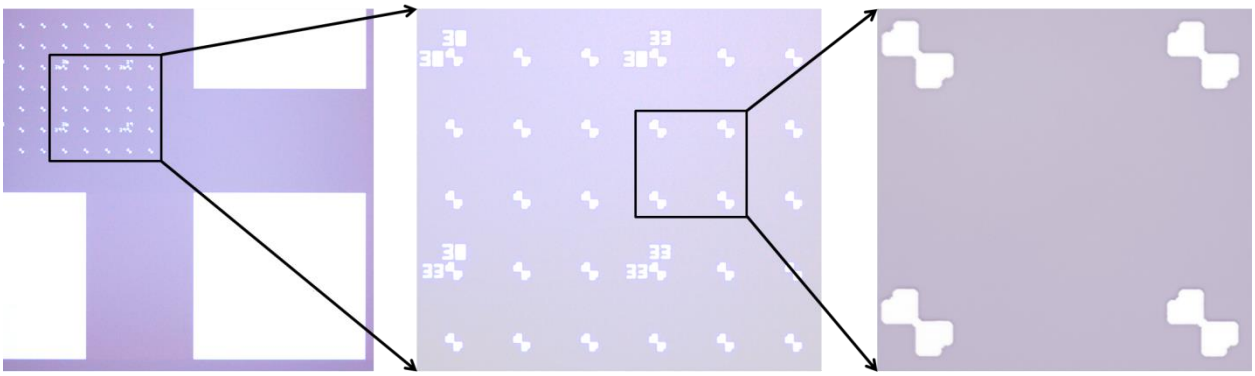

Figure 3.4 Optical images of markers at 10X, 50X and 100X magnifications.

3.3 Exfoliation of Single Layer and Multilayers MoS_2 Flakes

After the Noveselov et al who first mechanically exfoliated 2D materials (graphene, transition metal dichalcogenides)[1] and received a Nobel prize for their research on 2D materials, many other methods have been devised for synthesis of single layer and few layer of 2D materials. Chemical exfoliation, Chemical vapor deposition, epitaxial growth, chemical bath deposition and spray pyrolysis are few other methods by which single and few layers of 2D materials can be synthesized[2-10]. Among all these methods I chose mechanical exfoliation method (also known as scotch tape method) because for the fundamental study it serves our purpose well. Figure 3.6 illustrates the schematic diagram of mechanical exfoliation process.

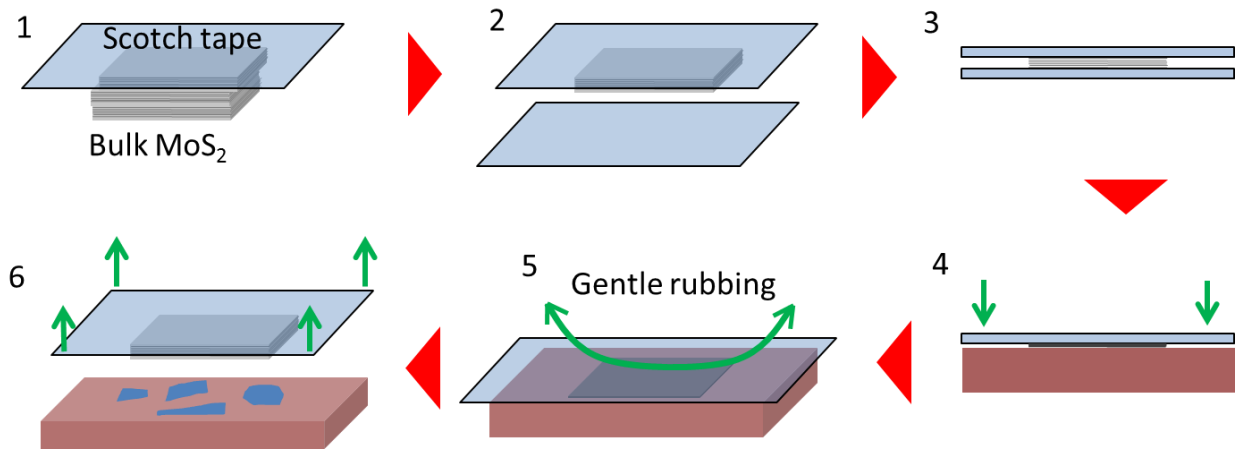

Figure 3.5 Mechanical Exfoliation process: (1) multiple layers peel off from bulk MoS_2 by scotch tape(2, 3) thinning down bulk MoS_2 to few layer (4) place the scotch tape onto pre patterned substrate (5) Evenly gentle rubbing on scotch tape with sponge (6) lift off scotch tape from the substrate.

Following are the steps for mechanical exfoliation:

1. Start from bulk single crystal of MoS_2 commercially available from SPI (SPI Supplies Brand, Natural Molybdenite) supply. Gently place the sticky side of scotch tape over bulk MoS_2 crystal and apply a very gentle pressure with the thumb. The purpose of gentle pressure is to make sure if there is any air trapped between bulk MoS_2 crystal and scotch tape, it will go away.
2. Peel off the scotch tape very slowly. Now flip scotch tape (sticky side up) over and gently lay down the opposite end of scotch (sticky side) over the just exfoliated layers of MoS_2 (from bulk).
3. Repeat this process for 4 to 5 times until the bulk crystal becomes very thin.
4. Now take a second piece of scotch tape, press it gently against the first piece of tape (facing sticky side each other) and slowly peel off again.

5. Now take the second piece of scotch tape and lay it over cleaned SiO_2/Si substrate. Again apply gentle pressure; slightly rub by sponge to get rid of any air trapped in between scotch tape and substrate.
6. Again peel off the scotch tape at a very slow rate about 1mm/sec and at very small peeling off angle generally less than 45 degrees.
7. Scan the sample under optical microscope to find out the single and multiple layers MoS_2 flakes.

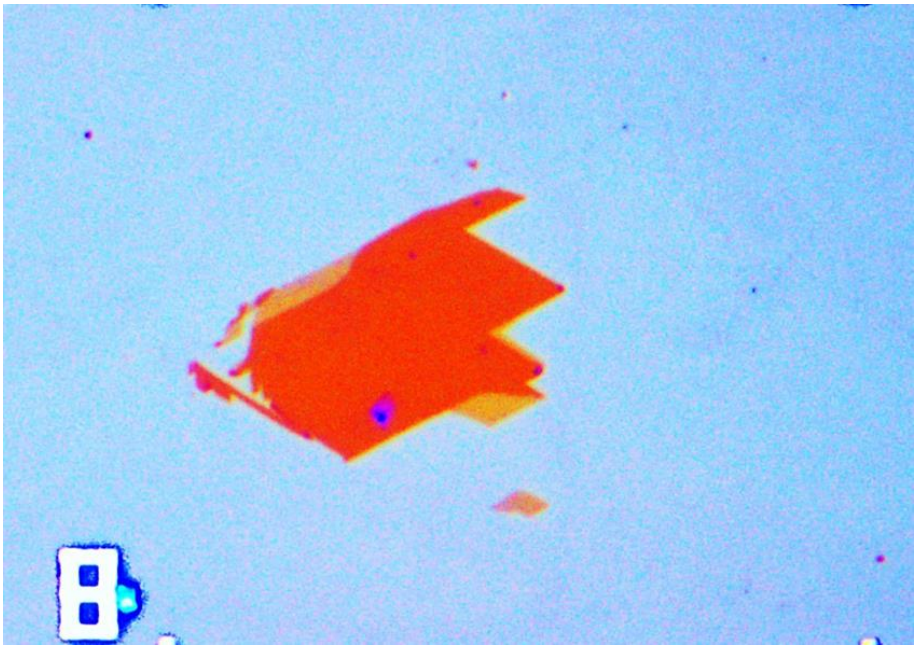

Figure 3.6 Optical image of mechanically exfoliated MoS_2 flake by method described above.

3.4 Deposition of Au NP

Figure 3.7 Actual image of thermal/e-beam evaporator used for deposition of Au NPs on flakes.

After exfoliating the MoS_2 flakes, all the samples were hot plate baked in order to ensure that the top surface of flake is cleans from any sticky residue that might be present during mechanical exfoliating. The hot baking was done at 100C for an hour. A usual practice is, after the hot plate backing, we do the AFM measurement. It benefits in two fold, giving information about the number of layers in the flake and also tell us about the cleanliness and roughness of the top surface of the flake. More details about AFM can be found in section 3.6.2. The Au was evaporated in the chamber shown in figure 3.7. This evaporator can be run in thermal or e-beam modes. The evaporator chamber is connected by rotary pump backed by turbo molecular pump.

It has already been proved that by depositing noble metal by PVD method on a substrate at a very slow rate up to few nm thick, a well dispersed NP can be formed over the surface. This method of producing NP on the surface has already been demonstrated on graphene and CNT[11-13]. Here in this study the Au metal was evaporated at a base pressure of 10-6 torr to form NP on the surface of MoS_2. The rate of deposition was kept constant at 0.01Å/sec.

First of all, we have tested the formation the Au NP on SiO_2/Si substrate only. The AFM images illustrated in Figure 3.9 (a), (b) and (c) confirm the formation of NP on SiO_2/Si substrate. From AFM measurements, the average lateral size of NP was found to be 19nm. The average height was found to be 1.7nm for 2nm deposition of Au.

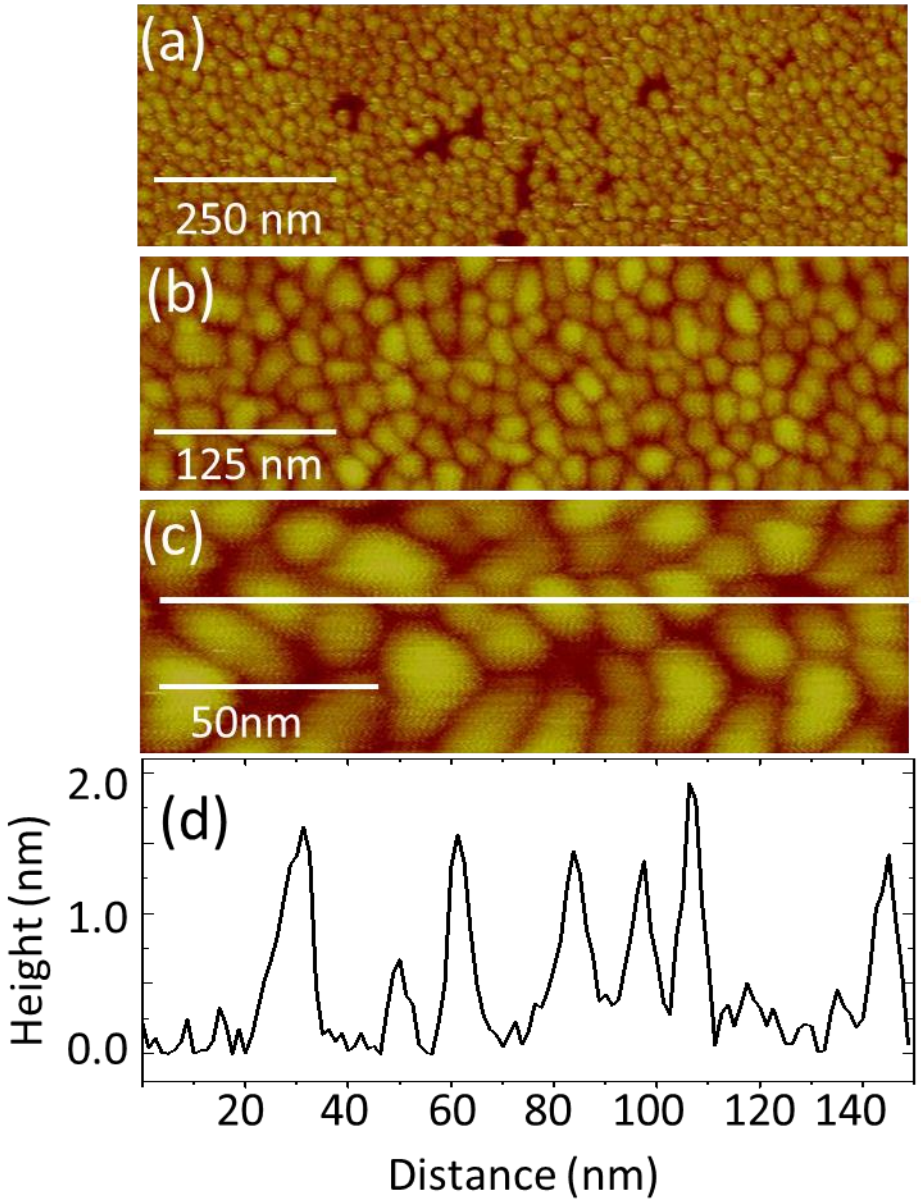

Figure 3.8 (a) AFM image of Au NPs on SiO_2/Si Substrate. (b), (c) high resolution images of the same sample. (d) height profile of NPs along white line shown in figure.

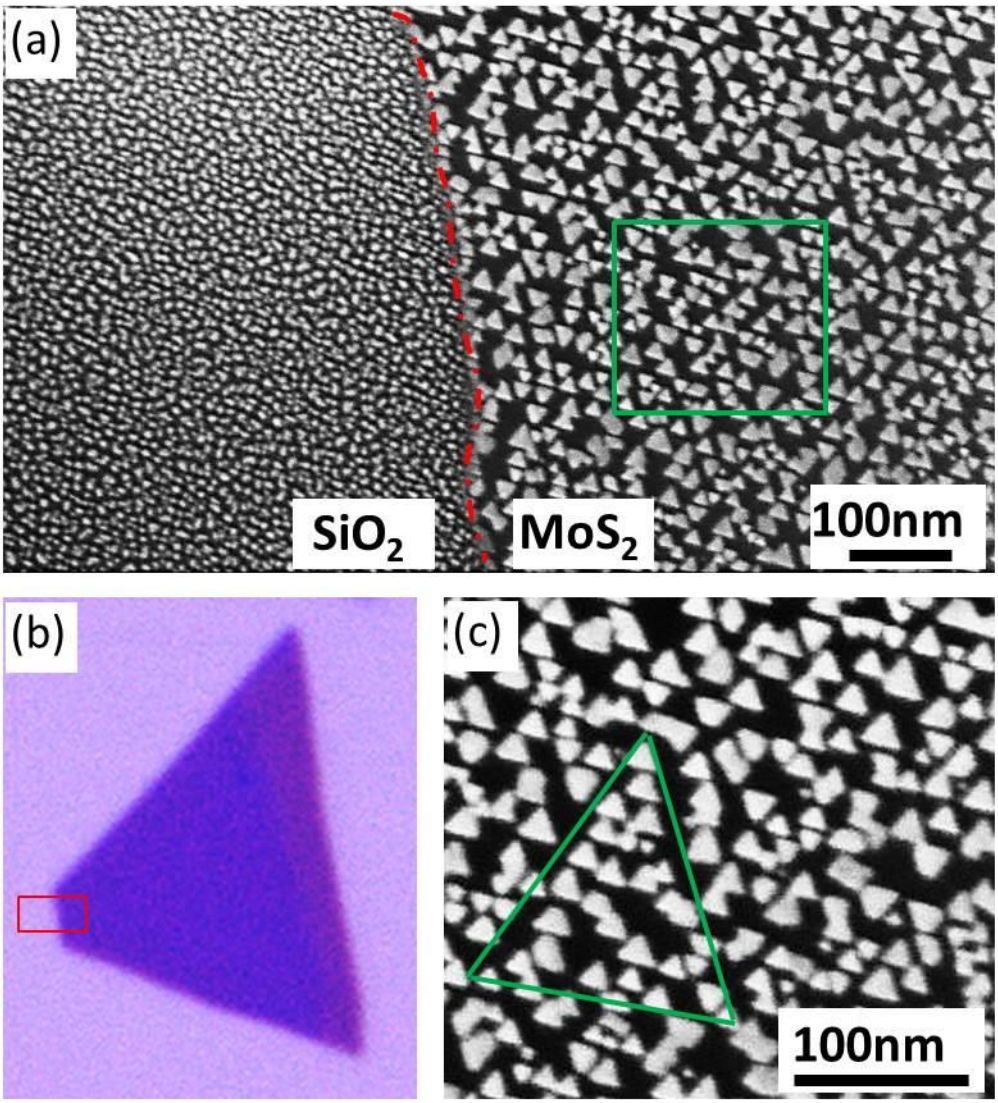

Figure 3.9 Au NP formation resulted from 1nm thickness on sample by thermal deposition. (a) SEM image of NPs on MoS_2. The dotted red line represents the edge of the flake (b) the optical image of pristine MoS_2 flake.(c) The high resolution image of the region boxed green in (a).

Later we evaporated the Au on pristine MoS_2 flake. The results are illustrated in figure 3.9. Figure 3.9a illustrates the SEM image of a flake after 1nm thickness of Au. The SEM image was purposefully take at the edge of the flake so that a clear difference in the shape of NPs can

be seen on SiO_2/Si and MoS_2 flake. The red dotted line serves the guide to the eye to represent the edge of MoS_2 flake. Well separated Au NPs with no particular shape can be seen on SiO_2 substrate whereas the NPs on MoS_2 are triangular in shape. The difference in shape of NPs originates from different wettability of the underneath surface (substrate).

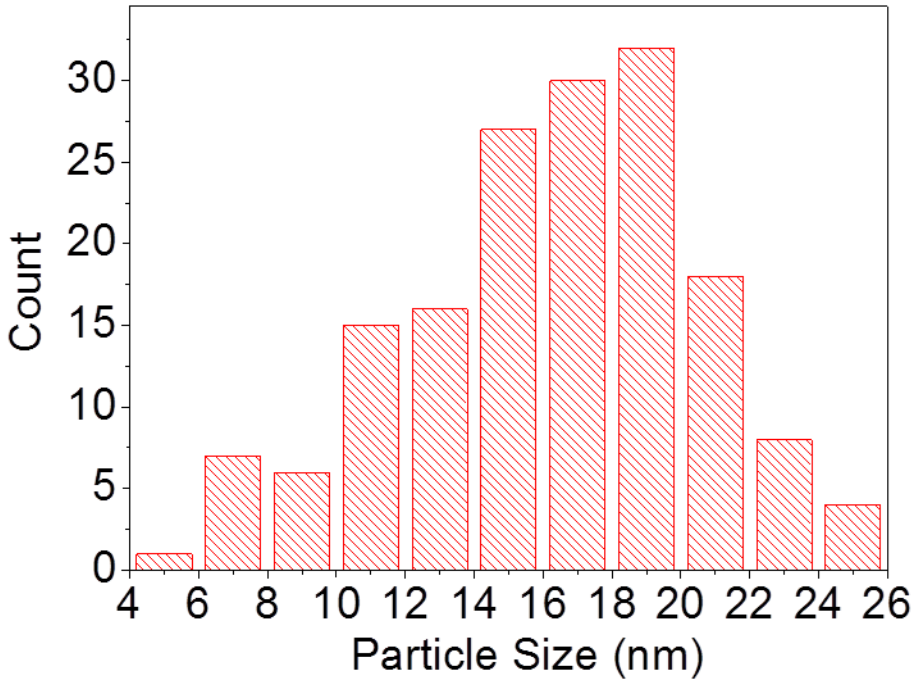

Figure 3.10 Size distribution of triangular Au NP on MoS_2 formed by thermal evaporation.

The lateral size of NPs was measure along the altitudinal direction of the equilateral triangle and a histogram of size distribution of NPs on MoS_2 is shown in figure 3.10. The lateral size of triangular NP varies from 5 nm to 25 nm. 70% of the total NPs lie in the range of 12-20 nm lateral size. The presences of different size of NPs suggest that the nucleation of new NPs and growth of old NPs is occurring at same time.

3.5 Fabrication of Electrodes

Electrodes were fabricated by both photo and electron beam lithography. Photo lithography was used to fabricate the large contact pads on the substrate. And later, electron beam lithography was used to fabricate the electrodes for contacting MoS_2 flake with the large contact pads. The electrodes were first designed using CAD software. The CAD design file was then exported to Nano Metric Patterning Software (NPGS) which generates a run file which can be simulated on the computer. Figure 3.11 illustrates the optical images at different stages of electrode fabrication steps.

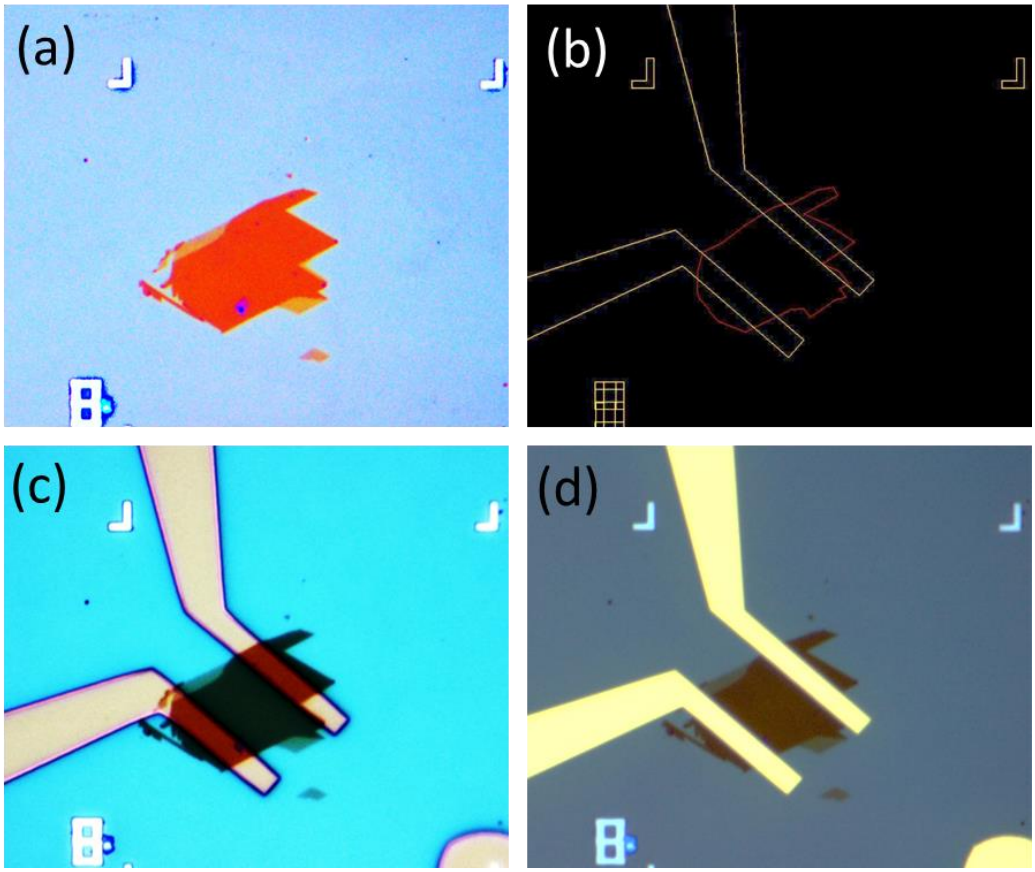

Figure 3.11 (a) Optical image of exfoliated flake (b) electrode layout designed in CAD software (c) optical image after e-beam lithography and development (d) optical image of final device electrodes.

The electrodes were defined on top of oxidized silicon substrates. One of the advantages of using highly doped (p-doped) Si-substrate is that it remains conducting even at very low temperature. Due to this advantage, such a heavily doped Si can be used as back gate during low temperature measurements. The sheet resistance of our substrate with 250 nm thermally grown oxide on it was < 0.005 Ω-cm and was purchased as 3 inch (100) Si wafer from Silicon Quest International.

3.5.1 Photolithography

Photo lithography is a very powerful technique to fabricate the micro structures. However due to the wave length limitation of light and its diffraction, nanometer features size cannot be fabricated by photolithography alone. Nevertheless, photolithography provides a valuable platform to other nano – lithographies.

Figure 3.13 illustrates the schematic of all the photolithography steps. In order to ensure the easier lift off, a two layer photo resist was spin coated over the substrate. A sensitive resist is used as bottom layer and less sensitive resist is spin coated on top[14]. By doing so, an undercut is created (as shown in figure 3.12) in the high sensitive bottom layer during etching process. Undercut helps in easier liftoff after metallization.

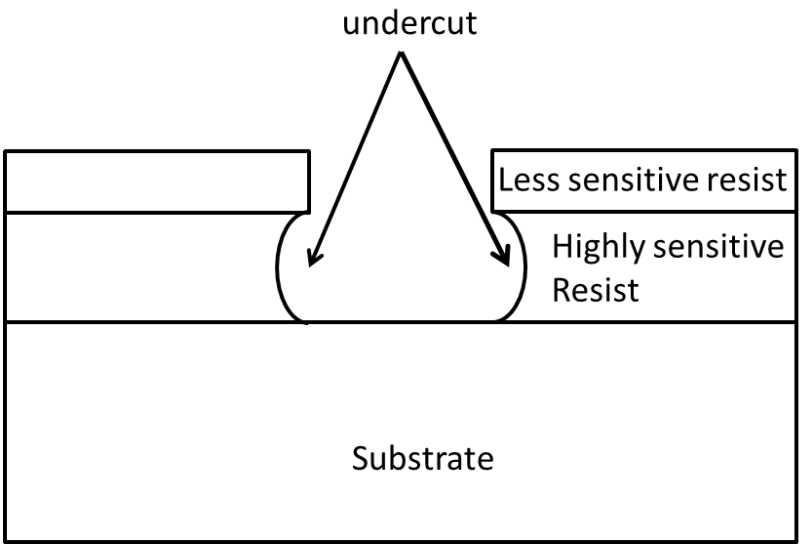

Figure 3.12 Schematic showing the formation of undercut during photo lithography process by using double layer lithography.

The first step of photolithography is cleaning of wafer. The wafer was cleaned with acetone and isopropyl alcohol (IPA) followed by dry nitrogen purging. The a first layer of photoresist (MicroChem (LOR-3A)) was spin coated at 3000 rpm for 30 seconds and baked at hot plate at 150C for 6 mins. Then after that, second layer of photoresist (Shipley S1318, from Micro Chem) was spin coated at 5000 rpm followed by and subsequently baking at 100^0C for 3 minutes. Shipley S1318 is a positive resist which means that we would obtain exactly the same pattern on the wafer as we had on our optical mask. After spin coating double layer resist, the 3 inch wafer was placed in Karl Seuss mask aligner and was exposed to UV light for 5 seconds. After the exposure, the wafer was developed in CD -26 developer for 30 seconds, rinsed in DI water and dried with dry nitrogen. All the steps involved in optically lithography process are chronologically illustrated in following figure.

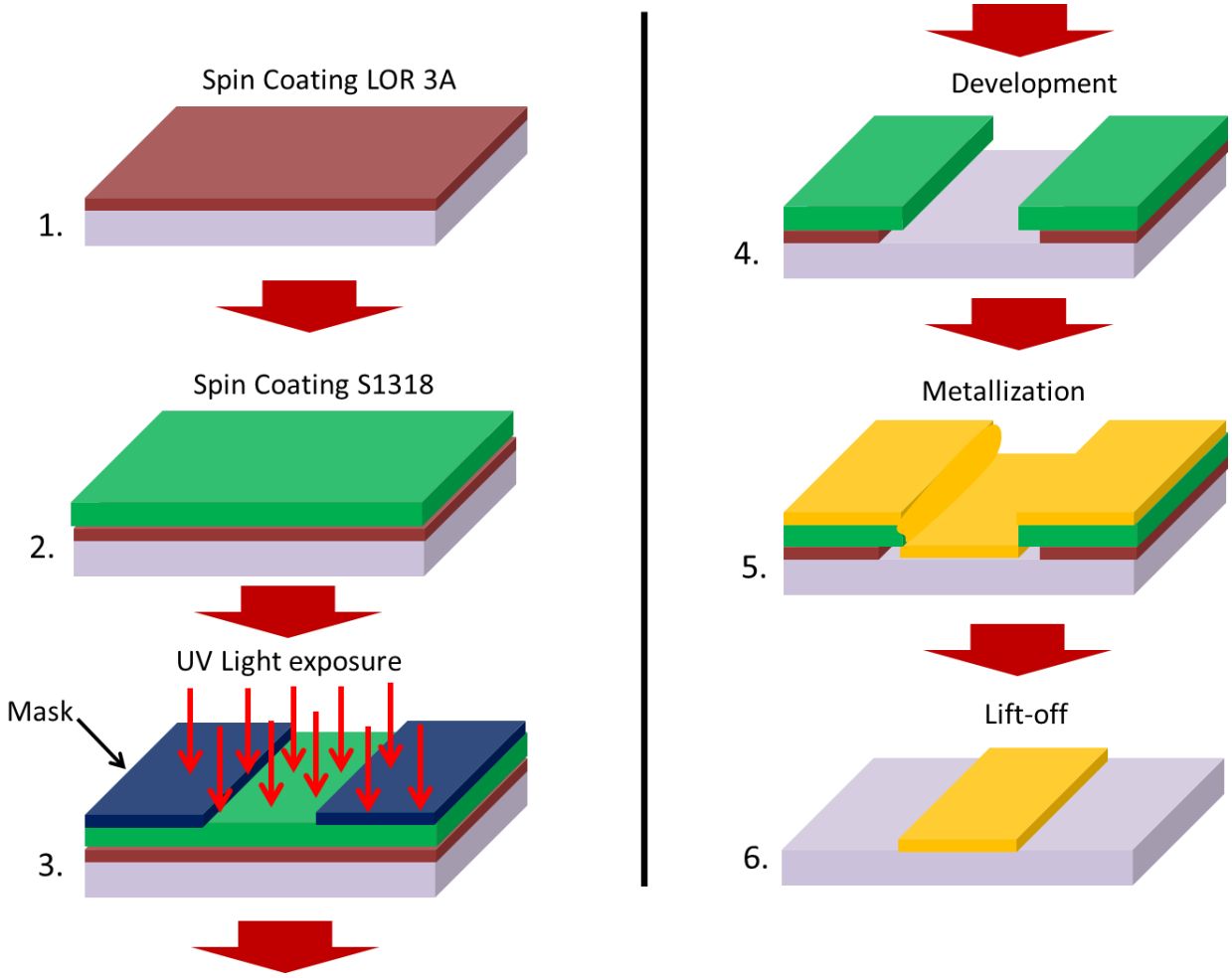

Figure 3.13 A chronological schematic diagram showing all the steps involved in double layer photolithography.

3.5.2 Metallization

Once the wafer has been exposed to UV light & developed, a combination of thermal evaporation and e-beam evaporation was used to deposit metal contact pads along with markers. We want a good adhesion of metal contact pads and markers to the substrate otherwise they won't survive the later acetone and IPA cleaning during the time of exfoliation. In addition to this, if adhesion is not firm; there are chances that the metallic electrode layers will get peeled off

during electrical measurements. Since Au alone does not possess good wettability property to SiO_2 substrate, so it doesn't stick very well with the surface. In order to overcome this difficulty, we have deposited 5 nm Cr as a sticky layer before evaporating of Au (40nm) layer. The evaporation rate was kept constant at 0.2A/sec at a base pressure of 10^{-6} torr.

3.5.3 Lift-off

Lift-off is the last step in fabrication process. After metallization, the wafer was immersed in PG remover (obtained from MicroChem) for 1-2 hours for lift off. A plastic pipet is used to squirt PG remover on the wafer in order to ensure that no metal is left. A sonication of 10-20 sec in an ultrasonic bath can help the lift off process if some unwanted deposited metal pieces are left there. After lift-off, the wafer is rinsed in acetone, IPA, and DI water, and blown dry with a stream of nitrogen gas.

3.5.4 Electron Beam Lithography

After fabrication of large contact pads using optical lithography (as shown in figure 3.14), smaller electrode arms were defined by EBL. NPGS integrated with scanning electron microscopy (SEM) system was used to define the electrodes in this step. Again similar as photolithography, a double layer resist recipe was used to define the small electrodes arm contacting MoS_2 flake to large contact pads for the same reason. At first a layer of resist MMA (Methyl Methacrylate) was drop casted and spin coated (at 4000rpm) on the sample. Immediately after the first layer, a second layer of resist PMMA (poly Methyl Methacrylate) was

spin coated at 4000rpm for 60 seconds. After spin coating, the sample was baked at 180C for 15 minus on hot plate. After the process, the resist thickness that we usually achieve is close to 250 nm which is good enough for 60nm metal deposition. Usually to have an easy lift off, the thickness of resist should be more than three times the thickness of metal to be deposited. The PMMA is a positive resist and was purchased from MicroChem. During the e-beam writing the resist was exposed to an area dose of 280 $\mu C/cm^2$ at 28 KeV using the Zeiss Ultra 55 Electron Beam Lithography System in Material Characterization Facility, University of Central Florida. Depending upon the minimum feature size, different sized apertures were used for e-beam writing. Alignment markers written by optical lithography help to accurately write small electrode arms with e-beam lithography. The schematic of large optical pad and small electrode arm are shown in figure 3.14.

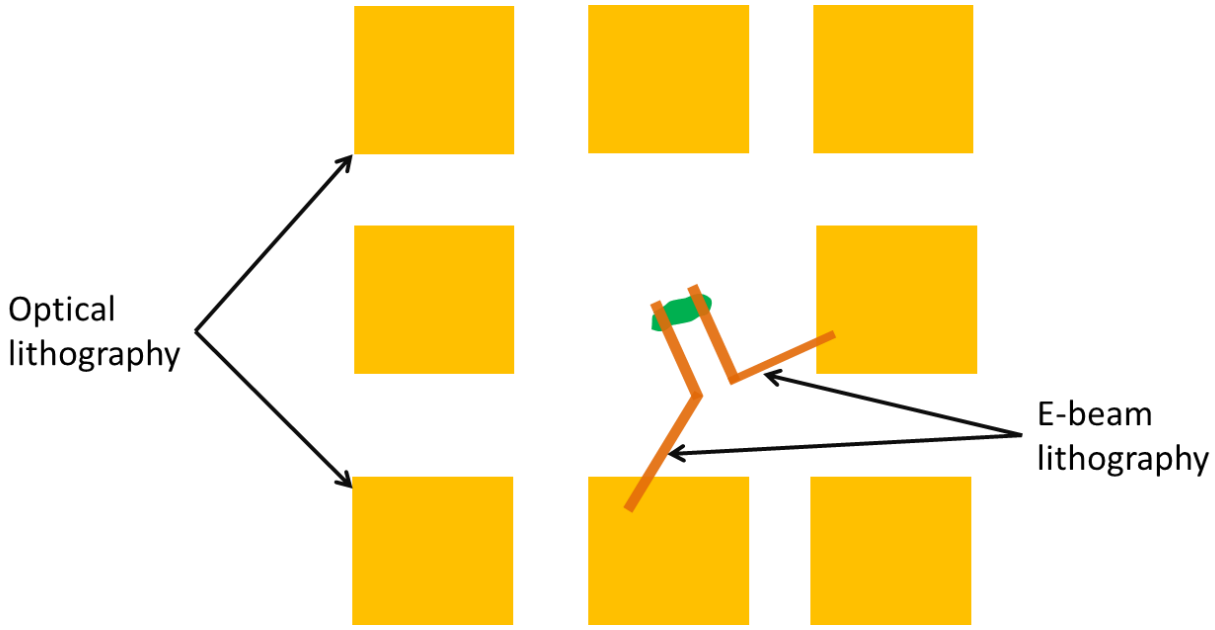

Figure 3.14 Schematic diagram electrode design fabricated by photolithography and e-beam lithography.

After the electron exposure to the desired resist area, the sample was then developed in developer solution (mixed solution) of Methyl-isobutyl-ketone : Isopropyl-alcohol (MIBK :IPA) at a ratio of 1:3 for 60 second followed by IPA (stopper solution) for 15 seconds and blown dry with nitrogen gas. As soon as development is over, usual practice is to check the patter under optical microscope to make sure we got the right pattern at right place. The developed portion can be well distinguished from the undeveloped one from its optical contrast. After making sure that electrodes are drawn at right place, we metalize the sample. A 40nm Au was thermally evaporated onto recently developed sample at a base pressure of 10^{-6}torr and at a very slow rate of 0.02A/sec. After metallization is over, the samples were then immersed into warm acetone (55°C-60°C) for 1 hour for lift-off.

3.6 Experimental Setups for Measurement

In this section, I shall discuss room temperature electron transport measurements setup, low temperature electron transport setup, optical properties measurement setup, AFM topological and height measurement setup

3.6.1 Raman and Photoluminescence Spectroscope

In this dissertation, all the Raman and PL measurements and mapping were recorded with Witec alpha300 RA confocal Raman system as shown in figure 3.15. The samples were illuminated with 532.0 nm laser light in ambient air environment at room temperature. The laser

power was set at 0.6 mW for all data acquisition in order to avoid damage to the sample including defect formation. The measurements were collected for an integration time of 1s. Emitted Stoke's Raman signal was collected by a Zeiss 100× objective (N.A = 0.9) and dispersed by a 1800 lines/mm grating for Raman measurement and a 600 lines/mm grating for PL measurements.

.

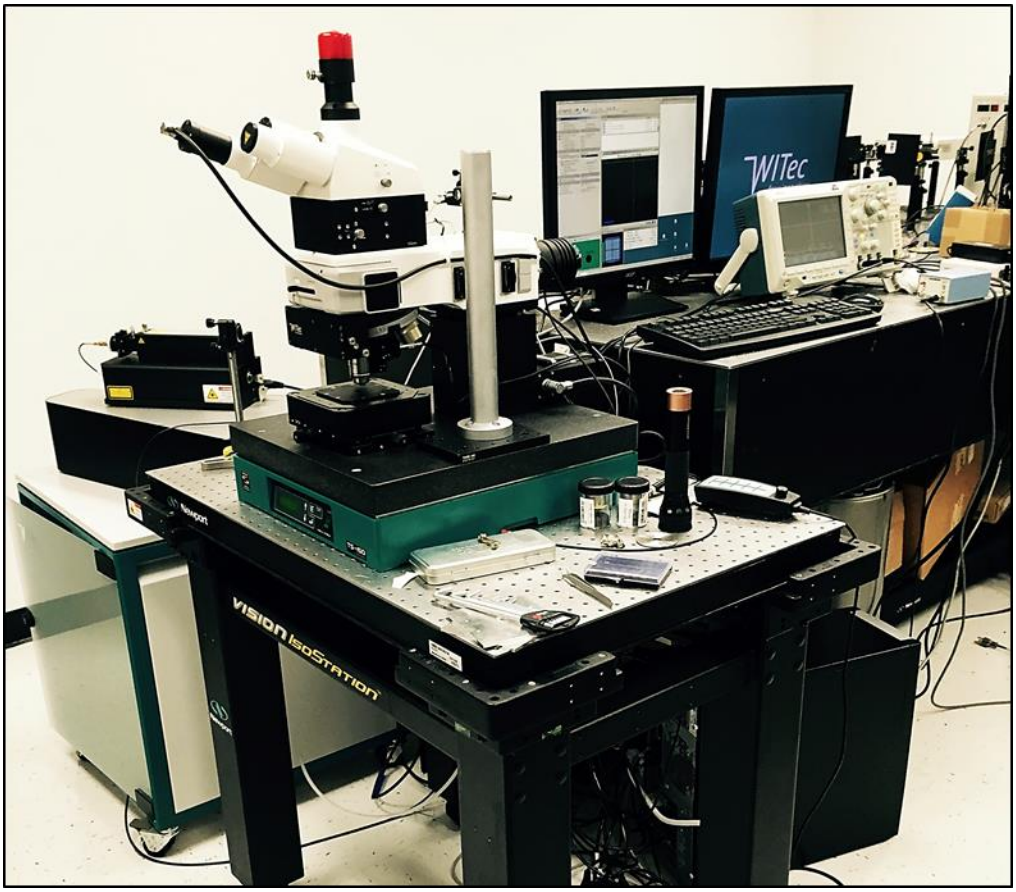

Figure 3.15 Actual image of WiTec Alpha 300 confocal Raman spectroscope.

3.6.2 Thickness and Height Measurement Setup (Optical and AFM)

All the exfoliated flakes were identified under optical microscope Olympus BX 51 with 100X objective. After initial identification of the flakes, topography images and height profiles

were taken with Vecco Dimension 3100 Atomic Force Microscope. AFM was operated at tapping mode for image extraction. Si (n-type) cantilever with force constant (K) = 25-75 N/m, length L=125μm and tip radius ~10nm were used for scanning samples. The operating frequency was kept between 200-400 Hz. Figure 3.16 illustrates the actual image of Optical and atomic force microscope.

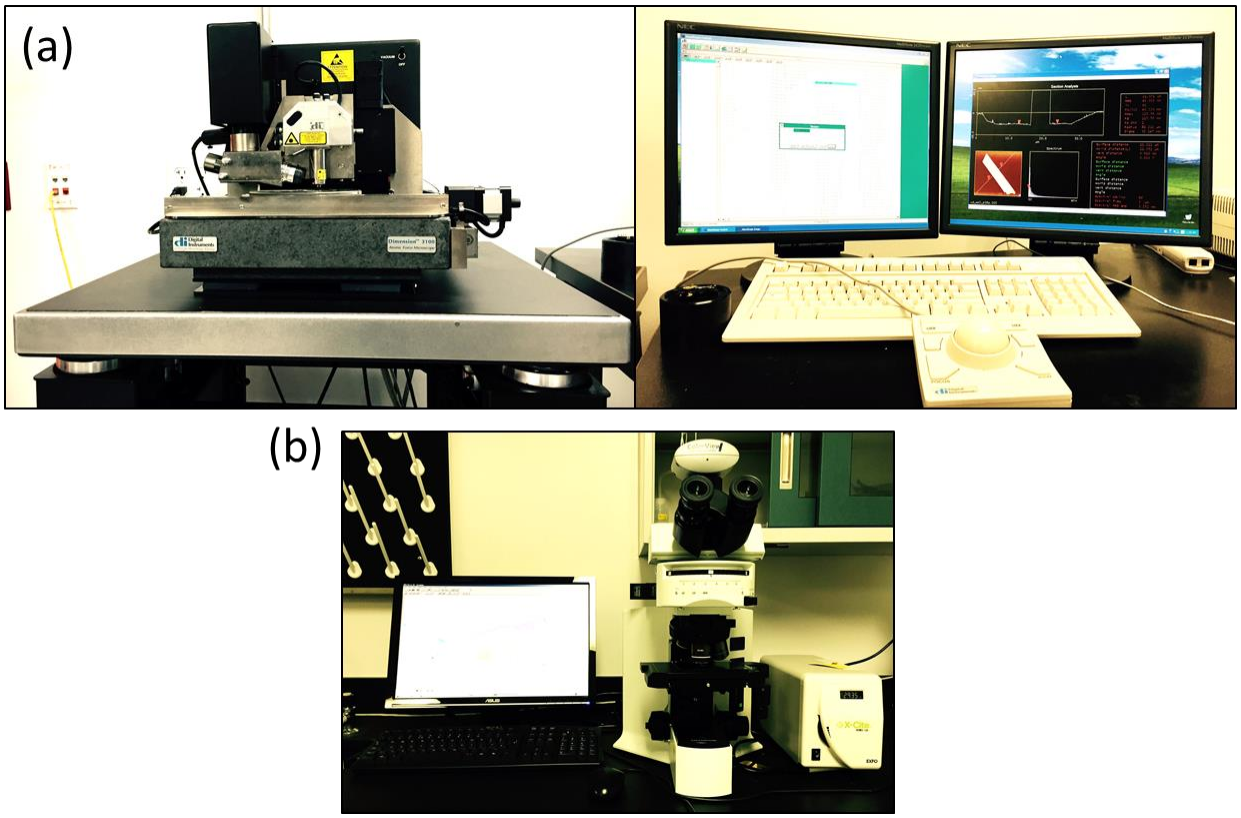

Figure 3.16 Actual images of AFM and optical microscope setup.

3.6.3 Electrical Measurement Setup

Electron transport measurements of pristine and Au decorated MoS_2 FET devices were recorded with a 3-terminal configuration: source, drain and gate, as shown in Figure 5.1. A dc power supply from electrometer (BNC 2090 from National Instrument) and a current

preamplifier (DL 1211) was used. The setup is capable of measuring sub pA signal. The gate voltage was applied by Keithley 2400. An Additional 1MΩ resistor was also connected between the gate of device and the Keithley 2400 in order to avoid any accidental application of large voltage to the devices. Figure 3.17 illustrates the setup for electrical measurement. LabVIEW software was used to record the data.

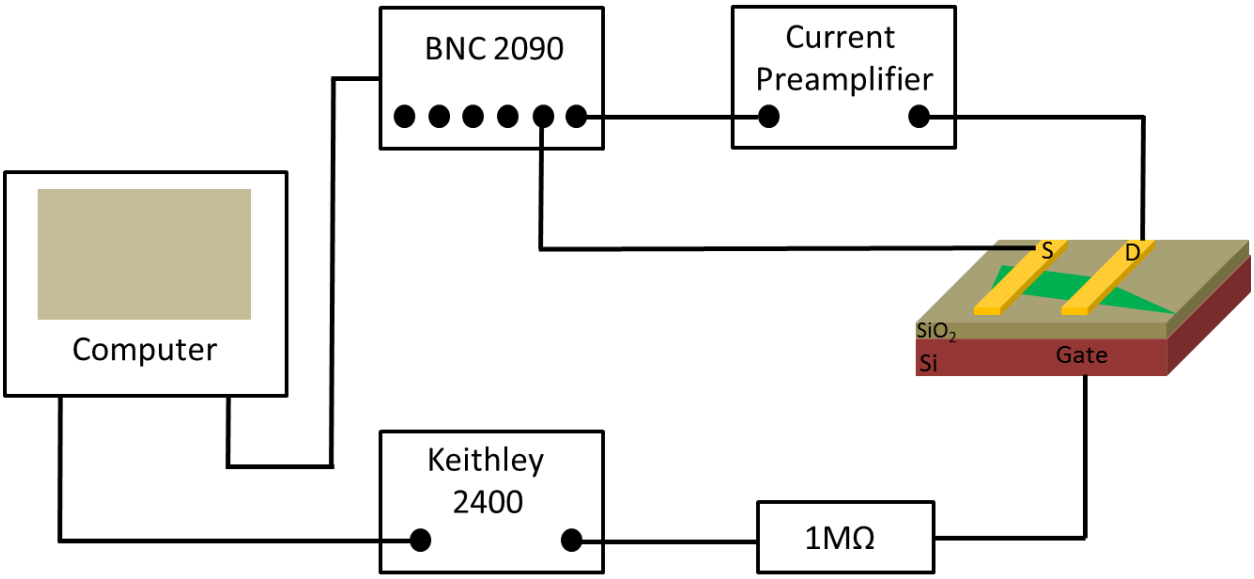

Figure 3.17 Three terminal measurement step-up for the room temperature electrical characterization MoS_2 FET.

All the low temperature measurements were done in cryostat. Before loading the sample to cryostat, they were bonded to chip carrier holder with Al wires with the help of wire bonder. Bottom of silicon substrate glued to chip carrier with silver paste served as back gate.

3.7 References

1 Novoselov, K. S. *et al.* Two-dimensional atomic crystals. *Proceedings of the National Academy of Sciences of the United States of America* **102**, 10451-10453, (2005).

2 Coleman, J. N. *et al.* Two-Dimensional Nanosheets Produced by Liquid Exfoliation of Layered Materials. *Science* **331**, 568-571, (2011).

3 Zeng, Z. *et al.* Single-Layer Semiconducting Nanosheets: High-Yield Preparation and Device Fabrication. *Angewandte Chemie International Edition* **50**, 11093-11097, (2011).

4 Ramakrishna Matte, H. S. S. *et al.* MoS2 and WS2 Analogues of Graphene. *Angewandte Chemie International Edition* **49**, 4059-4062, (2010).

5 Liu, K.-K. *et al.* Growth of Large-Area and Highly Crystalline MoS2 Thin Layers on Insulating Substrates. *Nano Letters* **12**, 1538-1544, (2012).

6 Zhan, Y., Liu, Z., Najmaei, S., Ajayan, P. M. & Lou, J. Large-Area Vapor-Phase Growth and Characterization of MoS2 Atomic Layers on a SiO2 Substrate. *Small* **8**, 966-971, (2012).

7 Lee, Y.-H. *et al.* Synthesis of Large-Area MoS2 Atomic Layers with Chemical Vapor Deposition. *Advanced Materials* **24**, 2320-2325, (2012).

8 Lin, Y.-C. *et al.* Wafer-scale MoS2 thin layers prepared by MoO3 sulfurization. *Nanoscale* **4**, 6637-6641, (2012).

9 Ji, Q. *et al.* Epitaxial Monolayer MoS2 on Mica with Novel Photoluminescence. *Nano Letters* **13**, 3870-3877, (2013).

10 Shi, Y. *et al.* van der Waals Epitaxy of MoS2 Layers Using Graphene As Growth Templates. *Nano Letters* **12**, 2784-2791, (2012).

11 Gingery, D. & Bühlmann, P. Formation of gold nanoparticles on multiwalled carbon nanotubes by thermal evaporation. *Carbon* **46**, 1966-1972, (2008).

12 Gaspar, D. *et al.* Influence of the layer thickness in plasmonic gold nanoparticles produced by thermal evaporation. *Sci. Rep.* **3** (2013).

13 Luo, Z. *et al.* Size-Selective Nanoparticle Growth on Few-Layer Graphene Films. *Nano Letters* **10**, 777-781, (2010).

14 Heiz, U., Landman, Uzi. Nanocatalysis. (2007).

CHAPTER 4: OPTICAL PROPERTIES OF MoS_2-Au HYBRID NANO SYSTEM

4.1 Introduction

MoS_2 is 2D semiconductor material with thickness dependent band gap property as its band gap changes from 1.2eV (indirect) in bulk form to 1.9 eV (direct) in monolayer form[1]. The direct band gap nature in ultrathin MoS_2 has led to exceptional photoluminescence properties[2]. In this chapter, I will discuss the effect of Au decoration on photoluminescence of MoS_2 flakes. In particular, I will study the effect of Au decoration on 2 layers and 4 layers MoS_2 flakes. To check the reproducibility of results, I have deposited 1nm and 2nm thick Au on MoS_2 flakes and results are presented in this chapter. Local variations in PL of pristine and Au decorated flakes have been studied by scanning the total flake area before and after Au decoration by acquiring PL mapping. PL mapping results have also been included in this chapter followed by discussion and conclusion.

4.2 Photoluminescence Quenching of MoS_2-Au (2nm) Hybrid Nano System

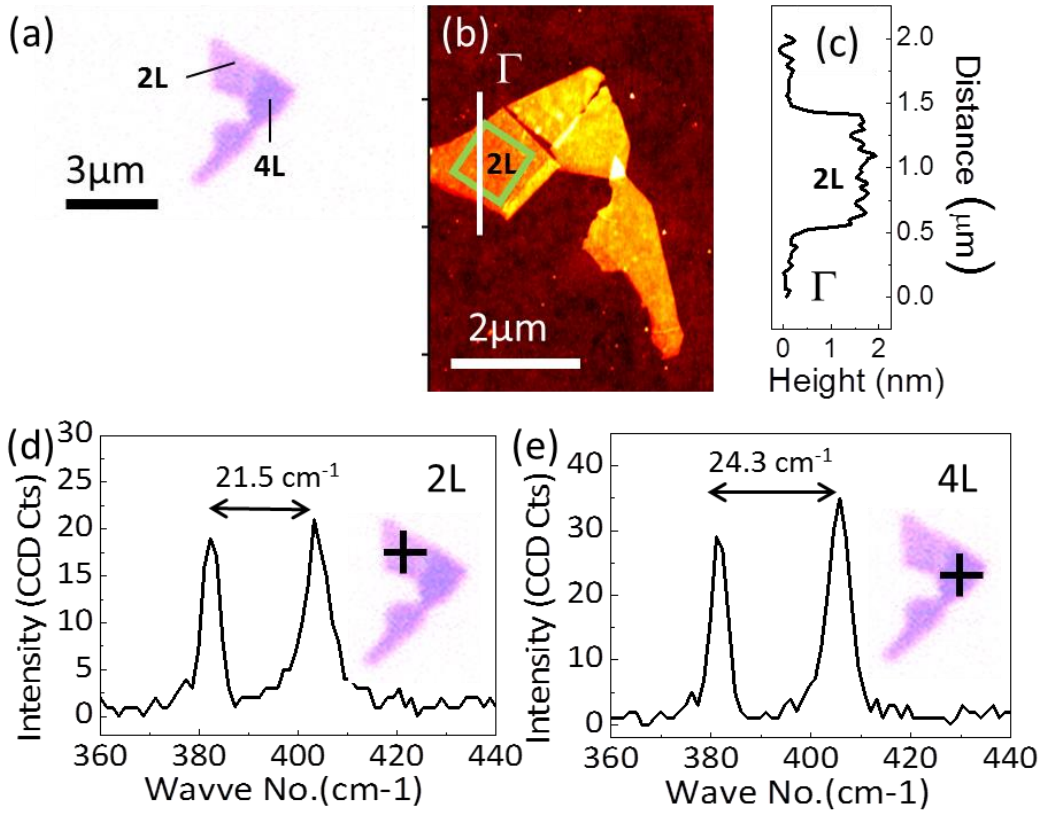

Figure 4.1 Identification of number of layers in exfoliated MoS_2 flake. (a) Optical micrograph of MoS_2 flake mechanically exfoliated on heavily doped Si/SiO_2 substrates. (b) AFM image of flake taken to identify the number of layers in it (c) AFM height profile extracted from AFM image from white line shown in the image (c), (d) Raman spectrum of flake taken from the region marked black cross in the inset.

Figure 4 shows the optical (Figure 4a) and AFM (Figure 4b) images of pristine MoS_2 flake. The optical image exhibits areas of different contrasts across the flake, which represents the pristine flake had different number of layers at different regions. After the initial contrast analysis, the flake was scanned under AFM to determine the number of layers in the pristine flake. The AFM image of pristine flake is shown in figure 4b. The number of layers of the exfoliated MoS_2 flake

was determined by AFM height measurements (as shown in Figure 4c) using the height profile (c) extracted from the AFM image (white Γ line) in Figure 4b. The transition from SiO_2 to MoS_2 indicates a thickness of 1.8 nm which is in good agreement with previously reported thickness of two layers of MoS_2 [3]. The number of layers in the flake was further confirmed by Raman spectroscopy. A Raman spectrum was extracted from different regions of the flake. Figure 4d and 4e illustrates the Raman spectrum extracted from a point marked by black cross in the inset of respective figures. The difference between the E^1_{2g} and A_{1g} peak positions were found to be 21.5 cm^{-1} for the 2 L and 24.3 cm^{-1} for the 4 L area.

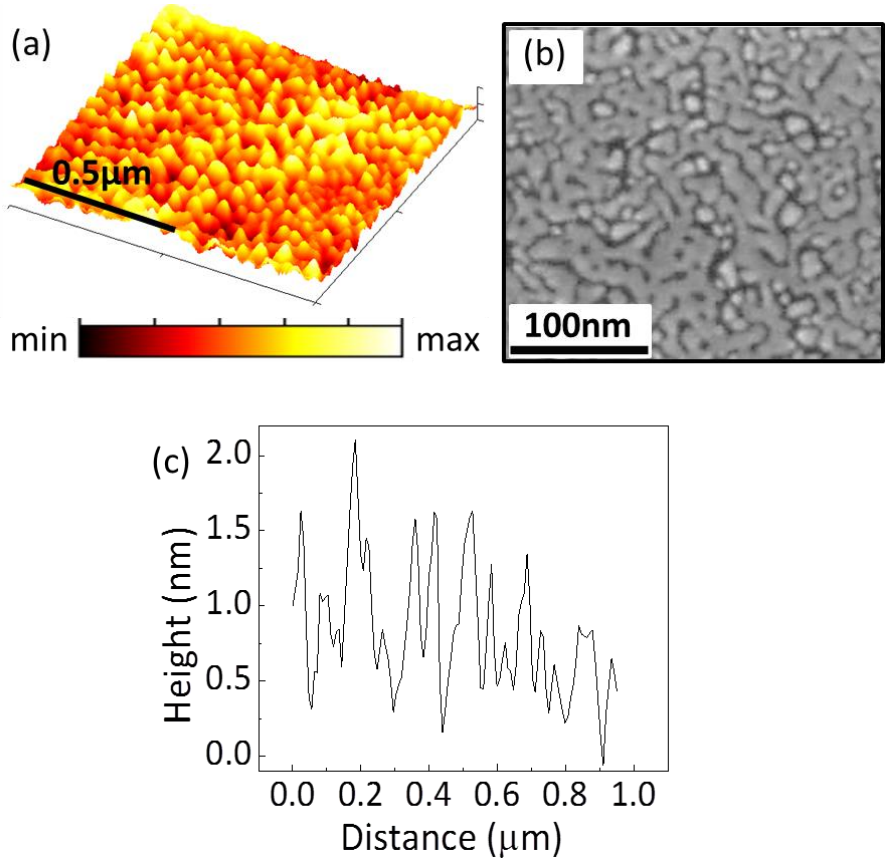

Figure 4.2 Formation of Au NP on MoS_2 resulting after 2nm of Au on pristine flake. (a) AFM, (b) SEM image of MoS_2 flake after 2nm Au deposition on it. (c) AFM height analysis of flake after 2nm Au deposition.

Figure 4.2 illustrates the AFM and SEM images of flake after 2nm Au deposition. An AFM (Figure 4a) and Scanning Electron Microscopy (SEM) characterization (Figure 4b) of the Au-MoS_2 hybrid system confirmed the formation of Au nanostructures. An average height of 1.6 nm for 2.0 nm Au deposition on MoS_2 was measured using root mean square (RMS) data analysis (4c) on the corresponding AFM image (Figure 4a). SEM images (Figure 4b) revealed elongated Au nanostructures, with feature size varying from 5 to 30 nm in width. AFM images indicate that the Au on MoS_2 exhibit some height variations within the elongated structures (Figure 4a) suggesting that they are made of several Au islands connected to each other at their base.

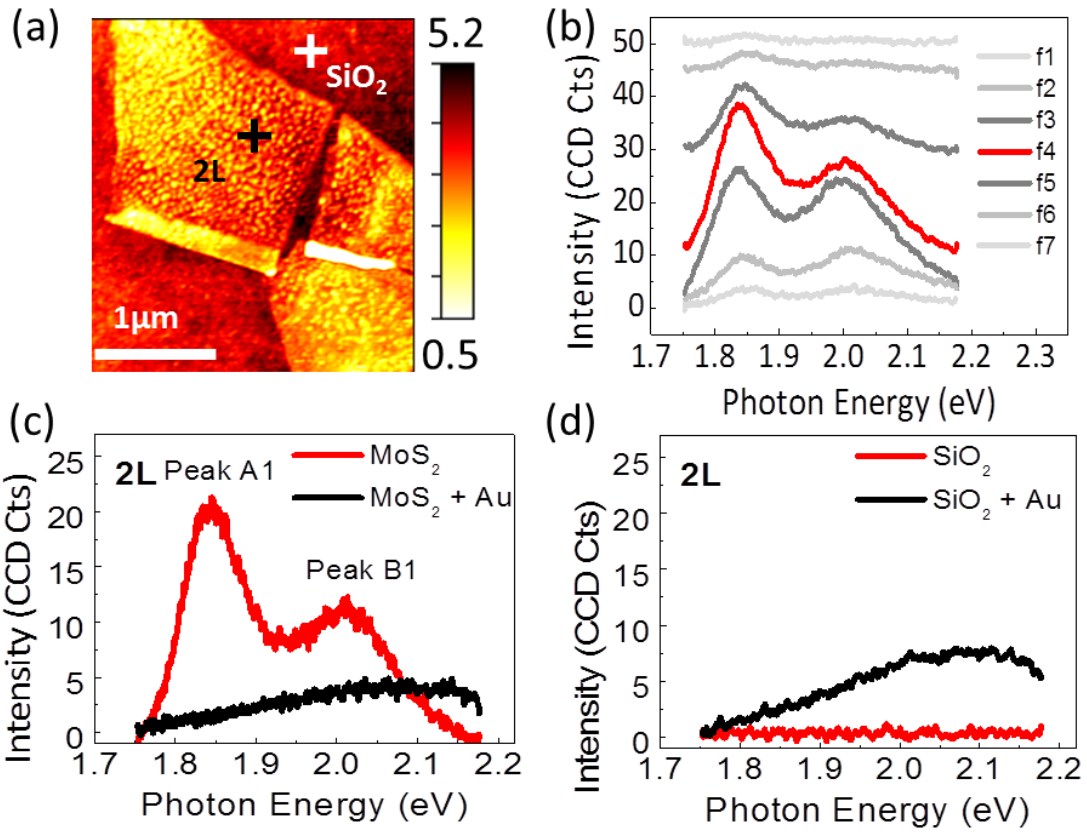

Figure 4.3 Effect of 2.0 nm Au deposition on MoS2 photoluminescence (PL). (a) AFM image of MoS_2 flake as exfoliated. Cross marks indicate the location of the PL data presented in (b). (b) PL signal as a function of focal plane from above the surface (f1) to several tens of nm below the

surface (f7). For clarity the curves were shifted of 4 units for each step. (c) PL spectra of 2 L MoS_2 flake as exfoliated (red) and after 2.0 nm Au deposition (black). (d) Plasmonic response of the bare SiO_2 substrate (red) and SiO_2 substrate covered with the Au nanoislands (black).

To investigate the effect of the Au nanostructures on the properties of MoS_2, we performed localized PL measurements on the pristine MoS_2 and Au decorated MoS_2 hybrid flake, at the same location. The PL measurements were carried out on a confocal Raman microscope system (see Chapter 3). Figure 4.3b shows the variations of the PL signal, acquired at locations labeled '2L' in Figure 4.3a, as a function of the selected focal plane of the excitation laser. Two emission peaks at 1.85 eV and at 1.98 eV can be seen (Figure 4.3b – red curve), corresponding to the A1 and B1 exciton peaks of MoS_2 [2], whose intensities change with the focal plane of the excitation laser focus. At some focal planes, the intensity of peak B1 was higher than (f6 in Figure 2b) or equal to (f5 in Figure 2b) peak A1, while at other focal planes highest intensity for peak A1 can be obtained (f4 in Figure 2b). Such variation is usually not discussed in reported PL studies. Hence we suggest that the variation in focal plane of excitation laser should be taken into account to increase the reproducibility of 2D and hybrid systems in view of more quantitative studies. After optimization, we selected f4 for all the measurements reported in this study.

Figure 4.3c shows the PL spectra acquired at the same location (marked '2L' on the flake in Figure 4.3a) on pristine MoS_2 (red curve) and after deposition of 2.0 nm Au on the MoS_2 surface (black curve). Recent work by Splendiani et al[2] described the prominent intensity of A1 peak in PL of pristine MoS_2 monolayers. However A1 peak at, 1.85 eV has also been observed for up to five layer (5 L) MoS_2, although with lower amplitude than in its single layer counterpart (i.e. all parameters other than number of layers should be identical for such comparison)[2,4,5]. The presence of A1 excitons around 1.85 eV in single layer MoS_2 is attributed to the direct gap

transition between the maximum of the valence band and the minimum of the conduction band at the K point of the Brillouin zone in monolayers MoS_2. As the direct excitonic transition at the Brillouin zone K point remains constant independently of the MoS_2 thickness, the indirect bandgap increases as the number of MoS_2 layers decreases[1,2], leading to a transition from indirect to direct gap occurring at the single layer level. The splitting between the A1 and B1 emission peaks is caused by the spin orbital and interlayer couplings and varies depending on the substrate[5]. The intensity of the B1 exciton peaks is negligible in suspended monolayer configurations and an enhancement of up to 10^4 has been reported for A1[1] while on substrate the intensity ratio of the A1/B1 is typically less than 10 [2,4,6-8]. The present work was carried out on a flake made of 2 L and 4 L MoS_2 on a Si/SiO_2 substrate. We find that in such conditions, the intensity ratio of the A1/B1 is about 2 in 2 L (Figure 4.3c) in close agreement with Liu et al[8]. For 4 L the intensity ratio was about 1.7 and a 20% decrease of the amplitude of the peaks was measured compared to 2 L. We then performed the PL measurement at the same location (marked '2L') after Au deposition. As shown in Figure 4.3c (black curve), both A1 and B1 excitons completely disappeared, suggesting that PL quenching has occurred.

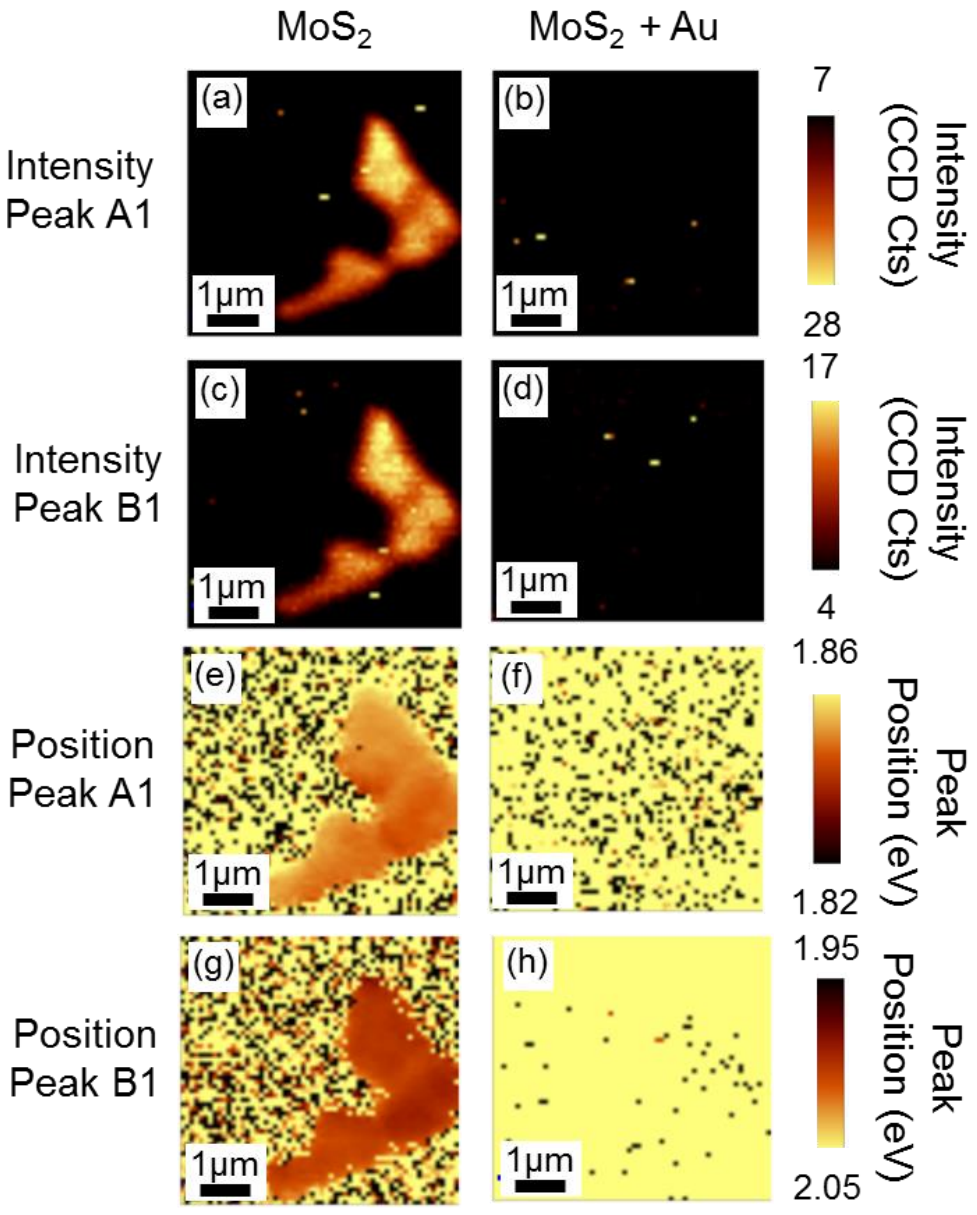

Figure 4.4 Photoluminescence (PL) mapping of MoS_2-Au hybrid nanoflake: Intensity (a) and position (e) of peak A1 across the exfoliated MoS_2 flake, Intensity (b) and position (f) of peak A1 across the exfoliated MoS_2-Au flake (after 2.0 nm Au deposition). Intensity (c) and position (g) of peak B1 across the exfoliated MoS_2 flake, Intensity (d) and position (h) of peak B1 across the exfoliated MoS_2-Au flake (after 2.0 nm Au deposition).

In order to see whether the PL quenching is observed throughout the flake after Au deposition or just at a few points, we acquired PL intensity maps and peak position contour plots for A1 and B1 peaks. The maps are presented in Figure 4.4. Figure 4.4a shows PL intensity mapping of the A1 peak throughout the pristine MoS_2 while Figure 4.4c corresponds to the map of the intensity of the B1 peak. We also considered the local variation in the position of the A1 and B1 PL peaks: Figure 4.4e and 4.4g represent the contour plot of the position of peak A1 and peak B1, respectively. Interestingly, we observed local variations in PL intensity and peak position but no PL quenching at any point on the pristine MoS_2 flake. The intensity of peak A1 varies locally from 22 to 25 CCD Cts within the 2 L region of the flake, while the intensity of peak B1 varies from 8 to 17 CCD Cts. In the 4 L region, the intensity of the A1 peak varied from 16 to 18 CCD Cts. Likewise, the position of peak A1 varies locally from 1.82 eV to 1.86 eV within the flake, while the position of peak B1 varies from 1.95–2.05 eV. Recent PL studies of MoS_2 also show small variations in peak position for both peak A1 and peak B1 [2,4,6,7] and intensity ratio of A1/B1[2,4,6,7] acquired using single point PL spectra. The variations could be attributed to non-homogenous interaction with the substrate, local defects in the flake or various edges configurations on the edges[4,7-9]. Although often neglected in single spectra studies[2,7,10], such 2D mappings could have a major impact on the understanding of the behavior of MoS_2 and defect- or hybrid MoS_2. The results highlight the need for 2D mapping of the flakes to avoid the misleading observation of a sheet that would be due to a localized change in the 2D flake.

The 2D mappings were repeated after Au deposition, as presented in Figure 4.4b (A1 intensity), d (B1 intensity), f (A1 position), h (B1 position). No peak could be observed in the range of 1.82–1.86 eV, as can be seen in the intensity map in Figure 4.4b and corresponding position

contour plot in Figure 4.4f. Similar observation holds in the range of 1.95–2.05 eV, as can be seen in the intensity map in Figure 4.4d and corresponding position contour plot in Figure 4.4h. Since Au nanostructures cover the entire MoS_2 surface, the observed PL quenching throughout the flake suggest strong charge transfer interaction between Au and MoS_2.

4.3 Photoluminescence Quenching of MoS_2-Au (1nm) Hybrid Nano System

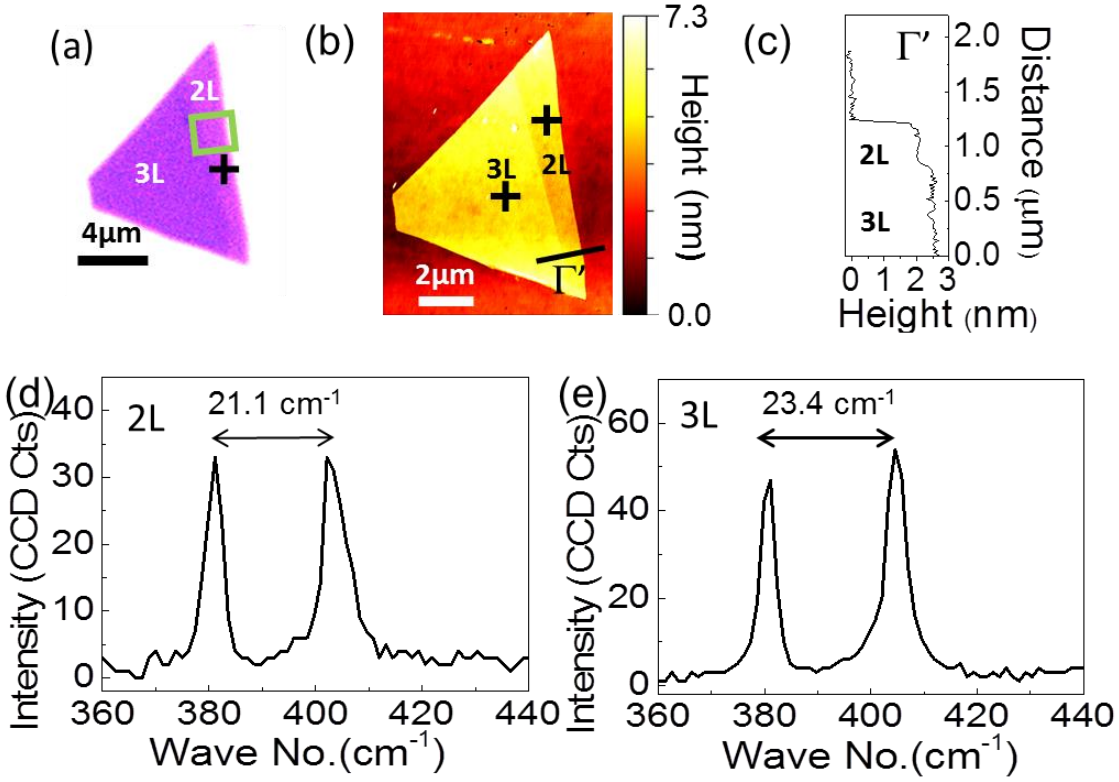

Figure 4.5 (a) optical image of exfoliated MoS_2 (b) AFM image of MoS_2 flake as exfoliated. Γ' line (black) corresponds to the profile cross-section extracted (c) to confirm the height of the flake layers. Raman Spectrum obtained from (d) two layers (2L) and (e) 3 layers (3L) MoS_2 flake before Au deposition. The difference between E_{2g} and A_{1g} peak is 21.1 and 23.4 cm^{-1} respectively which is indicative of 2 layers (2L) and 3 layers (3L) MoS_2 flakes.

In order to further confirm the PL quenching of Au on MoS_2, we repeated the study for 1.0 nm Au deposition on another MoS_2 flake. Figure 4.5a shows the optical image of the pristine MoS_2 flake considered for this sequence of measurements. The optical contrast (Figure 4.5a) and AFM topography (Figure 4.5b) images show 2 L (1.9 nm thickness) and 3 L (2.4 nm thickness) areas on the flake, which was further confirmed from Raman study (Figure 4.5d and 4.5e). The high resolution AFM image (Figure 4.6a) shows the morphology of the hybrid MoS_2 surface after 1.0 nm Au deposition with average height of 0.6 nm (extracted by RMS analysis, Figure 4.6c). SEM characterization (Figure 4.6b) of the MoS_2-Au hybrid system showed the formation of isolated triangular Au nanostructures on MoS_2, with size variation of 5 nm to 17 nm, corresponding to a lower coverage compared to the 2.0 nm deposition sample.

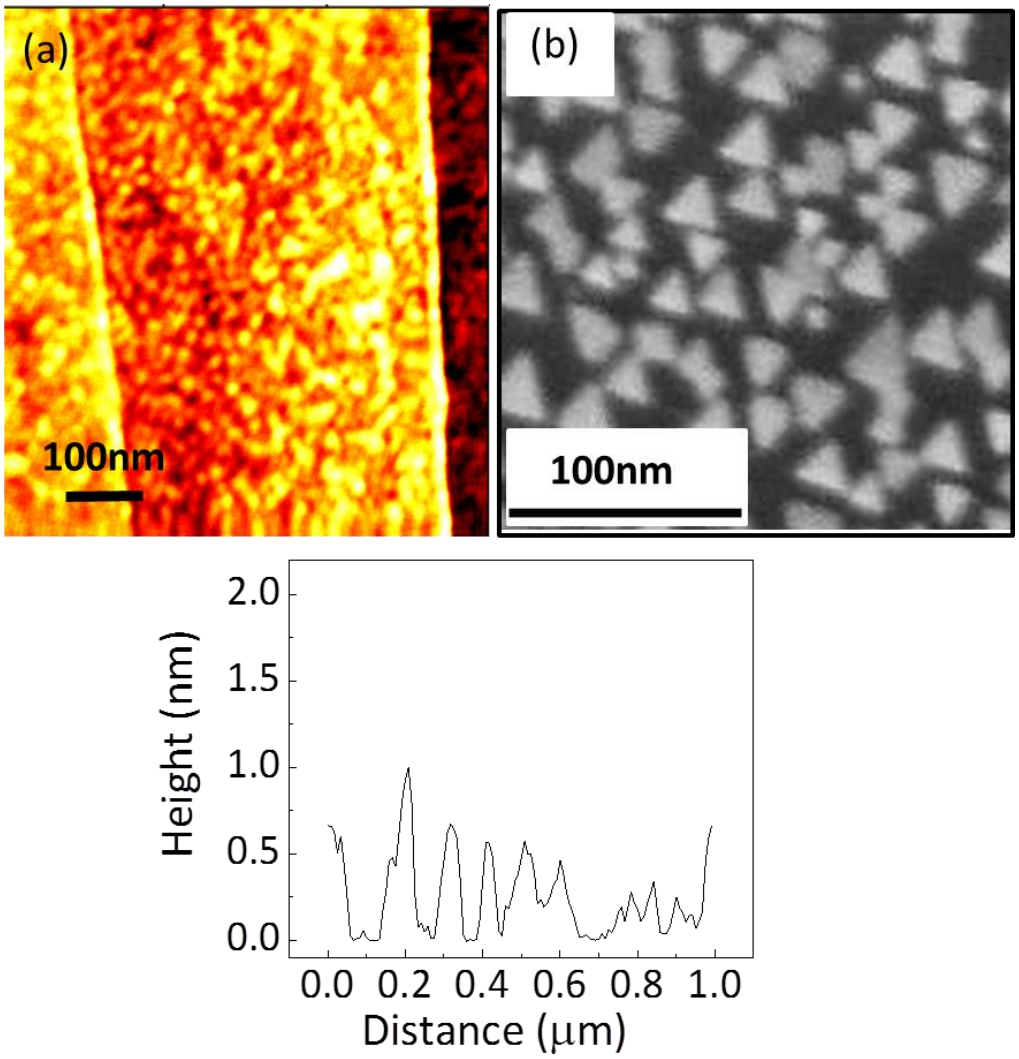

Figure 4.6 Formation of Au NP on MoS_2 resulting after 1nm of Au on pristine flake. (a) AFM, (b) SEM image of MoS_2 flake after 1nm Au deposition on it. (c) AFM height analysis of flake after 1nm Au deposition.

A PL spectrum of the flake was acquired (at the location indicated by the cross labeled '2L' in Figure 4.5a) on pristine MoS_2 (red curve in Figure 4.7). Small variations in the intensity of both emission peaks were observed in the 2 L and 3 L, and at the 2 L–3 L transition on pristine MoS_2 (Figure 4.8). A PL spectrum of the flake at the same location was acquired after 1.0 nm Au deposition (black curve in Figure 4.7). As in the 2.0 nm deposition case, we observed

a significant photoluminescence quenching of the A1 peak on MoS_2-Au, but a small reduction of the B1. The partial quenching of the B1 peak may be due to variations in the Au nanostructures dimensions and shape. To study a local variation in the flake we acquired intensity maps of these two peaks A1 and B1. Figure 4.9a–d show the PL intensity maps of A1 (Figure 4.9a, b) and B1 (Figure 4.9c, d) for pristine and hybrid MoS_2-Au. PL quenching was observed on both 2 L and 3 L in presence of Au (Figure 4.9b and Figure 4.9d). The measurements confirm the p-doping of MoS_2 by thermally deposited Au nanostructures on 2 L to 4 L MoS_2.

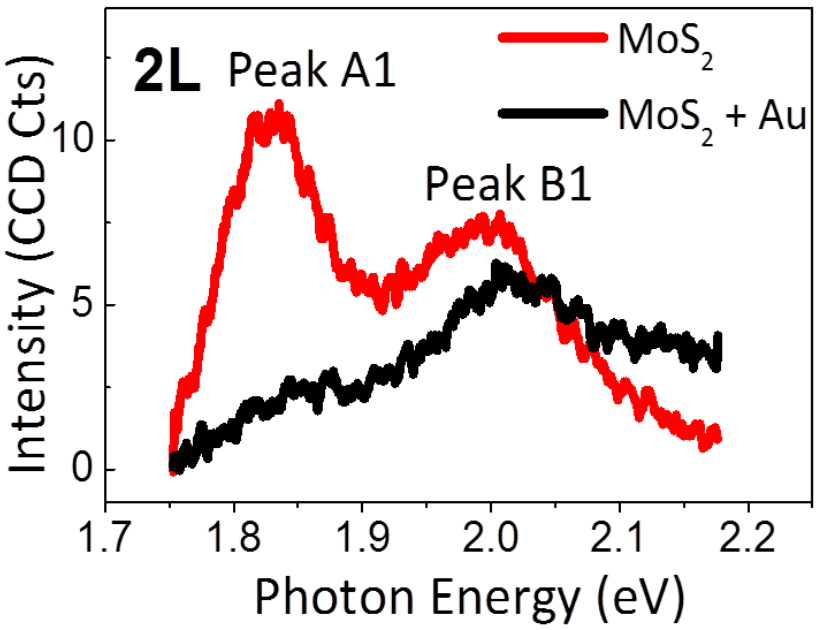

Figure 4.7 PL of pristine MoS_2 flake (red curve) and after 1nm Au deposition (black curve).

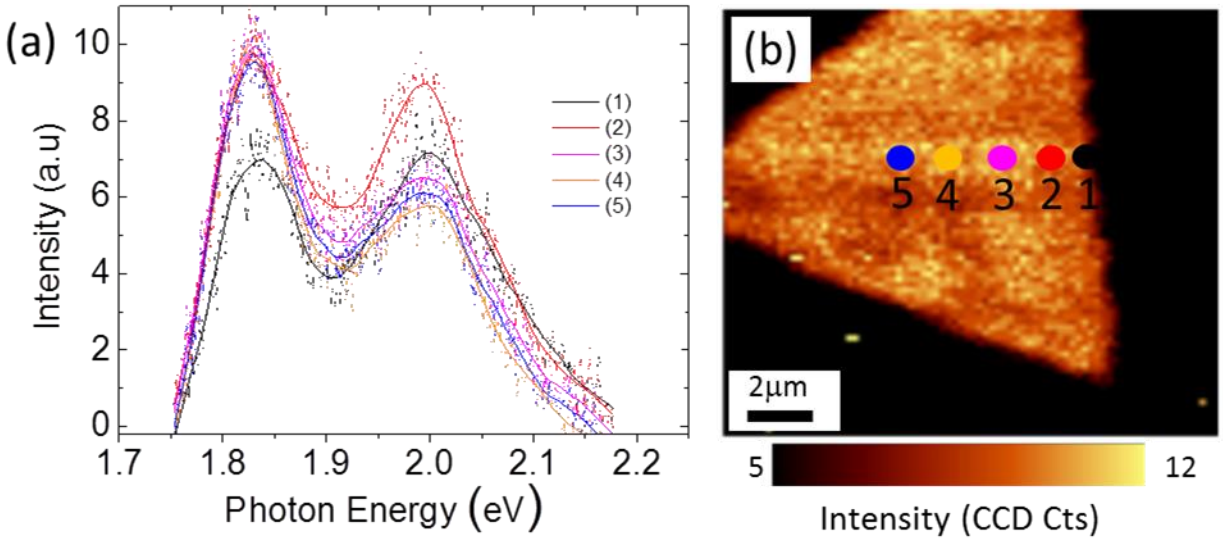

Figure 4.8 (a) Local variation in the PL intensity of pristine MoS_2 flake used for 1 nm Au deposition study. Spectra were taken at five different points along a line as shown in the intensity map of A1 peak (b). (1) in black shows the signal acquired at 2L close to the edge of the nanoflake, while (2) in red shows the PL signature of 2L closer to the 3L interface. (3)-(5) are representative of the 3L MoS_2 PL signature.

Different groups have reported decoration of MoS_2 with Au, using chemically synthesized nanostructures[11-16]. Some of these studies presented electrical transport data, with one study showing p-doping and the other showing n-doping. Our study, on the other hand, was performed using thermally deposited Au structures, and the PL study showed p-doping. Similarly, both p- and n- doping of Au on graphene has been observed[11,14,17,18]. Although the p-doping confirmed by our PL quenching result is in agreement with recent electrical transport data of MoS_2[11], this quenching is rather unexpected as Au nanostructures are well known for their plasmonic characteristics and their ability to enhance materials responses[19].

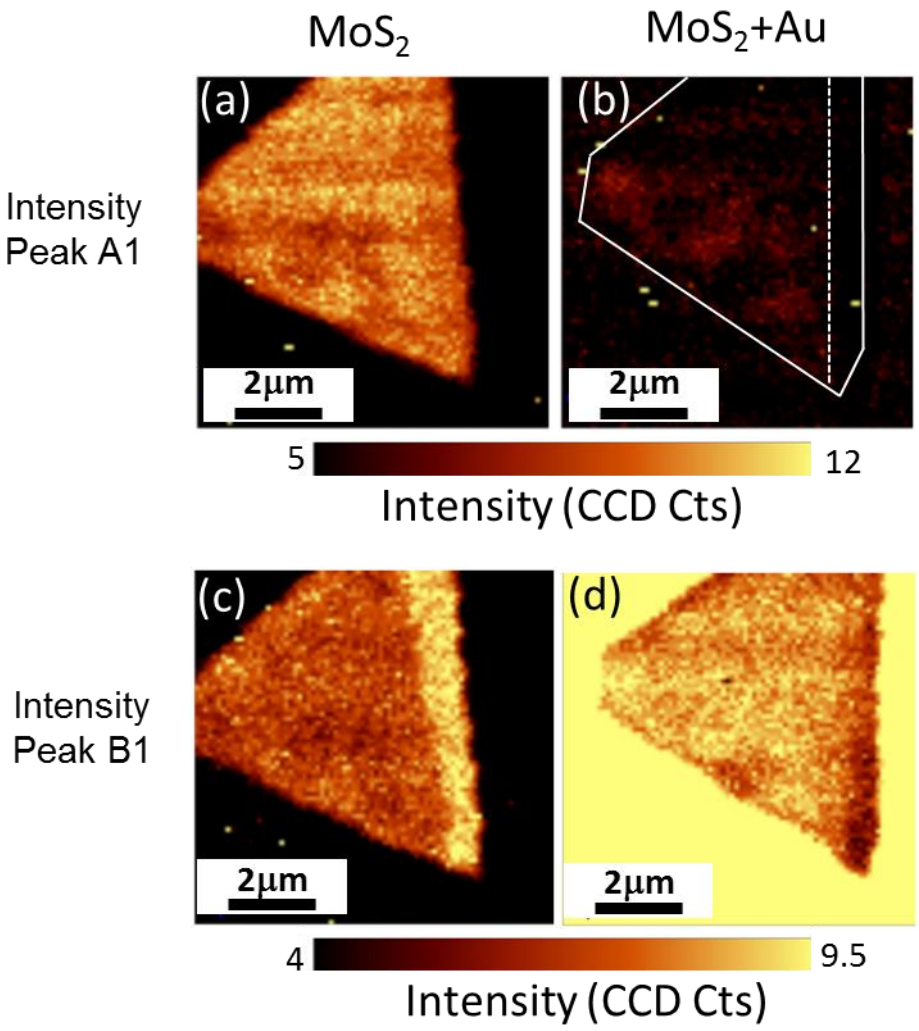

Figure 4.9 Photoluminescence (PL) mapping of MoS2-Au hybrid nanoflake**:** Intensity (a, c) of peak A1 and B1 across the exfoliated MoS_2 flake, Intensity (b,d) of peak B1 across the exfoliated MoS_2-Au flake (after 1.0 nm Au deposition).

Absorption around 500–600 nm has been reported for 40 nm Au nanoparticles in colloidal solutions[20] and on quartz substrates[21]. Moreover, no PL signal on the Si/SiO_2 substrate before Au deposition (Figure 4.3b (red curve), acquired at the location marked 'SiO_2' in Figure 4.3a), whereas a broad absorption centered around 2.1 eV (i.e. 590 nm) could be observed in the presence of Au nanostructures (Figure 4.3b (black curve)). Similar behavior was observed for

1.0nm deposited Au (see high intensity of the substrate in Figure 4.9d). This suggests plasmonic activity of the Au nanostructures on Si/SiO_2, but did not lead to any PL enhancement on MoS_2. Interestingly, recent study by Sohbani et al[13], indeed shows PL enhancement on Au coated silica nanospheres of ~180 nm indicating a strong size effect of the Au nanostructures on the PL and doping of MoS_2. This suggests that PL and doping of MoS_2 by metal nanostructures is likely related to their geometry and need to be addressed in future theoretical and experimental works.

4.4 Discussion

Recently, variations of PL intensity are reported for different substrates[5] and for liquid phase exfoliated MoS_2[10]. In substrate dependent studies, although no quenching was observed, small variations were attributed to the doping by the trapped charges of the substrate[5]. While for the Li-intercalated MoS_2 study, the absence of PL was due to a phase transition of MoS_2 to metallic phase[10]. In our present study, all measurements were carried out on the same substrate (Si/SiO_2 substrate) and the absence of PL quenching in the 2D mapping of pristine MoS_2 (without Au deposition) suggests that the substrate induced defects are not responsible for the observed PL quenching of MoS_2 after Au deposition. To determine whether the PL quenching is due to any structural change of MoS_2 caused by Au deposition, we performed X-ray photoemission spectroscopy (XPS) on pristine MoS_2 and after depositing Au. No change in the structure could be found according to a comparison of XPS peak position and peak FWHM (Figure 4.10). Thus it is clear that the PL quenching is not due to any structural change in the system.

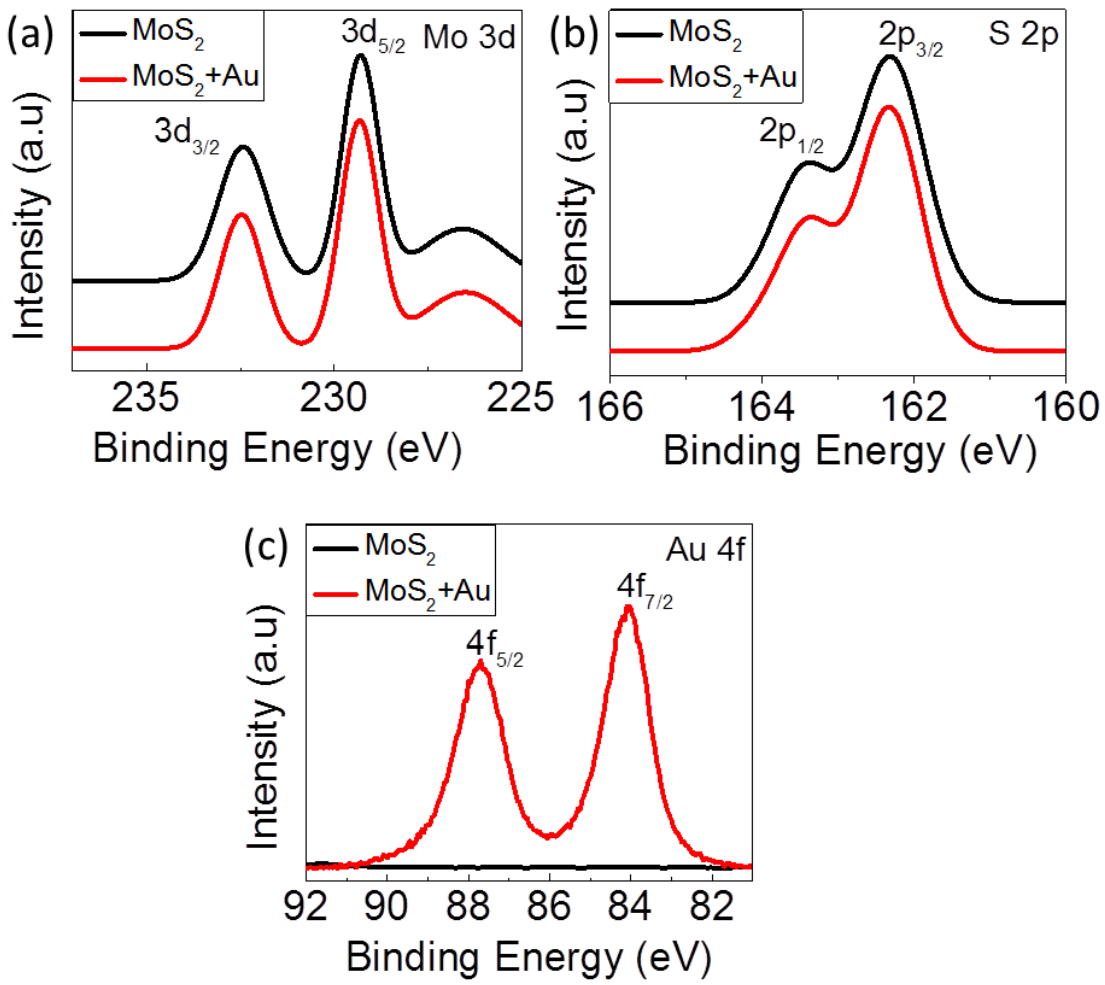

Figure 4.10 X-Ray Photoemission Spectroscopy analysis for (a) Mo (b) S and (c) Au binding energies of pristine MoS_2 and Au-MoS_2 hybrid.

Therefore, the variations of PL in our study suggest doping by the Au nanostructures. We infer that the PL quenching observed in the presence of Au can be attributed to a change in the electronic structure of the system. The Fermi level of a single layer of MoS_2 and Au was previously reported at 4.7 eV[22-25] and 5.1 eV [26,27] resulting in a 0.4 eV energy level offset (Figure 4.11a), which causes a band bending[23] in the MoS_2-Au hybrid (Figure 4.11b). Upon illumination, the electrons in the excited state of MoS_2 transfer to Au, leaving a hole behind, thus

cause p-doping in MoS_2. As electrons from MoS_2 are transferred to Au, they do not decay back to their initial ground state, leading to PL quenching in the hybrid system.

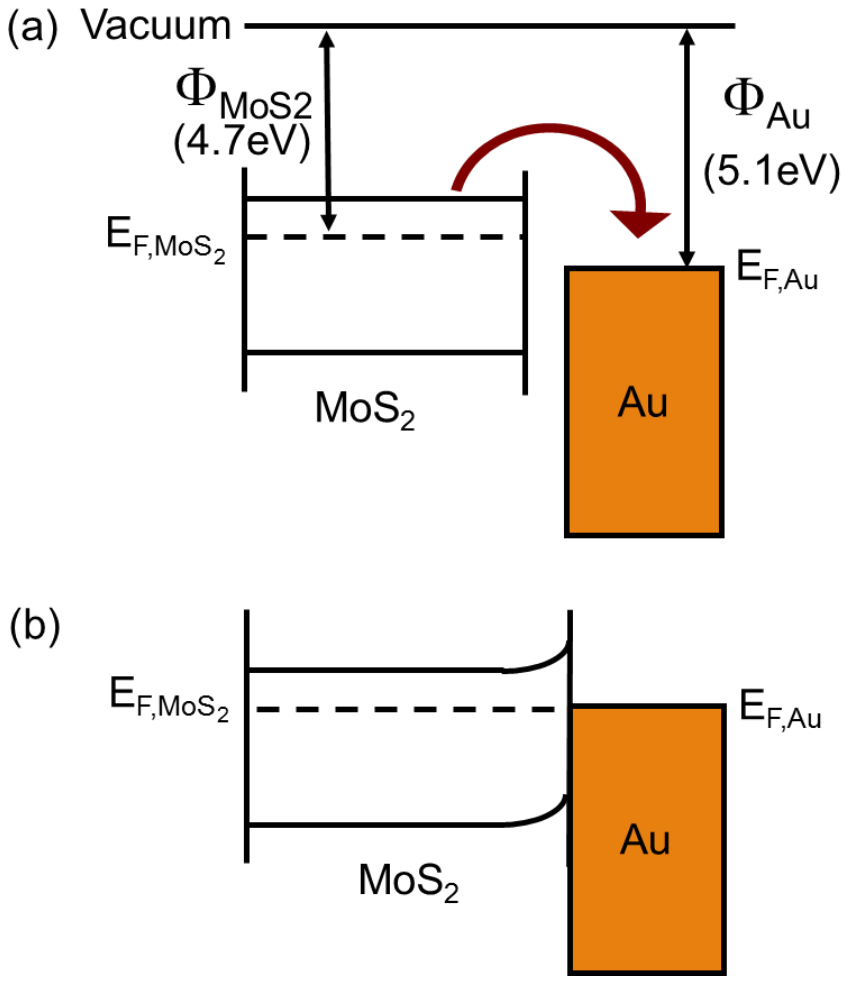

Figure 4.11 Electron transfer mechanism in MoS_2-Au hybrid nanoflake. (a) The energy band diagram for MoS_2 and Au shows the relative positions of Fermi level with respect to vacuum level before establishing a contact. The direction of the arrow represents the transfer of electrons from MoS_2 to Au after the contact is established, (b) The energy band diagram of MoS_2-Au showing band bending after establishing the contact between Au and MoS_2. Electron transfer from MoS_2 to Au causes p-doping and PL quenching.

4.5 Conclusion

In summary, we have investigated the PL behavior of pristine and Au decorated MoS_2. The size of the NPs was controlled by the thickness of Au deposited. The results show a drastic PL quenching as a result of the Au NPs on MoS_2, irrespective of the number of MoS_2 layers (from 2 L to 4 L). We suggest that the change in the electronic structure of the system consists of electrons transfer from MoS_2 to Au, as the work function of MoS_2 is lower than that of Au. Thus the electrons in the excited state of MoS_2 transfer to Au, leaving a hole behind, causing p-doping in MoS_2. In addition, our study demonstrates the need for more comprehensive studies of hybrid TMDs to fully understand the effect of dimension, materials, and spacing on the electronic properties of the system. However, the present results offer new options for localized tunability of the 2D TMDs properties as quenching will occur where patches of Au nanostructures are patterned. We expect these results to have numerous applications in nano-electronics and nano-optics.

4.6 References

1 Huang, X., Zeng, Z. Y. & Zhang, H. Metal dichalcogenide nanosheets: preparation, properties and applications. *Chemical Society Reviews* **42**, 1934-1946, (2013).

2 Splendiani, A. *et al.* Emerging Photoluminescence in Monolayer MoS2. *Nano Letters* **10**, 1271-1275, (2010).

3 Mouri, S., Miyauchi, Y. & Matsuda, K. Tunable Photoluminescence of Monolayer MoS2 via Chemical Doping. *Nano Letters* **13**, 5944-5948, (2013).

4 Buscema, M., Steele, G., Zant, H. J. & Castellanos-Gomez, A. The effect of the substrate on the Raman and photoluminescence emission of single-layer MoS2. *Nano Res.* **7**, 1-11, (2014).

5 Mak, K. F., Lee, C., Hone, J., Shan, J. & Heinz, T. F. Atomically Thin MoS_2: A New Direct-Gap Semiconductor. *Physical Review Letters* **105**, 136805 (2010).

6 Tongay, S. *et al.* Defects activated photoluminescence in two-dimensional semiconductors: interplay between bound, charged, and free excitons. *Scientific Reports* **3**, (2013).

7 Scheuschner, N. *et al.* Photoluminescence of freestanding single- and few-layer MoS_2. *Physical Review B* **89**, 125406 (2014).

8 Liu, Y. L. *et al.* Layer-by-Layer Thinning of MoS2 by Plasma. *Acs Nano* **7**, 4202-4209, (2013).

9 Su, L., Zhang, Y., Yu, Y. & Cao, L. Dependence of coupling of quasi 2-D MoS2 with substrates on substrate types, probed by temperature dependent Raman scattering. *Nanoscale* **6**, 4920-4927, (2014).

10 Eda, G. *et al.* Photoluminescence from Chemically Exfoliated MoS2. *Nano Letters* **11**, 5111-5116, (2011).

11 Shi, Y. *et al.* Selective Decoration of Au Nanoparticles on Monolayer MoS2 Single Crystals. *Scientific Reports* **3**, (2013).

12 Sreeprasad, T. S., Nguyen, P., Kim, N. & Berry, V. Controlled, Defect-Guided, Metal-Nanoparticle Incorporation onto MoS2 via Chemical and Microwave Routes: Electrical, Thermal, and Structural Properties. *Nano Letters* **13**, 4434-4441, (2013).

13 Sobhani, A. *et al.* Enhancing the photocurrent and photoluminescence of single crystal monolayer MoS2 with resonant plasmonic nanoshells. *Applied Physics Letters* **104**, (2014).

14 Shi, Y. *et al.* Work Function Engineering of Graphene Electrode via Chemical Doping. *ACS Nano* **4**, 2689-2694, (2010).

15 Scharf, T. W., Goeke, R. S., Kotula, P. G. & Prasad, S. V. Synthesis of Au–MoS2 Nanocomposites: Thermal and Friction-Induced Changes to the Structure. *ACS Applied Materials & Interfaces* **5**, 11762-11767, (2013).

16 Govinda Rao, B., Matte, H. S. S. R. & Rao, C. N. R. Decoration of Few-Layer Graphene-Like MoS2 and MoSe2 by Noble Metal Nanoparticles. *J Clust Sci* **23**, 929-937, (2012).

17 Ren, Y. *et al.* Controlling the electrical transport properties of graphene by in situ metal deposition. *Applied Physics Letters* **97**, (2010).

18 Huh, S., Park, J., Kim, K. S., Hong, B. H. & Kim, S. B. Selective n-Type Doping of Graphene by Photo-patterned Gold Nanoparticles. *ACS Nano* **5**, 3639-3644, (2011).

19 Jasuja, K. & Berry, V. Implantation and Growth of Dendritic Gold Nanostructures on Graphene Derivatives: Electrical Property Tailoring and Raman Enhancement. *ACS Nano* **3**, 2358-2366, (2009).

20 Aslan, K., Holley, P., Davies, L., Lakowicz, J. R. & Geddes, C. D. Angular-Ratiometric Plasmon-Resonance Based Light Scattering for Bioaffinity Sensing. *Journal of the American Chemical Society* **127**, 12115-12121, (2005).

21 Lereu, A. L. *et al.* Plasmon assisted thermal modulation in nanoparticles. *Optics Express* **21**, 12145-12158, (2013).

22 Sundaram, R. S. *et al.* Electroluminescence in Single Layer MoS2. *Nano Letters* **13**, 1416-1421, (2013).

23 Yin, Z. *et al.* Single-Layer MoS2 Phototransistors. *ACS Nano* **6**, 74-80, (2012).

24 Liu, K.-K. *et al.* Growth of Large-Area and Highly Crystalline MoS2 Thin Layers on Insulating Substrates. *Nano Letters* **12**, 1538-1544, (2012).

25 Choi, M. S. *et al.* Controlled charge trapping by molybdenum disulphide and graphene in ultrathin heterostructured memory devices. *Nature Communications* **4**, (2013).

26 Eastman, D. E. Photoelectric Work Functions of Transition, Rare-Earth, and Noble Metals. *Physical Review B* **2**, 1-2 (1970).

27 Michaelson, H. B. The work function of the elements and its periodicity. *Journal of Applied Physics* **48**, 4729-4733, (1977).

CHAPTER 5: ROOM TEMPARATURE ELECTRONIC TRANSPORT PROPERTIES OF Au DECORATED MoS_2

5.1 Introduction

In this chapter I will investigate the room temperature electronic properties of Au decorated MoS_2. Two kinds of Field Effect Transistors (FETs) samples were fabricated and investigated: (1) FETs containing few layers (2-4 layers) MoS_2 flakes and (2) FETs containing multilayer (20-30 layers) MoS_2 flakes. Here I will demonstrate an approach to systematically tune the transport properties of MoS_2 FET by controlling the thickness of Au deposited on it. I will present the evidence of tuning the threshold voltage (V_{th}) and field effect mobility (μ) of MoS_2 FET over a large range. I will also present quantitative results for charge transfer from MoS_2 to Au at various thickness of Au. In the end, I will discuss the reason for variation in field effect mobility with a simple approach. My findings of in plane engineering of electrical properties of MoS_2 can be applied to other 2D materials to tune their properties as well.

5.2 Device Schematic and Fabrication

The schematic layout of MoS_2 FET is illustrated in figure 5.1. MoS_2 flakes were mechanical exfoliation with the help of a scotch tape from the bulk single crystal of MoS_2. The method of exfoliation has already been explained in chapter 3 in details. The highly doped Si with 250 nm thermally grown oxide on top was used as substrate for fabrications of FETs. In order to facilitate and pin point the location of exfoliated flake on the substrate, the substrate was patterned with numbered identifiable markers with the help of optical lithography. The details

about the shape, size and density of markers are explained in Chapter 3. The substrate was rinsed with Acetone, IPA and DI water followed by 20 min oxygen plasma in order to ensure the cleanliness of its top surface. All the exfoliated flakes were immediately transferred on to pre-patterned Si substrate. Figure 5.1 illustrates the schematic layout of MoS_2-Au FET.

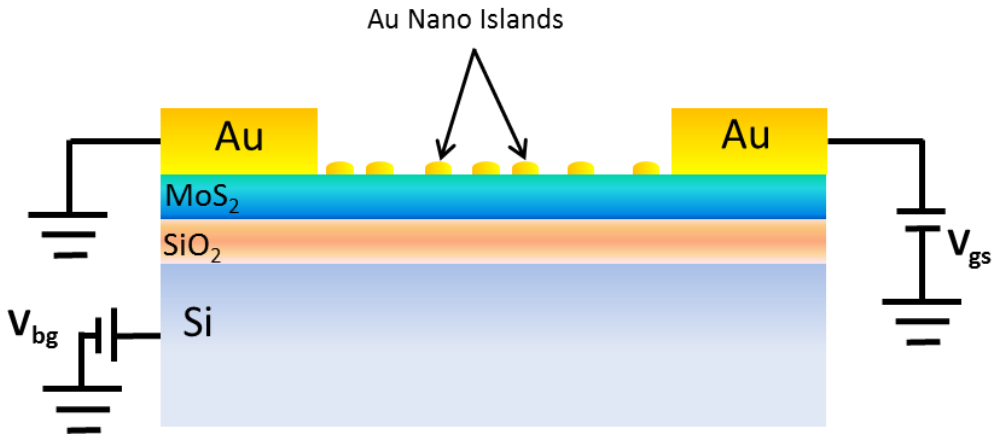

Figure 5.1 Schematic layout of MoS_2-Au field effect transistor.

Electrical contacts to MoS_2 exfoliated flake were patterned with the help of standard electron beam lithography. 35nm Au electrodes (shown yellow in color) were deposited on top of the flake for electron transport measurements. Double layer resist methyl methacrylate/ poly(methyl methacrylate) (MMA/PMMA) was spun over the substrate to ensure the easy liftoff. The resist was baked for 15 mins followed by electron beam exposure and development in developer solution (MIBK:IPA::1:3). For electrodes, the Au was deposited at a very slow rate of 0.03A/sec to ensure a good electrical contact with the flake and mechanical stability of the electrodes. For formation of Au NPs over MoS_2 flake, the Au was deposited controbally and at a very slow deposition rate of 0.01 A/sec at a base pressure of 10^{-6} torr.

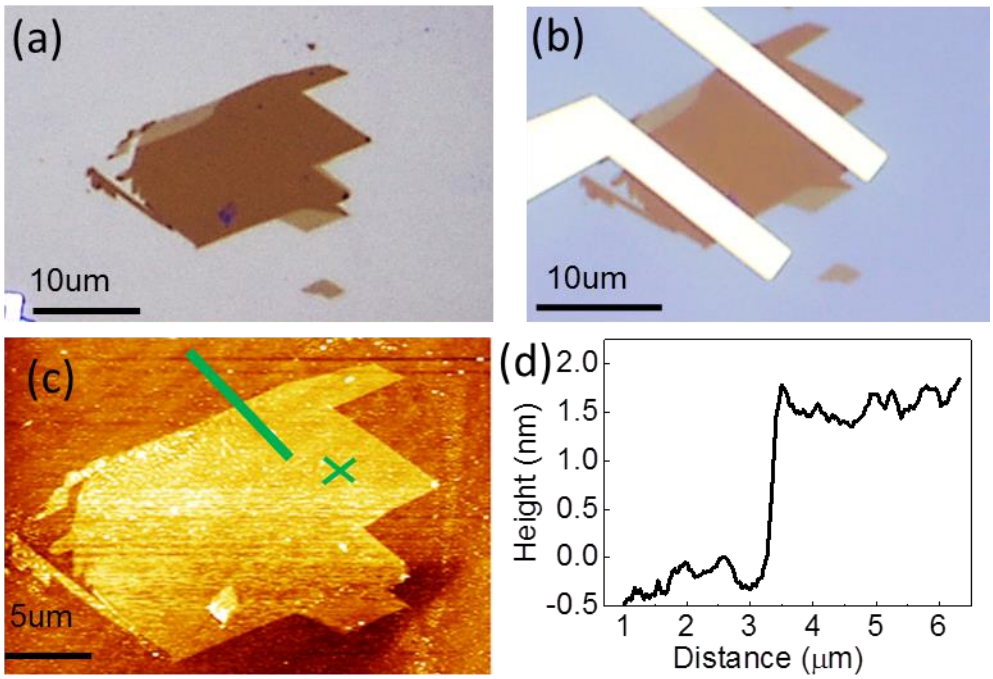

Figure 5.2 Identification of number of layers in exfoliated MoS_2 flake. (a) Optical micrograph of MoS_2 flake mechanically exfoliated on heavily doped Si/SiO_2 substrates. (b) Optical micrograph of fabricated MoS_2 FET (c) AFM image of exfoliated MoS_2 flake. (d) Height profile of the flake extracted from the green line shown in AFM image.

Figure 5.2 the shows the optical and AFM height measurement analysis of representative flake to identify the number of layers. Figure 5.2a illustrates the optical image of the flake used an initial indicator for estimation of number of layer. With the AFM height measurement analysis as shown in figure 5.2c, the height of the flake was found to be 1.5nm which corresponds to 2 layers. The height profile extracted is shown in figure 5.2d.

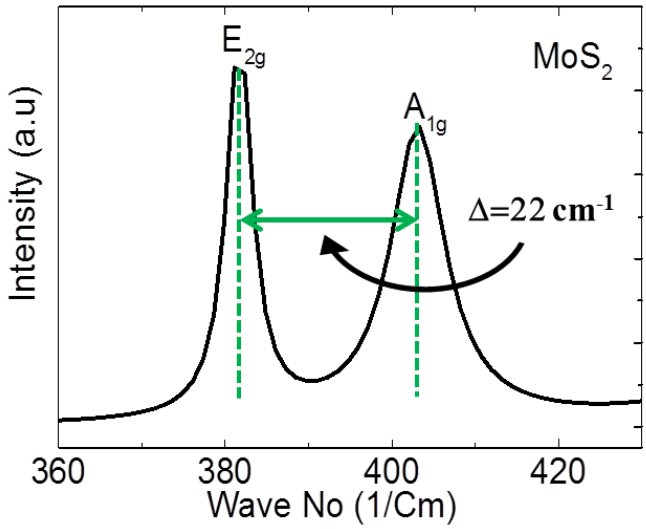

Figure 5.3 Raman spectrum of MoS_2 flake used to fabricate the representative device. Two peaks were identified as E_{2g} and A_{1g} separated by 22 cm^{-1} from each other.

Furthermore the number of layers in representative device flake was confirmed by Raman Spectroscopy. The Raman spectrum of the exfoliated flake is shown in figure 5.3. The spectrum was extracted from the area marked green cross in figure 5.2c. Two predominant peaks at position 381cm^{-1} and 403cm^{-1} wave number were identified as E_{2g} and A_{1g} modes of vibrations. The peaks were found to be separated by Δ = 22cm^{-1} wavenumber. This Δ = 22cm^{-1} separation between these modes confirms that the representative device has flake with 2 MoS_2 layers[1].

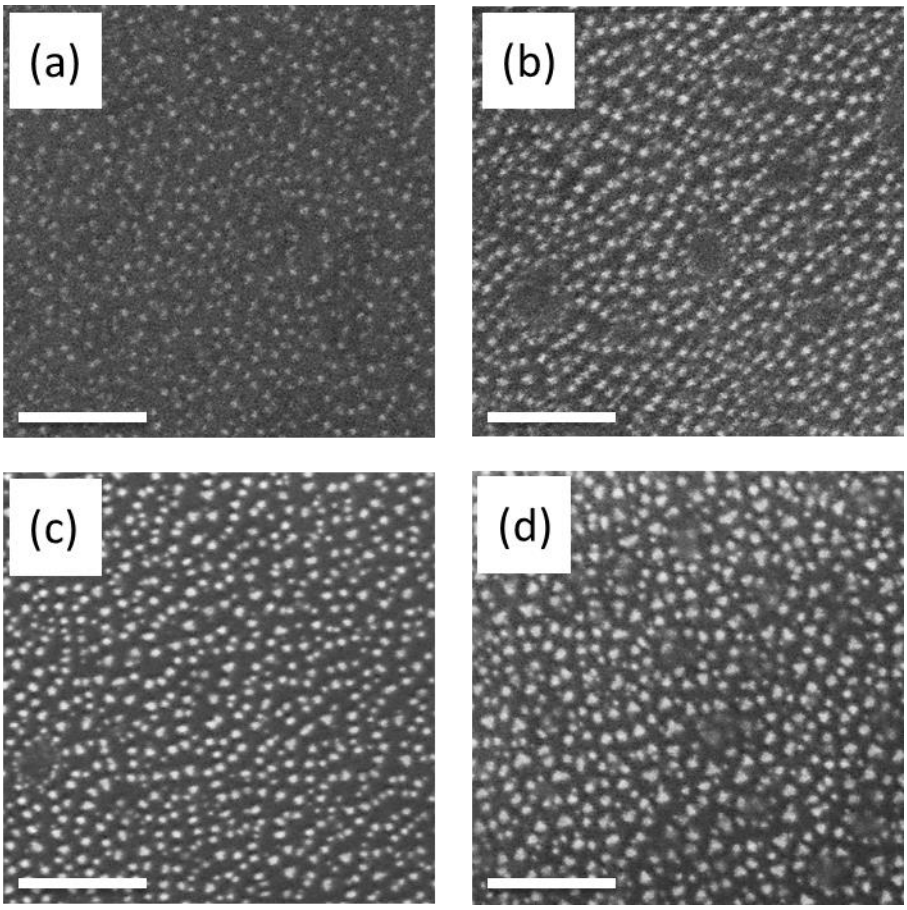

Figure 5.4 FE SEM images of MoS_2 flake decorated with different thickness of Au (a) 0.2nm (b) 0.4nm (c) 0.6nm and (d) 0.8nm. Scale bar shown in the figure is 100nm.

Figure 5.4a, 5.4b, 5.4c and 5.4c illustrates the FE SEM image of MoS_2 flakes after 2^{nd}, 4^{th}, 6^{th} and 8^{th} deposition respectively. The scale bar shown in figure is 100nm. The particle size distributions (Histogram) of NPs on decorated flakes were calculated by Gatan software as show 5.4b. It was found that 81%, 73%, 67% and 49% of particles lie in the range of 5-7nm, 6-8nm, 7-9nm and 9-11nm respectively for 2^{nd}, 4^{th}, 6^{th} and 8^{th} deposition respectively. From the curve fitting function, I have determined the average median size of NPs. The average size was found to increasing with Au thickness. For 2^{nd}, 4^{th}, 6^{th} and 8^{th} deposition the average median size was

found be 6.3nm, 7.5nm, 8.4nm and 9.9nm respectively. The increase of the size of Au NPs can be explained by the cohesive energy of Au. The cohesive energy of Au lies in the range of (3.7-4.0 eV)[2-4]. On the other hand, Au NPs which are only physiosorbed on the surface of MoS_2 are held by week Van der Waals force which is expected to be far less than cohesive energy of Au. Hence the NPs tend to increase their size. From the SEM images, the number of NPs per unit area was calculated after 8th deposition and found to be $4.2x10^{11}$ /cm^2. If I assume the NPs are spherical in shape (for simplicity) I can estimate the total interfacial area. For the 8th deposition, the interfacial area was calculated per cm2 of MoS_2 flake and found that 33% of area is covered by Au NPs after 8th deposition.

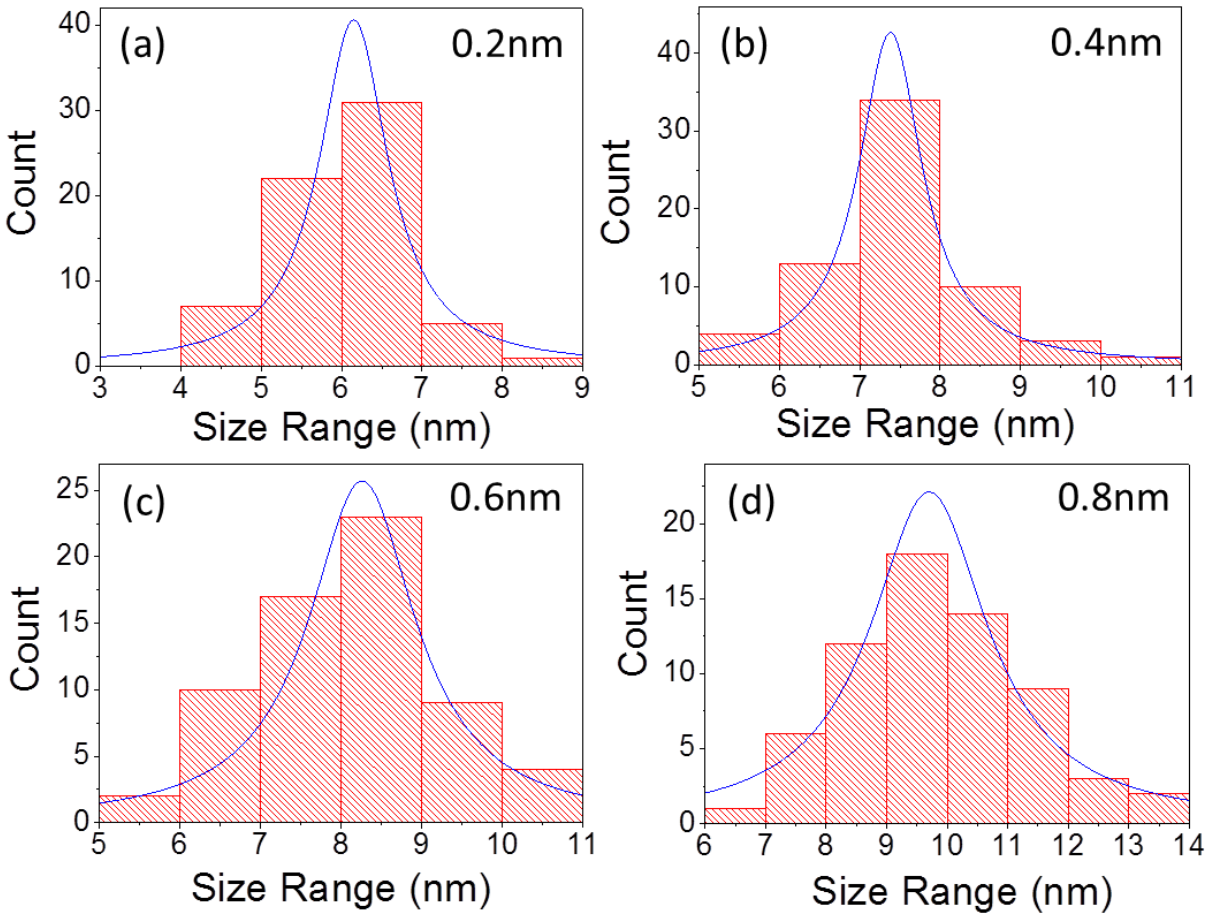

Figure 5.5 Particle size distribution of nano particles on decorated flakes resulted from (a) 0.2nm (b) 0.4nm (c) 0.6nm and (d) 0.8nm Au deposition.

5.3 Room Temperature Electronic Transport Properties Au Decorated Few Layer MoS_2

Figure 5.6 shows the variation in transfer characteristics (drain-current I_D as a function back gate voltage V_G) measured at fixed source-drain bias voltage V_{DS}=100mV for 2 layer MoS_2 FET at different thickness of Au. The black curve represents the transfer characteristics of MoS_2 FET when the Au thickness is 0nm (i.e. pristine flake). The drain current (I_D) changes several orders of magnitude with the applied positive gate voltage (V_G) which is a signature of n-type FET.

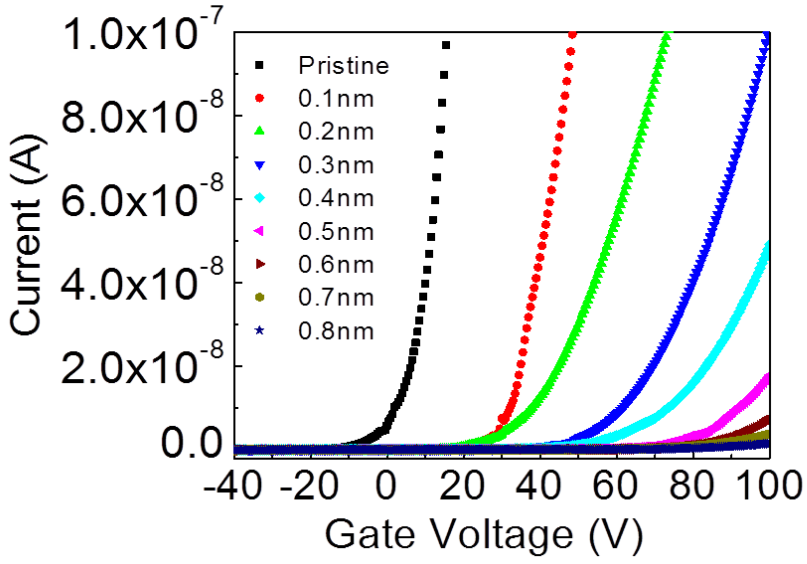

Figure 5.6 Au thickness dependent transfer characteristic of few layers MoS_2 FET measured at fixed drain to source voltage (V_{GS}) = 100mV.

The threshold voltage (V_{th}) can be extracted by extrapolating from the linear region of transfer characteristic curve from the point of maximum slope (where transconductance is maximum) to zero drain current. The threshold voltage (V_{th}) was found to be at 2V for pristine MoS_2. After the transport characteristic measurement of pristine MoS_2 FET, 1st deposition (for 100 sec) was performed over the MoS_2 flake and the transport characteristics were measured again. Red curve shows the transfer characteristic of MoS_2 after 1st deposition. It can be clearly noticed that the threshold voltage has been shifted from 2V (for pristine MoS_2) to 29V after 1st deposition with 1 order of magnitude decrease in the drain current. After the transport measurement one more Au deposition was done onto the flake and transport characteristics of FET were measured again and so on. The current trend of shifting V_{th} towards positive side of V_G and reduction in I_D with deposition of more and more Au on flake continues for subsequent depositions and is evident in figure 5.6. We kept increasing the thickness of Au on MoS_2 flake in steps until the current in the device becomes zero. We observed a systematic change in the V_{th} with the amount of Au thickness.

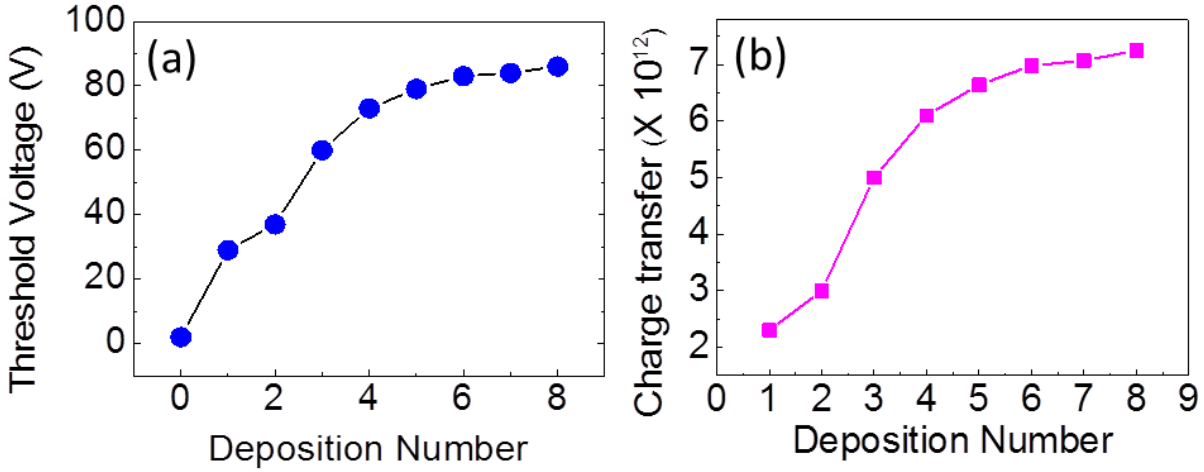

Figure 5.7 Au thickness dependent threshold voltage change and charge transfer in few layers MoS_2 FET.

Figure 5.7a shows the change in V_{th} the thickness of Au. We observed that V_{th} can be controllably tuned over a large range between 2V to 86V by controlling the thickness of Au. However the change in V_{th} tends to saturate after 5th deposition. The V_{th} value can be used to estimate the carrier concentrations[2,3] at fixed V_G by the following formula:

$$Q_{tot} = Cg|V_G - V_{th}| \quad \text{.....(5.1)}$$

Where Q_{tot} is the total charge, C_g is the gate capacitance, V_G is gate voltage and V_{th} is the threshold voltage. Equation 6.1 can be used to quantitatively estimate the charge transfer from by calculating the change in V_{th} value by following formula:

$$Q_{trf} = C_g \Delta V_{th} \quad \text{.....(5.2)}$$

Where Q_{trf} is the total charge transfer as a result of doping and ΔV_{th} is the change in the threshold voltage. The gate capacitance was measure from the parallel plate capacitor model and for $C_g = \varepsilon A/d$, where ε is the permittivity of the medium, A is the area and d is the distance between to plates. Figure 5.7b shows the amount of charge transfer resulted from various Au thickness. We have observed that after only 1st deposition of Au, a total of $2.3x10^{12}/cm^2$ charge gets transferred from MoS_2 to Au. It is worth mentioning that from the energy band diagram of MoS_2-Au system, it is proved that a charge transfer will happen from MoS_2 to Au[4]. In pristine MoS_2 the charge density could be ~10^{13} /cm^2 [5]. Initially the charger transfer increases linearly with thickness but after 5th deposition the charge transfer tends to saturate which is expected as

charge transfer is dependent upon V_{th} which have already shown saturation 5th deposition. After 5th deposition the total charge transfer is 6.98x10^{12}/cm^2 as can be seen in figure in 5.7b. Assuming the maximum upper limit of charge in intrinsic MoS_2 suggested by Novoselove et.al. which is 1x10^{13}/cm^2, here in our case; we have almost 70% of charge transferred to Au NP after 6th deposition.

Now we examine the variation in field effect mobility (μ) of few layers MoS_2 FET with thickness of Au deposition. The μ vs thickness plot of few layers MoS_2 FET is illustrated in figure 5.8. The μ of MoS_2 FET was calculated from linear portion of transfer characteristics taken at fixed drain to source voltage, V_{DS} = 100mV by using the following formula[6,7]:

$$\mu = \frac{dI_{DS}}{dV_G} \frac{L}{WC_iV_{DS}}$$

Where C_i is the capacitance per unit area, L, W are channel length and channel width respectively, V_{DS} is drain to source voltage and dI_{DS}/dV_G is the slope of linear region of transfer characteristic of FET.

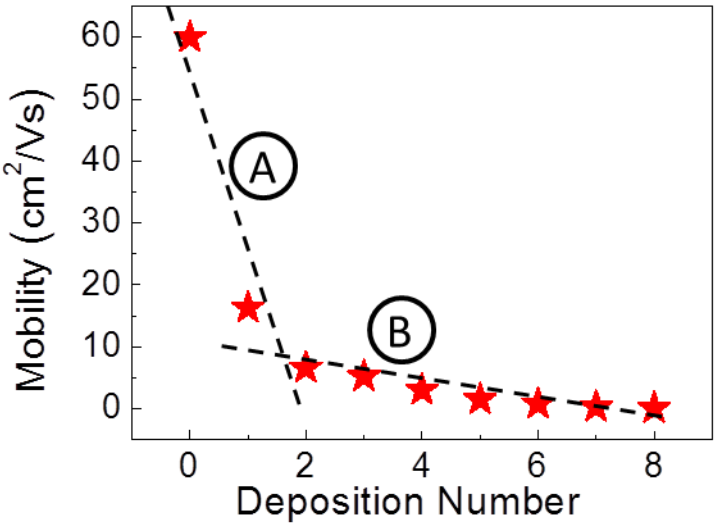

Figure 5.8 Variation of field effect mobility of few layers MoS_2 FET with various thicknesses of Au. Two regions were identified in μ Vs Thickness curve marked "A" and "B" in figure.

We identified two regions; region "A" and region "B" in μ vs thickness curve of MoS_2 FET. The region "A" spans from pristine to deposition #2, where the decrease in μ is very steep. However in region "B" which spans from deposition #3 to further, the drop in μ value is comparatively less steep than region "A".

5.4 Room Temperature Electronic Transport Properties Au Decorated Multi-Layer MoS_2

Now we examine the Au decorated multilayer MoS_2 hybrid FET. Figure 5.9a illustrates he optical micrograph of multilayer MoS_2 FET. The height profile is extracted for the AFM measurement from the line drawn green in optical image and is shown in figure 5.9b. The average height of flake was found to be 18nm which corresponds to about 27 MoS_2 layers in

flake. A Raman spectrum was also taken from the point marked green cross in the optical image and shown in figure 5.9c. The difference between the E_{2g} and A_{1g} mode of vibrations Δ was found to be equal to 26 cm^{-1} which confirms that the flake has multilayers in it.

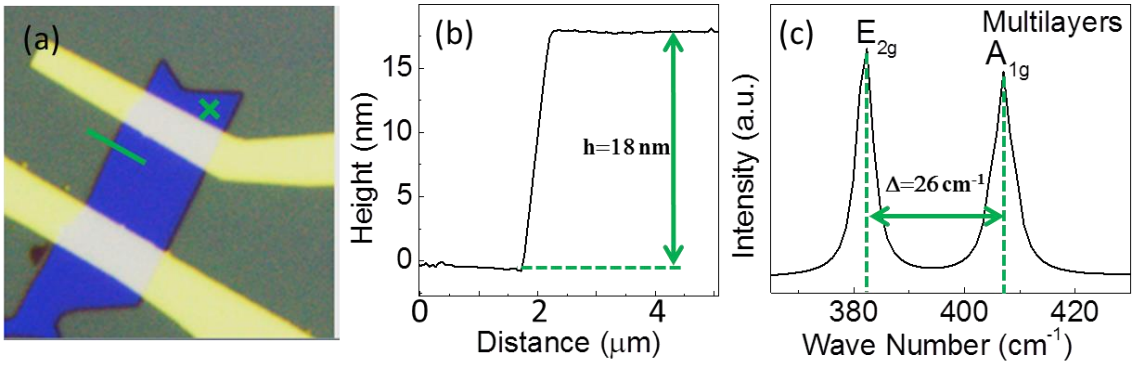

Figure 5.9 (a) optical micrograph of multilayer MoS_2 FET (b) Raman spectrum of Multilayer flake extracted from point marked green cross in optical image and (c) AFM height profile extracted form line marked green in optical image.

Figure 5.10 shows the variation in transfer characteristics (drain-current I_D as a function back gate voltage V_G) measured at fixed source-drain bias voltage V_{DS}=100mV for few layer MoS_2 FET at different thickness of Au. The black curve represents the transfer characteristics of MoS_2 FET when the Au thickness is 0nm (i.e. pristine flake). The drain current (I_D) changes several orders of magnitude with the applied positive gate voltage (V_G) which is a signature of n-type FET.

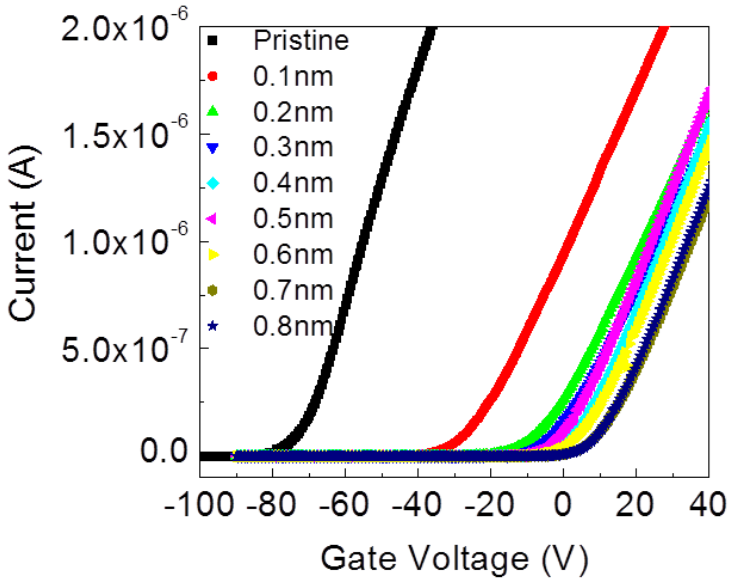

Figure 5.10 Au thickness dependent transfer characteristic of multi layers MoS_2 FET measured at fixed drain to source voltage (V_{GS}) = 100mV.

The threshold voltage (V_{th}) was again extracted by extrapolating from the linear region of transfer characteristic curve from the point of maximum slope (where transconductance is maximum) to zero drain current. The threshold voltage (V_{th}) for pristine MoS_2 was found to be at 2V. After the transport characteristic measurement of pristine multilayer MoS_2 FET, 1st deposition was performed over the MoS_2 flake and again the transport characteristics were measured. Red curve in figure 5.10 shows the transfer characteristic of multilayer MoS_2 after 1st deposition. In agreement with the previously measured few layer MoS_2 FET transfer curve, the multilayer MoS_2 FET also shows a change in V_{th} with the deposition of Au thickness. However in contrast to few layer FET, in case of multilayer MoS_2 FET, after 2nd deposition the change in V_{th} was very little.

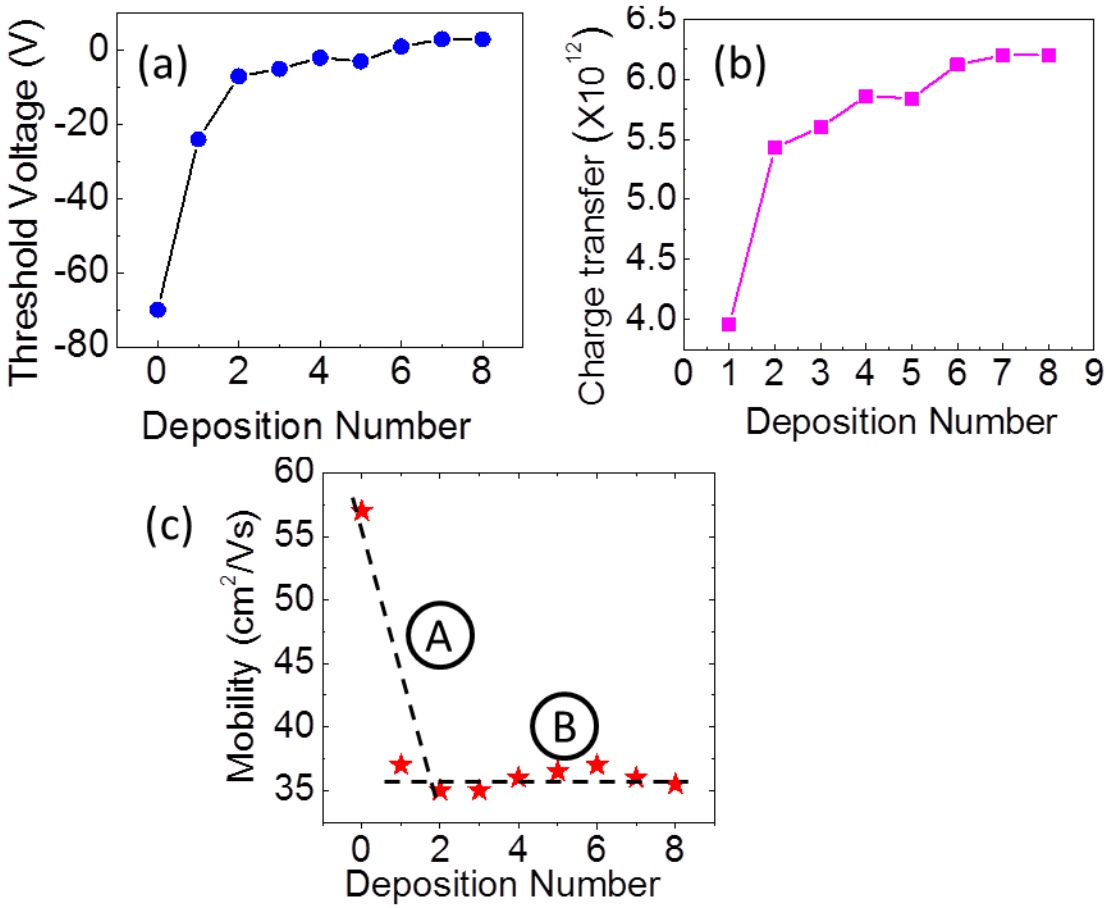

Figure 5.11 Variation in V_{th} (a), charge transfer (b) and μ (c) of multilayer MoS_2 FET with Au thickness.

Figure 5.11a illustrates the V_{th} change with thickness of Au. V_{th} for multilayers FET changes almost linearly up to 2nd deposition and slows down after 2nd deposition and eventually saturates. This trend of V_{th} shift matches well with the previously shown few layers MoS_2 FET. From V_{th} values, we again quantitatively estimated the charge transfer by using equation 5.2. Figure 5.11b illustrates the charge transfer with at different thicknesses. Thickness vs charge transfer curve also shows similar trend. Now again we calculated the mobility in each step of Au deposition. Figure 5.11c illustrates the mobility vs thickness curve for multilayer MoS_2 FET. We observed the decrease in mobility was very steep up to 2nd deposition which is in agreement with

the 2 layer device, but after the 2nd deposition there has been no noticeably change in mobility in multilayer FET.

5.5 Discussion

In this section I will discuss about the change in V_{th} towards the positive side of gate voltage in both few layers and multilayers devices as shown in previous figure 5.6 and figure 5.10 and change in μ with thickness of Au as shown in figure 5.8 and 5.11c respectively. The V_{th} in simple words is defined as the gate voltage at which the device turns on. If we reduce the majority carries in MoS_2 (which are electrons) as explained in section 5, we would expect the device to switch on at later voltage. Such a change in V_{th} towards the positive side of gate voltage is indicative of p-doping of MoS_2. P-doping of MoS_2 by Au is also supported by the band alignment and work function of the materials[4]. The work function of MoS_2 (Φ_M) is at 4.7eV and work function of Au (Φ_{Au}) is at 5.1eV as reported in previous reports[4], results in 0.4eV offset in Fermi levels of MoS_2 and Au. Such an offset causes a significant band bending of energy level in semiconductor side. As a result upon making the Au-MoS_2 contact, the electron form MoS_2 gets transferred to Au. Hence MoS_2 gets p-doped.

Now I will discuss the reduction of μ with thickness of Au. The μ vs thickness curve shown in figure 5.8 shows two regions "A" and "B". In region "A" the decrease in μ is very steep whereas in region "B" the decrease is relatively less sharp. I believe that in region "A" the decrease in the μ is because of two major reasons. First contribution comes from p-doping caused by Au NP. Due to the reduction in carriers[8] and the overall current in device reduces. This can be clearly seen in transfer characteristic of device (figure 5.6) that due to decrease in carriers in MoS_2, the

slope of linear regions also decreases and hence the field-effect mobility of FET. Second contribution comes from the obstruction posed to the flow of electrons by the localized depletion regions formed underneath the Au NP when MoS_2 and Au NP come in contact with each other. These localized depletion regions comes into picture when a metal NP comes in contact to semiconducting material[9].

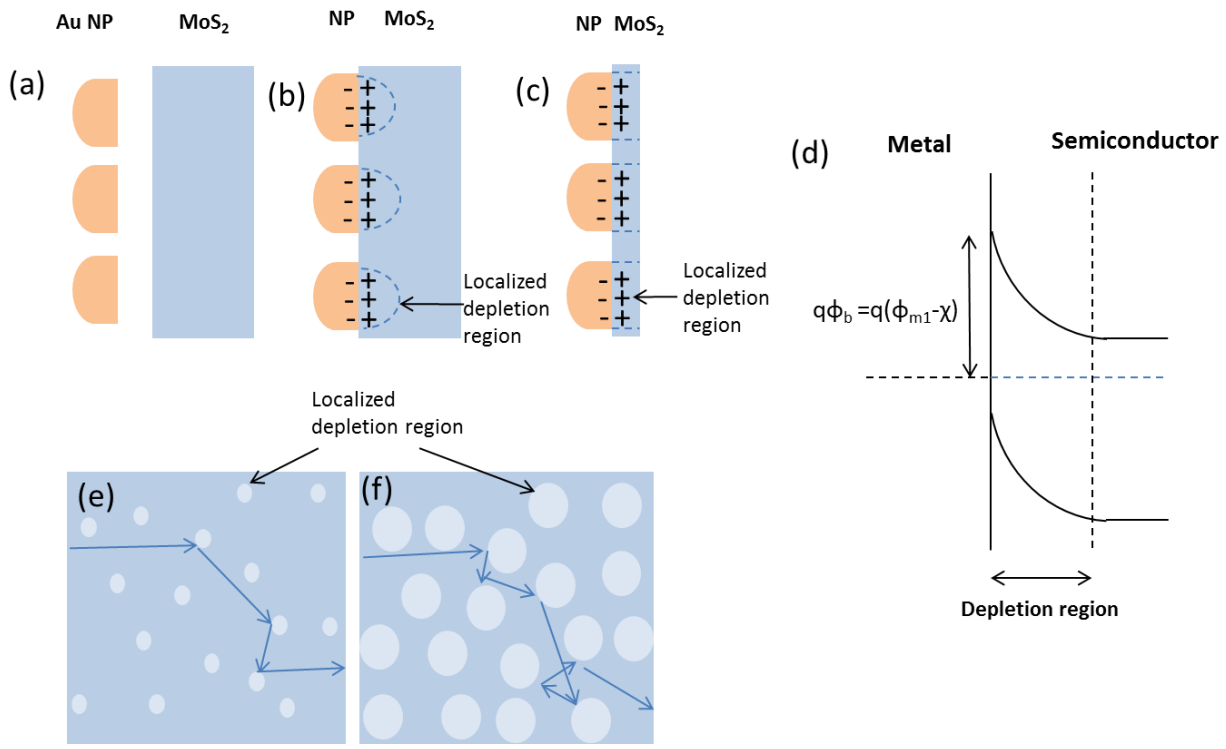

Figure 5.12 Formation of depletion region in MoS_2 underneath Au NPs. (a) illustrate the schematic of Au NP and multilayer MoS_2 before contact, (b) illustrates the formation of localized depletion regions in multilayer MoS_2 underneath Au NPs, (c) illustrates the localized depletions regions in few layer MoS_2 and (d) illustrates the energy band alignments in MoS_2 and Au after they come in contact with each other and the formation of localized depletion region as a result of band bending (e),(f) illustrates the schematic representation obstruction posed by localized depletion regions to flow of electrons.

Figure 5.12 illustrates the schematic diagram showing the formations of localized depletion regions in MoS_2 underneath the Au NP upon coming in contact with NPs. The size of

these depletion regions can be controlled by controlling the size of deposited NPs. Figure 5.12b and 5.12c illustrates the schematic for side view of formation of localized depletion regions underneath the Au NP for multilayer and few layers MoS_2. Figure 5.12d shows the energy band alignment of Au and MoS_2 after the contact and formation of localized depletion regions. Figure 5.12e and 5.12f shows the top view of the schematic representing smaller and larger localized depletion regions in MoS_2. The arrows in the figures are drawn to represent the flow of charge in MoS_2. In region "A", since the size of NPs is small, hence the size of depletion regions is also small. Therefore second contribution is not dominant in region "A". Hence the dominant contribution in reduction of field effect mobility only comes from p-doping.

In region "B", the doping tends to saturate (as change in V_{th} is very slow) whereas the size of localized depletion regions becomes larger and larger making it difficult for charge to flow in MoS_2. Hence again we see a reduction of mobility in this region, but the dominant reason I believe is because of the large size of localized depletions regions. A further careful study is needed to examine this region. Here we suggest that in order to tune the carrier concentration in MoS_2 by Au doping, we should limit the device to work in region "A".

5.6 Conclusion

In conclusion, we fabricated the MoS_2 FET device and decorated it with various thickness of Au and studied its electrical and transport properties. We showed that a very slow evaporation (0.01A/sec) of Au on MoS_2 surface results in formation of NP over the surface of MoS_2. We further demonstrated the simple and easy method to systematically tune p-doping in MoS_2. We also demonstrated that by controlling the amount of Au on MoS_2, we can tune the

carrier concentration and the threshold voltage over the large range from 2V to 86V. We quantitatively calculated the amount of charge transfer from MoS_2 to Au. We interpreted that the decrease in field effect mobility of the device is due to two major contributing factors: p-doping of MoS_2 and formations of localized depletions underneath Au NP which pose more obstruction to the flow of electrons in the MoS_2.

5.7 References

1 Lee, C. *et al.* Anomalous Lattice Vibrations of Single- and Few-Layer MoS2. *ACS Nano* **4**, 2695-2700, (2010).

2 Radisavljevic, B. & Kis, A. Mobility engineering and a metal–insulator transition in monolayer MoS2. *Nat Mater* **12**, 815-820, (2013).

3 Mak, K. F. *et al.* Tightly bound trions in monolayer MoS2. *Nat Mater* **12**, 207-211, (2013).

4 Bhanu, U., Islam, M. R., Tetard, L. & Khondaker, S. I. Photoluminescence quenching in gold - MoS2 hybrid nanoflakes. *Sci. Rep.* **4**, (2014).

5 Novoselov, K. S. *et al.* Two-dimensional atomic crystals. *Proceedings of the National Academy of Sciences of the United States of America* **102**, 10451-10453, (2005).

6 RadisavljevicB, RadenovicA, BrivioJ, GiacomettiV & KisA. Single-layer MoS2 transistors. *Nat Nano* **6**, 147-150, (2011).

7 Islam, M. R. *et al.* Tuning the electrical property via defect engineering of single layer MoS2 by oxygen plasma. *Nanoscale* **6**, 10033-10039, (2014).

8 Yun, W. S., Han, S. W., Hong, S. C., Kim, I. G. & Lee, J. D. Thickness and strain effects on electronic structures of transition metal dichalcogenides: 2H-MX_2 semiconductors (M= Mo, W; X=S, Se, Te). *Physical Review B* **85**, 033305 (2012).

9 Sze S. M., N. K. K. Physics of Semiconductor Devices, 3rd Edition. (2006).

CHAPTER 6: CONCLUSION

6.1 Summary

In this dissertation, Optical and electronic properties of Au decorated MoS_2 have been investigated. First two chapters build up a background for the study. In chapter is about characterization of the flake, device fabrication and measurement.

In chapter 4, we have investigated the optical properties of thermally deposited Au decorated MoS_2 nanoflakes. The size of the NP was controlled by the thickness of Au deposited. We reported a drastic PL quenching after decorating MoS2 with Au NP. We suggest that the electrons gets transferred from MoS_2 to Au thereby cause a p-doping in MoS_2 flake.

In chapter 5, we have investigated the electronic transport properties of Au decorated MoS_2 at room temperature. We fabricated the MoS_2 FET and decorated it with various thickness of Au and studied its electrical and transport properties. We demonstrated the formation of Au NP by thermal deposition at a very slow rate and also demonstrated that the electronic properties can be tuned by changing the thickness of Au. We tuned threshold voltage over the large range from 2V to 86V by changing the thickness of Au. In addition, we quantitatively calculated the amount of charge transfer from MoS_2 to Au. We interpreted that the decrease in field effect mobility of the device is due to two major contributing factors: p-doping of MoS_2 and formations of localized depletions underneath Au NP which pose more obstruction to the flow of electrons in the MoS_2.

6.2 Future Directions

As an extension of this work, I believe atomically thin, planner pn junction can be fabricated. Figure 6.1 illustrates the concept to fabricate MoS_2 pn junction by Au doping. First of all the MoS_2 flake is exfoliated on SiO_2/Si substrate. Then two electrodes are defined with the help of e-beam lithography. A thin layer of PMMA is then spun over the flake and a small window is opened by using the e-beam lithography again. By doing so, half of the flake will be exposed and other half will remain under PMMA. By doing so, we can selectively p dope half of the flake with Au. End the end, we will remove the PMMA form the flake.

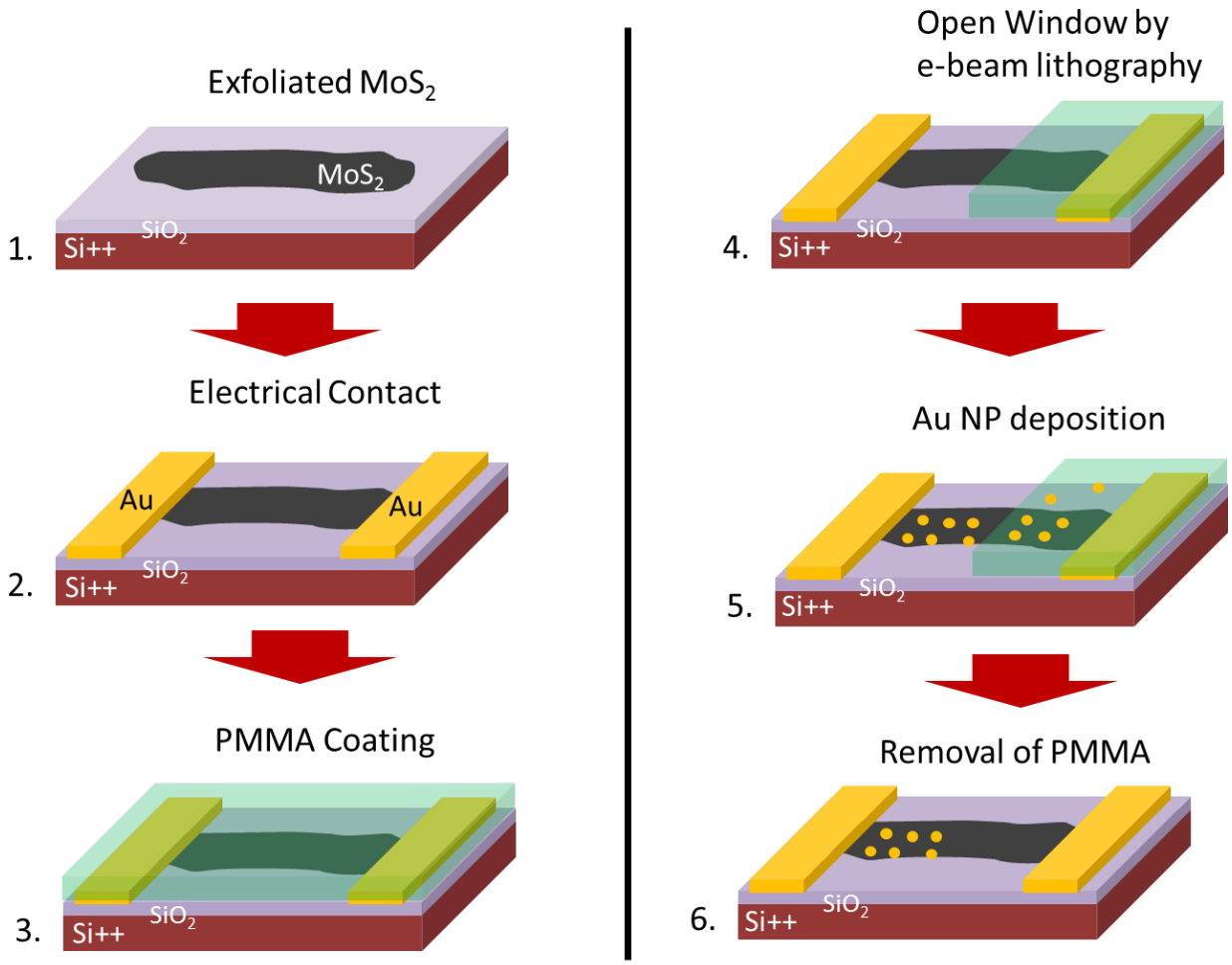

Figure 6.1 Fabrication steps for only MoS_2 pn junction (1) Exfoliation of MoS_2 on Si/SiO_2 substrate (2) Metallization of gold (Au) electrode on the selected flake (3) coating of PMMA (4) opening up of a small window by e-beam lithography for Au deposition(5) top view of final device